D2.1 - Report describing the experiments performed at each reactor and associated data uncertainties

Version 2.0
February 2026

Szabolcs Czifrus[1], András Szabolcs Ványi[1,2], Tamás Belgya[3], Yann Perin[4], Mathieu Hursin[5,6], Klemen Ambrožič[7,8]

[1]Department of Nuclear Energy, Budapest University of Technology and Economics, Hungary
[2]Fuel and Reactor Materials Department, Institute for Atomic Energy Research, HUN-REN Centre for Energy Research, Hungary
[3]Budapest Neutron Centre, Institute for Energy Security and Environmental Safety, HUN-REN Centre for Energy Research, Hungary
[4]Reactor Safety Division, Gesellschaft für Anlagen- und Reaktorsicherheit (GRS) gGmbH, Germany
[5]Laboratory for Reactor Physics and Systems Behavior, EPFL - Swiss Federal Technology Institute of Lausanne, Switzerland
[6]Laboratory for Reactor Physics and Thermal-Hydraulics, Paul Scherrer Institute, Switzerland
[7]Reactor Physics Division, Jožef Stefan Institute, Slovenia | [8]Faculty of Mathematics and Physics, University of Ljubljana, Slovenia

Funded by the European Union

Disclaimer

Funded by the European Union. Views and opinions expressed are however those of the author(s) only and do not necessarily reflect those of the European Union or the European Atomic Energy Community ('EC-Euratom'). Neither the European Union nor the granting authority can be held responsible for them.

Document information

Grant Agreement	n°101163288
Project Title	Experiments for Validation and Enhancement of the REactor preSsure vessel fluence assessmenT
Project Acronym	EVEREST
Project Coordinator	Yann Perin – GRS
Project Duration	01.09.2024 – 30.08.2028 (48)
Related Work Package	WP2
Related Task(s)	T 2.1, T 2.3
Lead Organisation	JSI
Contributing Partner(s)	BME, HUN-REN, JSI, GRS, EPFL
Due Date	March 1st, 2026
Submission Date	February 27th, 2026
Dissemination level	PU

History

Date	Version	Submitted by	Reviewed by	Comments
24.02.2026	Version 1.0	Klemen Ambrožič	Mathieu Hursin	Initial version
26.02.2026	Version 2.0	Laurine Duivon	Karine Lavoisier Mathieu Hursin	Final Version

Signatures

Author Signature	WPL Signature	Coordinator Signature
 Klemen Ambrožič	 Mathieu Hursin	 Yann Perrin

Funded by the European Union

Funded by the European Union. Views and opinions expressed are however those of the author(s) only and do not necessarily reflect those of the European Union or the European Atomic Energy Community ('EC-Euratom'). Neither the European Union nor the granting authority can be held responsible for them.

Table of contents

Funded by the European Union

Funded by the European Union. Views and opinions expressed are however those of the author(s) only and do not necessarily reflect those of the European Union or the European Atomic Energy Community ('EC-Euratom'). Neither the European Union nor the granting authority can be held responsible for them.

Funded by the European Union

Funded by the European Union. Views and opinions expressed are however those of the author(s) only and do not necessarily reflect those of the European Union or the European Atomic Energy Community ('EC-Euratom'). Neither the European Union nor the granting authority can be held responsible for them.

List of figures

Funded by the European Union

Funded by the European Union. Views and opinions expressed are however those of the author(s) only and do not necessarily reflect those of the European Union or the European Atomic Energy Community ('EC-Euratom'). Neither the European Union nor the granting authority can be held responsible for them.

Funded by the European Union

Funded by the European Union. Views and opinions expressed are however those of the author(s) only and do not necessarily reflect those of the European Union or the European Atomic Energy Community ('EC-Euratom'). Neither the European Union nor the granting authority can be held responsible for them.

Funded by the European Union

Funded by the European Union. Views and opinions expressed are however those of the author(s) only and do not necessarily reflect those of the European Union or the European Atomic Energy Community ('EC-Euratom'). Neither the European Union nor the granting authority can be held responsible for them.

List of tables

Funded by the European Union

Funded by the European Union. Views and opinions expressed are however those of the author(s) only and do not necessarily reflect those of the European Union or the European Atomic Energy Community ('EC-Euratom'). Neither the European Union nor the granting authority can be held responsible for them.

Summary

This report describes the experiments performed at the Budapest Research Reactor, the BME Training Reactor and the JSI TRIGA Mk-II research reactor. The emphasis in this report is on the experimental data:

- Axial reaction rate profiles for determination of fast and thermal neutron flux profile, at various positions in the reactor core.
- Control rod reactivity worth measurements.
- Coolant temperature measurements at different locations in the core and in the pool tank.
- Reactor power and fuel temperature evolution during a fast reactor transient.

The measurement techniques used in each particular setup, as well as their core configurations, and potential sources of uncertainties are described and evaluated. In some cases, results from models used at the time of analysis are also shown alongside experimental data. Numerical experimental datasets are made available, serving as a benchmark for future advance Multiphysics modelling efforts of the EVEREST project.

Keywords

Research reactor, experimental data, Axial profile reaction rate measurements, excess reactivity measurements, coolant temperature, pulse database

Abbreviations and acronyms

Acronym	Description
WP	Work Package
BRR	Budapest Research Reactor
BME	Budapest University of Technology and Economics
JSI	Jožef Stefan Institute
TRIGA	Training Research Isotope production by General Atomics
HPGe	High purity germanium detector
NAA	Neutron Activation Analysis
LEU	Low-enriched uranium
SiC	Silicon carbide
DPA	Displacement per atom
IFE	Instrumented fuel element
PHA	Pulse Height Analysis
MCS	Multi-Schannel Scaling
CFD	Computational Fluid Dynamics
RANS	Raynolds-Averaged Navier Stokes
CAD	Computer Aided Design

Funded by the European Union

Funded by the European Union. Views and opinions expressed are however those of the author(s) only and do not necessarily reflect those of the European Union or the European Atomic Energy Community ('EC-Euratom'). Neither the European Union nor the granting authority can be held responsible for them.

1. Introduction

1.1. Background

The precise characterization of nuclear research reactors relies on the accurate determination of fundamental parameters, primarily neutron flux and core reactivity. Because neutron flux cannot be measured directly, experimental campaigns typically measure the products of neutron-induced nuclear reactions. Techniques such as Neutron Activation Analysis (NAA) utilize specific target isotopes—relying on thermal reactions (e.g., ^{197}Au, ^{235}U or fast reactions (e.g., ^{54}Fe, ^{58}Ni)—to deduce flux components based on characteristic radioactive decay and gamma emissions. To assess both subcritical and supercritical reactor states, reactivity measurements are primarily conducted using the inverse kinetics method. Derived directly from point reactor kinetics equations, this method expresses reactivity as a function of time-dependent neutron detector count rates, providing a highly reliable measurement without the need for additional complex instrumentation.

1.2. Objectives

The primary objective of this document is to present comprehensive, benchmark-quality experimental data derived from extensive operational and transient campaigns. By compiling meticulous facility specifications, structural geometries, and high-resolution empirical measurements, this deliverable provides a foundation for computational validation. The datasets detailed herein are specifically intended to support the rigorous benchmarking of high-fidelity neutron transport codes (such as MCNP (Rising et al., 2025) and Serpent (Leppänen et al., 2025)), thermal-hydraulic fluid dynamics simulations (such as ANSYS CFX (ANSYS, 2011)), and advanced multi-physics coupling frameworks.

1.3. Scope

This deliverable outlines the physical characteristics, calibration procedures, and specific experimental datasets from three distinct European research reactors:

- Budapest Research Reactor (BRR): A 10 MW vessel-type reactor primarily utilized for materials science. The scope covers its facility design and recent experimental campaigns focused on developing continuous axial flux profiles within fast-flux irradiation channels using high-purity iron and aluminium-gold activation wires.
- BME Training Reactor: A 100 kW light-water moderated, pool-type reactor. The documented scope includes a recent high-precision activation-based power calibration, integral and differential control rod reactivity worth measurements, relative axial reaction rate profiling, and comprehensive thermal-hydraulic temperature mapping during various operational transients.
- JSI TRIGA Mark II Reactor: A 250 kW pool-type reactor uniquely capable of generating 1 GW power bursts during prompt-super-critical pulse operations. The scope encompasses absolute axial reaction rate validations, high-precision fission rate profiling using miniature ^{235}U and ^{238}U fission chambers, pool-wide temperature mappings to validate natural convection, and the comprehensive JSI TRIGA Pulse Database—an exhaustive 26-year empirical archive of transient nuclear operations.

Funded by the European Union

Funded by the European Union. Views and opinions expressed are however those of the author(s) only and do not necessarily reflect those of the European Union or the European Atomic Energy Community ('EC-Euratom'). Neither the European Union nor the granting authority can be held responsible for them.

2. General Methodology

2.1. Reaction rate measurements

Neutron flux measurements cannot be performed directly, and are usually performed by measuring the products of neutron-induced nuclear reactions, such as fission, scattering (SiC detectors) or via a number of other neutron-induced nuclear reactions, which emit reaction products promptly, and are often used as reactor power monitoring detectors, or by converting a stable isotope into radioactive one i.e. neutron activation, which then decays with a characteristic decay time. In the latter case, the decay products can be either charged particles i.e. in the case of Self Powered Neutron Detectors (SPNDs), or characteristic gamma radiation, by which the exact amount of the activated nuclei can be deduced, and is commonly known as the Neutron Activation Analysis (NAA).

In all cases, the reaction probability is described by an intrinsic property of the target nuclei structure called the microscopic reaction cross section, which is generally energy dependent:

- Thermal reactions: The binding energy of the additional neutron alone is sufficient to excite the target nucleus to undergo some sort of nuclear reaction. Isotopes commonly used for the estimation of thermal neutron flux are ^{3}He(n,p)^{3}H, ^{6}Li(n,α)^{3}H, ^{10}B(n,α)^{7}Li, ^{197}Au(n,γ)^{198}Au and ^{235}U(n,fiss).
- Fast reactions: The binding energy of the neutron alone is not sufficient, to cause a nuclear reaction so additional energy in the form of neutron's kinetic energy is required for the reaction to be possible. Isotopes commonly used for the estimation of the fast neutron flux component are ^{115}In(n,n')^{115m}In, ^{58}Ni(n,p)^{58}Co, ^{58}Ni(n,2n)^{57}Ni, ^{54}Fe(n,p)^{54}Mn, ^{24}Mg(n,p)^{24}Na, ^{27}Al(n,α)^{24}Na, as well as ^{238}U(n,fiss) and ^{237}Np(n,fiss).

The energy reaction cross sections mentioned previously are shown in Figure 2-1 .

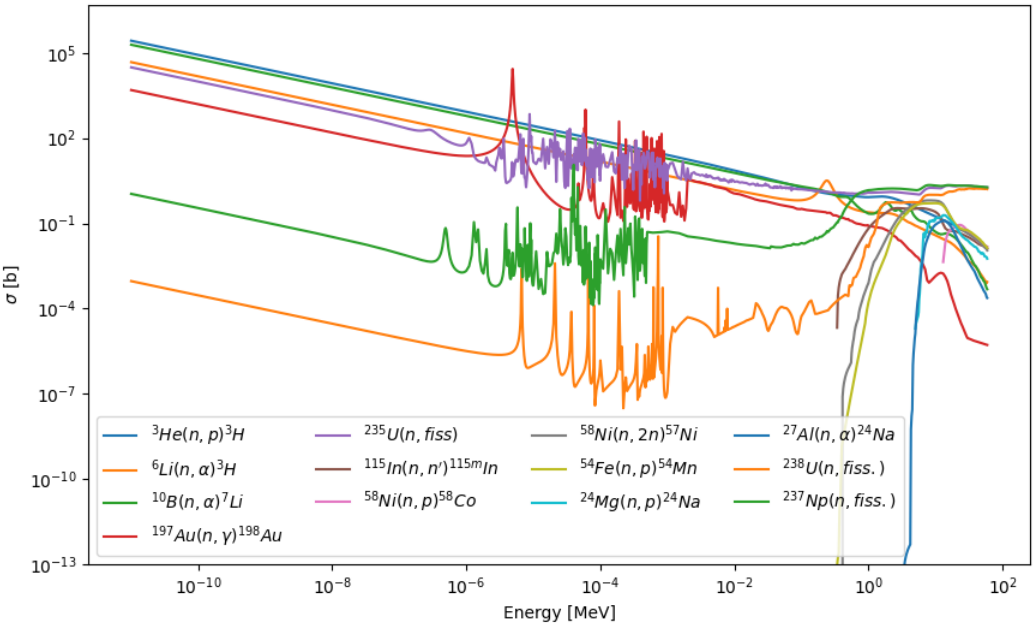

Figure 2-1: Reaction cross sections commonly used to detect neutron flux.

Broadly speaking, it is not uncommon that thermal reactions have cross sections higher even at MeV energy range, compared to fast neutrons. It is therefore common practice to perform two measurements with thermal reactions, an ordinary one, where both thermal and fast component are measured, and a second one, where the sample is enclosed inside cadmium shielding, which absorbs the thermal neutrons, so that only fast

Funded by the European Union

Funded by the European Union. Views and opinions expressed are however those of the author(s) only and do not necessarily reflect those of the European Union or the European Atomic Energy Community ('EC-Euratom'). Neither the European Union nor the granting authority can be held responsible for them.

neutrons act on the sample. The thermal neutron flux can then be deduced by the difference in activation, using the so-called cadmium ratio method (Anderson et al., 1947).

While we specifically mentioned thermal (0.1 meV – 0.5 eV) and fast neutron components (above 0.1 MeV), a gap exists in between, in the epithermal region. Recent advances in neutron flux measurements have identified the possibility to extend the range of thermal reaction into the epithermal region using boron compounds such as BN and B_4C with varying degrees of boron concentration and enrichment (Radulović et al., 2024).

One of the more established and precise methods is the NAA, where the decay of the radioactive isotope is accompanied by a number of gamma emissions, which is unique for each isotope. Special care must be taken in order to properly account for neutron self-absorption, and the absorption of the resulting gamma radiation in the sample itself, before reaching HPGe detector. That is why neutron activation foils are commonly made in the shape of thin discs, to minimize the effect.

In order to assess the geometrical effects of self-shielding and the response of the detector to a particular gamma ray energy i.e. detector sensitivity, Monte Carlo particle transport methods are commonly used. Special care must also be taken with respect to measurements of the irradiation time, flux and power levels, and then the measurement time, particularly if absolute reaction rate calculations are required. HPGe's will record radiation due to the background as well, so a reference background measurement should be taken and subtracted.

2.2. Reactivity measurements

Reactivity measurements performed in research reactors are primarily based on methods relying on the point reactor kinetics equations. These techniques include:

- pulsed neutron source methods;
- asymptotic period methods;
- inverse kinetics method.

Reactivity measurements presented in this document were performed using the inverse kinetics method. In contrast to the mentioned alternative techniques, inverse kinetics is rather general as it is applicable to both subcritical and supercritical reactor states and does not require additional instrumentation beyond an appropriately positioned neutron detector. The method is derived directly from the point kinetics equations, which are reformulated to express the reactivity as a function of the time-dependent neutron detector count rate. For a reactor without external neutron source, the inverse kinetics equation the form in Equation (1).

$$\frac{\rho(t)}{\beta_{eff}} = 1 + \frac{\frac{\Lambda}{\beta_{eff}}\frac{d\varphi}{dt} - \sum_{i=1}^{N}\frac{\beta_i}{\beta_{eff}}\lambda_i \int_{-\infty}^{t} \varphi\,(t')e^{-\lambda_i(t-t')}dt'}{\varphi(t)} \quad (1)$$

where β_{eff} is the total effective delayed neutron fraction, β_i and λ_i are the delayed neutron fractions and decay constants for delayed neutron group i, Λ is the generation time and φ is the amplitude function, or in practical measurement cases the detector count.

2.3. Temperature measurements

The operation of a nuclear reactor is highly dependent on fuel and coolant temperatures. Elevated temperatures shift the thermal neutron spectrum peak to higher energies and broaden reaction rate cross-section resonances through the Doppler effect. Furthermore, thermal expansion decreases coolant density, which, in the case of water, reduces neutron moderation. This leads to a harder neutron spectrum that induces more radiation damage in reactor structural materials via atom displacements (DPA). Predicting this DPA

Funded by the European Union

Funded by the European Union. Views and opinions expressed are however those of the author(s) only and do not necessarily reflect those of the European Union or the European Atomic Energy Community ('EC-Euratom'). Neither the European Union nor the granting authority can be held responsible for them.

accumulation and the resulting material embrittlement is a fundamental component of ageing management and lifetime extension justifications for commercial nuclear power plants. To ensure inherently safe operation, these combined thermal-neutronic effects must produce a negative temperature feedback coefficient. Accurately capturing these dynamics requires coupled neutron transport and thermal-hydraulic modelling, which in turn demands rigorous validation using high-fidelity experimental data.

This report describes several experimental campaigns conducted at the BME Training reactor and the JSI TRIGA reactor to provide this crucial validation data. To characterize the thermal-hydraulics, coolant temperature profiles were mapped both within the reactor core and above it in the reactor pool tank. These in-core and above-core measurements were performed using distributed arrays of multi-point thermocouple lances inserted into specific core grid positions, allowing for the precise capture of the three-dimensional thermal plume and the onset of natural circulation within the pool.

Moreover, transient fuel temperature measurements during pulse operation are presented to demonstrate the most significant thermal-neutronic coupling in the nuclear fuel. The JSI TRIGA reactor utilizes a unique Uranium-Zirconium Hydride (U-ZrH) fuel matrix that drives a prompt negative temperature feedback mechanism. Capturing this rapid coupling during a millisecond power pulse requires specialized Instrumented Fuel Elements (IFEs). These IFEs are equipped with embedded K-type thermocouples located directly within the fuel meat and are connected to high-frequency data acquisition systems. This specific instrumentation allows for the precise measurement of the prompt temperature jump before significant heat transfer to the coolant occurs, directly recording the prompt reactivity decrease that safely terminates the pulse.

Funded by the European Union

Funded by the European Union. Views and opinions expressed are however those of the author(s) only and do not necessarily reflect those of the European Union or the European Atomic Energy Community ('EC-Euratom'). Neither the European Union nor the granting authority can be held responsible for them.

3. BME Training Reactor

The measurements described and presented in this section were carried out between 2019 and 2023. The experimental descriptions were documented in (Ványi, 2023) and (Ványi et al., 2021),(Ványi, Hursin, Aszódi, et al., 2023),(Ványi, Hursin, & Czifrus, 2023) journal publications, where further details can be found. Subsection 3.1 presents a brief overview of the BME reactor, Subsection 3.2 discusses the power calibration, while Subsection 3.3 describes the different experiments that were carried out in the facility (reactivity worth measurements in Subsection 3.3.1, axial reaction rate profile measurements in Subsection 3.3.2, vessel temperature measurements in Subsection 3.3.3, different transients with temperature feedback in Subsection 3.3.4).

3.1. Facility overview

The Training Reactor of BME (BME TR) is a light-water moderated and cooled pool-type research reactor. The reactor core is located at the bottom of a cylindrical vessel, which has a height of 6 m and a diameter of 1.4 m (see Figure 3-1). The vessel is surrounded by a 200 cm thick concrete shielding. Between the vessel and the shielding, there is a thin gap filled with air. For safety reasons, on the top of the tank continuous air extraction is installed.

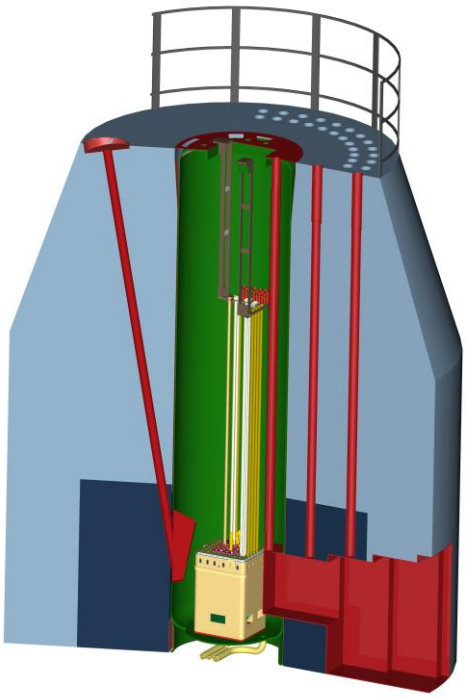

Figure 3-1: Reactor core, reactor vessel and concrete shielding

The moderator and coolant of the reactor is demineralised water. The primary circuit inlet nozzle is located at the bottom of the vessel and opens into a diffuser unit. The diffuser leads the coolant directly to the fuel assemblies, while the whole unit is housed in an aluminium box, which has windows on all lateral sides, allowing the coolant to recirculate from the vessel (see Figure 3-2). The primary circuit outlet nozzle is located 110 cm above the core (see Figure 3-3), while a spillway is installed at the top of the vessel.

Funded by the European Union

Funded by the European Union. Views and opinions expressed are however those of the author(s) only and do not necessarily reflect those of the European Union or the European Atomic Energy Community ('EC-Euratom'). Neither the European Union nor the granting authority can be held responsible for them.

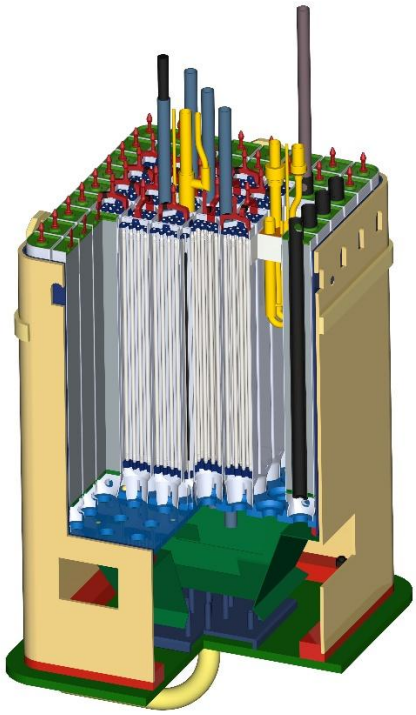

Figure 3-2: Overview of the reactor core

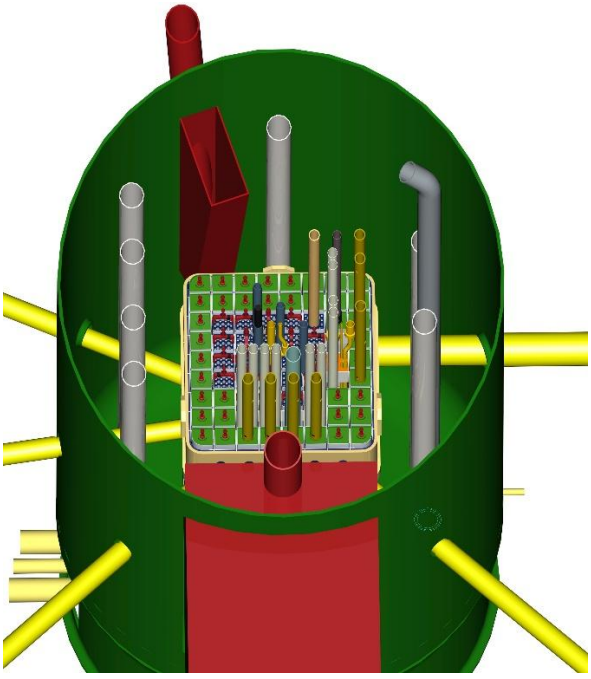

Figure 3-3: Overview of the reactor core, the detector tubes and the outlet nozzle

The reactor core consists of twenty-four elements of regular (i.e. containing sixteen fuel pins in a regular rectangular lattice) and modified (i.e. either the number of pins is reduced or the lattice is irregular) type EK-10 fuel assemblies, which nominally contain 10% enriched uranium dioxide in metal magnesium matrix. The fuel assemblies are surrounded by forty-one elements of solid graphite reflector blocks. All structural components inside the tank (such as fuel rod and assembly cladding, control rod guide tubes, etc.) are made of an alloy containing more than 99.5% aluminium.

Funded by the European Union

Funded by the European Union. Views and opinions expressed are however those of the author(s) only and do not necessarily reflect those of the European Union or the European Atomic Energy Community ('EC-Euratom'). Neither the European Union nor the granting authority can be held responsible for them.

The reactor accommodates three vertical dry and twenty vertical wet irradiation channels, five horizontal beam tubes, a large irradiation tunnel and a pneumatic rabbit sample-delivery system with three branches. The start-up of the reactor is assisted by a conventional plutonium-beryllium neutron source. The monitoring instrumentation of the reactor core is located in seven protecting tubes around the core, in the vessel.

The criticality control of BME TR is ensured by two safety and two control rods (see positions and notations in Figure 3-4):

- Safety rod 1 (abbreviation: SR1) is located between the fuel assemblies E6 and F5, containing boron carbide pellets;
- Safety rod 2 (abbreviation: SR2) is located between the fuel assemblies D5 and E4, containing boron carbide pellets;
- Manual control rod (abbreviation: MAN) is located between the fuel assemblies C6 and D5 containing boron carbide, controlled manually;
- Automatic control rod (abbreviation: AUT) is located between the fuel assemblies C4 and D3; it consists of a stainless-steel tube covered by a thin layer of cadmium. This rod can be operated both manually and in automatic mode by the control unit.

The rod positions are given in millimetres: z = 0 mm corresponds to the fully inserted state, while z = 600 mm to the completely withdrawn state.

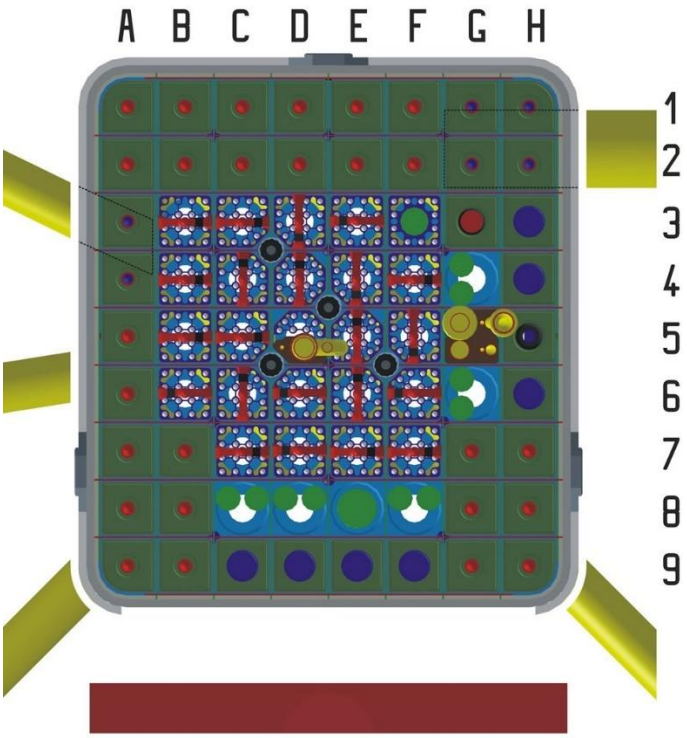

Figure 3-4: Horizontal cross-section of the reactor core

The reactor can be operated in two modes. In manual mode, the operator assumes full control of the absorber rods, while in automatic mode the central control unit keeps the reactor critical by continuously adjusting the automatic control rod level to the critical position.

Funded by the European Union

Funded by the European Union. Views and opinions expressed are however those of the author(s) only and do not necessarily reflect those of the European Union or the European Atomic Energy Community ('EC-Euratom'). Neither the European Union nor the granting authority can be held responsible for them.

According to the operational limits and conditions of the facility, the temperature of the coolant in the primary circuit must be remain between 20 °C and 60 °C during operation. By turning on the primary circuit pump, forced flow can be induced. The moderator can be cooled by the secondary loop or heated by an electrical heater.

The reactor has not been completely refuelled since its initial commissioning. In 1977, the F3 assembly was switched to an identical, fresh fuel unit, while in 1980 an additional regular assembly was inserted to the B6 position of the core. Based on the operation logs, the released thermal energy is approximately 18.8 MWdays, which corresponds to an average burnup of 0.7 MWd/kgU for the fuel.

The original structural drawings of BME TR were collected from (Kovács, 2011), sorted and were finally realised in a modern CAD software. The work was made difficult by the great number of reactor parts and the sometimes-contradictory archives. Nevertheless, the resulting posters (such as Figure 3-1 to Figure 3-4), the digital two-dimensional structural drawings (see (Kovács, 2011) or (Ványi, 2023)) and the three-dimensional model offered valuable information for demonstration and further modelling purposes.

Parameters that were not discussed above are presented in (Ványi, 2023) along with the official drawings of the control rods and some of the fuel assemblies. More structural drawings can be found in (Kovács, 2011), while more detailed and comprehensive descriptions can be found in the (Klujber & Horváth, 2021) benchmark description.

3.2. Reactor power calibration

The last power calibration of BME TR took place in 1970 according to the methodology cited and described in Subsection 3.3.5 of (Ványi, 2023). Recently, the need for a new, more precise power calibration arose to better assess and compare high-fidelity simulation and high-resolution measurement results.

The new power calibration of BME TR is based on foil activation measurements and corresponding Serpent Monte Carlo simulations. Furthermore, a calorimetry-based estimation was performed as well to support the calibration results. The detailed description of the calibration procedures is presented in Appendix B of (Ványi, 2023).

In the case of the activation-based calibration, the measured, then evaluated neutron flux values were plotted against the corresponding calculated values and a linear fit was performed with fixed zero y-wise offset using the method of least squares regression. The fitting uncertainty was determined by Monte Carlo error propagation. The fitted parameter (i.e. the measured to calculated flux ratio) was found to be 1.44 ± 0.03, which means that according to this calibration, the current 100 kW nominal reactor power corresponds to 144 ± 5 kW power.

In the case of the calorimetry-based estimation. the calibration procedure was carried out for three separate measurements yielding a final 1.43 ± 0.08 measured-to-nominal power ratio considering additional sensitivity analysis.

In conclusion, the relationship between the reactor power and the displayed nominal power can be expressed as shown in Equation (2).

$$P_{reactor} = 1.44 \cdot P_{nominal} \tag{2}$$

where the uncertainty of the coefficient is 0.03.

Funded by the European Union

Funded by the European Union. Views and opinions expressed are however those of the author(s) only and do not necessarily reflect those of the European Union or the European Atomic Energy Community ('EC-Euratom'). Neither the European Union nor the granting authority can be held responsible for them.

3.3. Experiments

3.3.1. Reactivity worth measurements

The measurements described below were carried out on different periods between 2019 and 2021. Due to the COVID-19 pandemic in this period, the change in the burnup of the fuel was negligible between the measurements.

The measurements of this subsection were carried out using the ex-core neutron detectors of the low power pulse mode detector chains I1 and I2 of BME TR. Both detectors are type CFUL08 fission chambers with an estimated dead time of 150 ns. The protecting tube of I1 is located about 140 mm from the graphite assemblies D1 and E1, while the tube of I2 is about 160 mm from graphite assembly A6. The exact axial positions of the detectors are not known. Each measured detector count time stamp was recorded and then converted into 10 Hz data.

3.3.1.1. Integral control rod reactivity worth measurements

The integral rod worth measurements for the two control rods were carried out by the rod drop method on three occasions in 2021.

The experiments were carried out at 20 °C moderator temperature, according to the following scheme corresponding to the measurement of the automatic control rod worth.

At the beginning of each measurement, the reactor power was set to 0.2 W z_{MAN} = 400 mm, z_{AUT} = 445 mm and operated in this state for 10 minutes so that the delayed-neutron precursor nuclei would reach their equilibrium concentration. Then the reactor was switched to manual mode, and the automatic rod was moved to 600 mm. As a result, the reactor power started to increase with a doubling time of about 40 s. At 1.5 W the operator dropped the automatic rod and waited a few minutes for the power to decrease.

The same methodology was applied for the measurement of the manual control rod with the initial critical state being z_{MAN} = 600 mm, z_{AUT} = 186 mm, the supercritical control rod state z_{MAN} = 600 mm, z_{AUT} = 300 mm and the corresponding doubling time 20 s.

The reactivity for the subcritical and the supercritical states as well as the associated uncertainties were calculated with an in-house script that is based on the method of inverse kinetics. The control rod reactivity worth values were obtained by appropriately subtracting the subcritical and supercritical reactivities. The evaluated results are presented in Table 3-1.

Table 3-1: Measured integral control rod reactivity worth measurements

Measured rod	Other rod position (mm)	Evaluated reactivity worth ($)
AUT	z_{MAN} = 400 mm	0.859 ± 0.004
MAN	z_{AUT} = 300 mm	1.893 ± 0.004

3.3.1.2. Differential control rod reactivity worth

The experiments were carried out at 20 °C moderator temperature on two occasions in 2021. The measurements were performed according to the following procedure:

In the case of the measurement of the automatic rod, the reactor power was set to 0.5 W power critical state with the manual rod being at 400 mm position. The reactor was operated in automatic mode in this state for 10 minutes so that the delayed-neutron precursor nuclei would reach their equilibrium concentration. Then the reactor was switched to manual mode, and the automatic rod was fully withdrawn at a constant speed of 5 mm/s. The reactor was operated in this supercritical state until the power increased to 2 W. At that point,

Funded by the European Union

Funded by the European Union. Views and opinions expressed are however those of the author(s) only and do not necessarily reflect those of the European Union or the European Atomic Energy Community ('EC-Euratom'). Neither the European Union nor the granting authority can be held responsible for them.

the automatic control rod was fully inserted, and withdrawn at a constant speed, until the power of 2 W was reached again.

This scheme was repeated 6 times. In the case of the manual control rod, the procedure was the same with the automatic rod being fixed at 300 mm.

The measurements were evaluated with an in-house inverse kinetics solver script. The control rod S-curves were determined by averaging each measured period. The associated uncertainties were determined by the deviation of the single curves from the average. The obtained automatic and manual differential control rod reactivity worth results are presented in Figure 3-5 and Figure 3-6 respectively.

The axial positional offsets of the control rods relative to the core centre were determined by identifying the position of the maximum in the numerical derivative of the S-curves. The resulting offsets were -1.9 ± 0.5 cm and -3.6 ± 0.5 cm for the automatic and manual control rods, respectively.

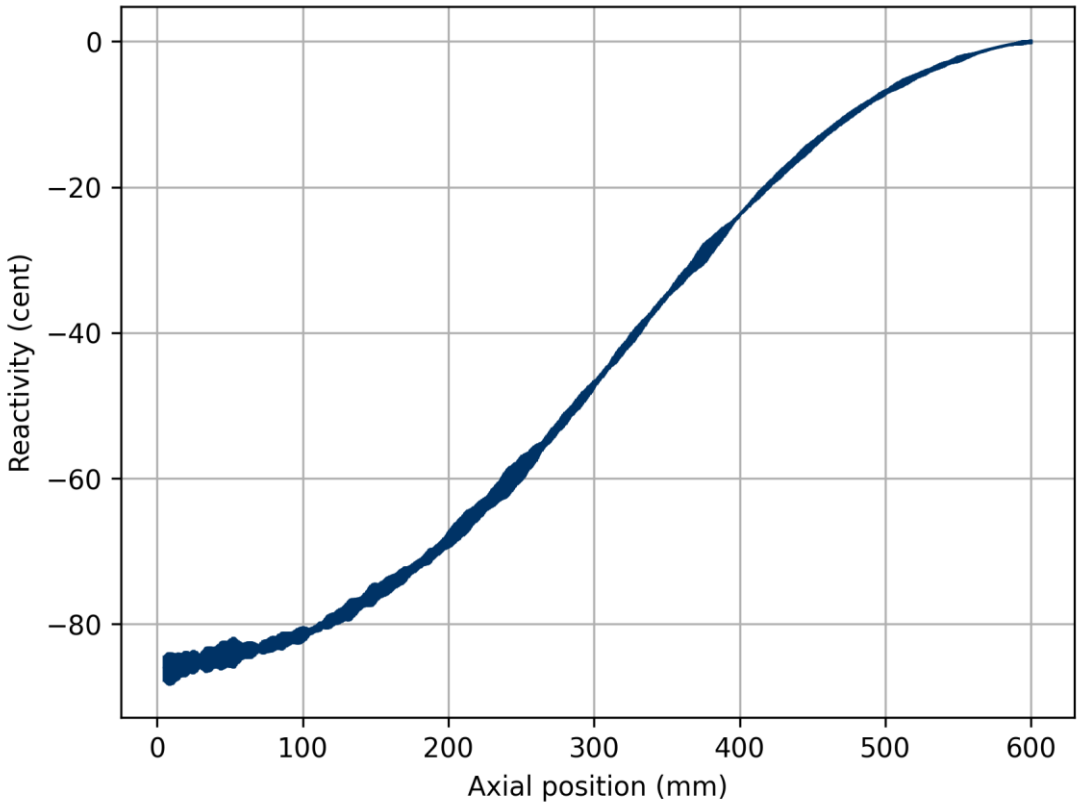

Figure 3-5: Measured differential reactivity worth of the automatic control

Funded by the European Union

Funded by the European Union. Views and opinions expressed are however those of the author(s) only and do not necessarily reflect those of the European Union or the European Atomic Energy Community ('EC-Euratom'). Neither the European Union nor the granting authority can be held responsible for them.

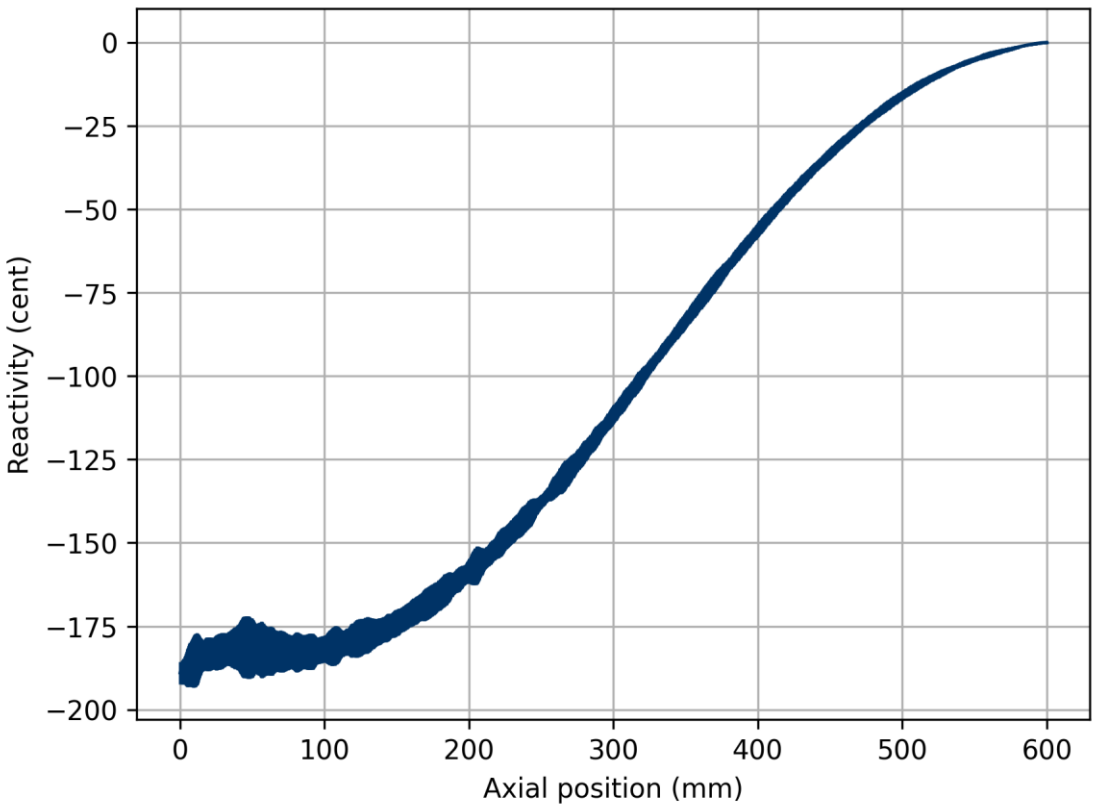

Figure 3-6: Measured differential reactivity worth of the manual control

3.3.1.3. Fuel and graphite assembly reactivity worth

Assembly worth measurements were performed for the fuel assemblies B3, C3, E3; and for the graphite reflector blocks A2, A3, A6, B1, B2, B7, C1, D1, E1 in 2021. The applied methodology is similar to that used for the control rod worth measurements. At the beginning of each measurement, the reactor power was set to 5 W power critical state (in such low power reactor states these should be referred to as quasi-critical states), and the MAN rod position was fixed at 400 mm. The reactor was operated in this state for 10 minutes so that the delayed-neutron precursor nuclei would reach their equilibrium concentration. Following the waiting time, the measured assembly was carefully removed from the core (the operation took 2-3 seconds), therefore, the power decreased exponentially. The counts were registered by the aforementioned type CFUL08 neutron detector. The reactivity values for the subcritical and the supercritical states, along with their associated uncertainties were evaluated by the in-house script based on the method of inverse kinetics. The assembly reactivity worth values were obtained by appropriately subtracting the evaluated reactivities of the subcritical and supercritical states. Uncertainties were determined with Monte Carlo error propagation taking into account the uncertainties of the delayed neutron parameters, the detector counts and the detector dead time. The evaluated values are presented in Table 3-2.

Table 3-2: Measured fuel assembly and graphite reflector block reactivity worth values

Assembly position	Assembly type	Measured reactivity worth (¢)
B3	Fuel	146.1 ± 1.6
C3	Fuel	265.9 ± 3.2
E3	Fuel	241.3 ± 2.8

Funded by the European Union

Funded by the European Union. Views and opinions expressed are however those of the author(s) only and do not necessarily reflect those of the European Union or the European Atomic Energy Community ('EC-Euratom'). Neither the European Union nor the granting authority can be held responsible for them.

A2	Graphite reflector	10.5 ± 0.1
A3	Graphite reflector	17.1 ± 0.2
A6	Graphite reflector	24.8 ± 0.3
B1	Graphite reflector	8.1 ± 0.1
B2	Graphite reflector	30.7 ± 0.3
B7	Graphite reflector	39.9 ± 0.4
C1	Graphite reflector	13.2 ± 0.1
D1	Graphite reflector	16.0 ± 0.2
E1	Graphite reflector	12.7 ± 0.1

3.3.1.4. Critical control rod positions

The critical control rod positions were measured on two occasions in 2021. The temperature in the reactor was 20 °C.

The measurements were carried out according to the following. The reactor power was set to 5 W power, the reactor was switched to automatic mode, and the manual control rod was fully withdrawn to z_{MAN} = 600 mm. The reactor was operated in this state for 10 minutes so that the delayed-neutron precursor nuclei would reach their equilibrium concentration. During this time, generally, the automatic rod position was changed within a 5 mm interval by the central control unit, keeping the reactor critical. Following the 10 minutes waiting time, the automatic rod position was noted along with an associated interval of uncertainty. Then the manual control rod was moved to 580 mm and further down to 380 mm and the procedure described above was repeated each time. The measurement series were averaged, and uncertainties were associated based on the experienced movements of the automatic control rod. Also, these uncertainty values were translated into reactivity by making use of the measured differential control rod reactivity worth presented in Subsection 3.3.1.2. The evaluated critical control rod positions are presented in Table 3-3.

Table 3-3: Measured critical control rod positions.

z_{MAN} (mm)	z_{AUT} (mm)	Δρ (¢)
380	528 ± 4	0.3
400	445 ± 4	0.7
420	395 ± 2	0.4
440	355 ± 2	0.4
460	322 ± 2	0.5
480	292 ± 2	0.5
500	266 ± 2	0.5
520	242 ± 2	0.4
540	223 ± 2	0.4

Funded by the European Union

Funded by the European Union. Views and opinions expressed are however those of the author(s) only and do not necessarily reflect those of the European Union or the European Atomic Energy Community ('EC-Euratom'). Neither the European Union nor the granting authority can be held responsible for them.

560	207 ± 2	0.4
580	195 ± 2	0.3
600	186 ± 2	0.3

3.3.2. Axial reaction rate measurements

In 2020, relative axial reaction rate measurements (please see section 2.1) were carried out with the activation method using Dy(5%)-Al alloy wires. In total, 14 measurements were carried out in 10 different positions.

3.3.2.1. Introduction

From the point of view of the activation, only the radiative capture reaction of Dy-164 is relevant. The cross-section of this reaction is approximately 1/v for thermal energies and decreases quickly for neutron energies larger than 1 eV. Although several resonances can be found between 10^2 eV and 10^4 eV, over 99% of the activation in a thermal reactor is caused by neutrons with energies below the cadmium cut-off (about 0.5 eV). The reaction chain of Dy-164 is the following:

$$^{164}\mathrm{Dy} \xrightarrow{n,\gamma} {}^{165m}\mathrm{Dy} \xrightarrow{\gamma(1.3\ \mathrm{min})} {}^{165}\mathrm{Dy} \xrightarrow{\beta^-(2.35\ \mathrm{h})} {}^{165}\mathrm{Ho}\,.$$

Therefore, the registered β counts of the wire segments are proportional to the thermal neutron flux they were exposed to.

3.3.2.2. Equipment

In order to perform the irradiation, the wire was put into a thin plexiglass tube, which was then inserted into the specified fuel sub-channel or vertical irradiation channel. After starting the reactor, the power was increased to 1 kW, which was maintained for 6 minutes. Following the irradiation, the Dy wire was first cooled for 30 minutes, then it was removed from the plexiglass tube, and was fixed to a metal rail, which was inserted in the measuring equipment. The measuring equipment consisted of a sample holder rail, movable by a stepper motor, and a stationary scintillation β-detector equipped with a collimator with a window of 5 mm width. A computer program was used to control the movement of the rail under the detector. For the measurements described in this chapter, the rail was moved in steps of 5 mm length, and the measurement time was set to 10 s. After the measurement, decay correction was performed on the registered data set.

3.3.2.3. Evaluation

The number of detected counts can be expressed as shown in Equation (3).

$$\varphi(\boldsymbol{r}, t_w) = \int_{t_w}^{t_w+t_m} \eta\, A(\boldsymbol{r}, t_w) e^{-\lambda t'} dt' = \tag{3}$$

$$= \frac{\eta A(\boldsymbol{r}, t_w)(1 - e^{-\lambda t_m}) e^{-\lambda t_w}}{\lambda} =$$

$$\phi_{th}(\boldsymbol{r}) \left\{ \frac{G\overline{\sigma_d} N_d \left(1 - e^{-\lambda t_a}\right)}{\lambda} \right\} e^{-\lambda t_w} \left(1 - e^{-\lambda t_m}\right)$$

where φ is the number of registered counts, η is the detector efficiency, A the sample activity, λ the decay constant of Dy-165, Φ_{th} the thermal neutron flux, G the self-shielding factor. $\overline{\sigma_d}$ the average thermal cross-section, N_d the number of Dy-164 nuclei, t_w the time interval between a fixed time (e.g. shutdown of the reactor or beginning of the measurement of the first segment) and the beginning of the measurement of the given segment, t_a the activation and t_m the measurement times.

Funded by the European Union

Funded by the European Union. Views and opinions expressed are however those of the author(s) only and do not necessarily reflect those of the European Union or the European Atomic Energy Community ('EC-Euratom'). Neither the European Union nor the granting authority can be held responsible for them.

As the geometry, activation time and measurement time are the same for each segment of the wire, by dividing each registered count by the corresponding $e^{-\lambda t_w}$ values one may obtain a quantity proportional to the reaction rate and the thermal neutron flux as well.

3.3.2.4. Irradiations

All the irradiations were performed at 1 kW nominal reactor power and lasted about 6 to 7 minutes. The main characteristics of the performed irradiations are summarised in (Ványi et al., 2021). In the case of the position notation, the first letter and number are the assembly identifiers, while the second number depicts the sub-channel number. The sub-channel numbering starts from the corner closest to the A1 position and continues from left to right, from top to bottom (see Figure 3-4). With the exception of irradiation RP-#2, each irradiated wire was measured twice in the measuring equipment.

Table 3-4: Main characteristics of the performed axial reaction rate measurements.

Measurement ID	Control rod positions		Measurement position
	z_{AUT} (mm)	z_{MAN} (mm)	
RP-#1	360	440	E6/1
RP-#2	340	450	B6/7
RP-#3	340	450	B4/1
RP-#4	339	450	B3/1
RP-#5	340	450	B3/8
RP-#6	540	380	C6/9
RP-#7	323	460	F3
RP-#8	342	450	E3/9
RP-#9	195	600	C6/9
RP-#10	341	450	C6/9
RP-#11	325	460	E7/1
RP-#12	351	445	D6/9
RP-#13	195	600	D6/9
RP-#14	543	380	D6/9

3.3.2.5. Results and discussion

The raw detector count rates were corrected for radioactive decay and subsequently normalized. Except for RP-#2, the two independent measurement series were averaged; for simplicity, the maximum value of each resulting axial distribution was then normalized to unity.

The evaluated relative axial reaction rate profiles are shown in Figure 3-7 to Figure 3-13. The axial positions correspond to the geometry of the measurement rail. In each case, the steep gradient of the distribution indicates the direction toward the bottom of the reactor core. As can be observed, in several measurements the orientation of the activation wire was inadvertently reversed during installation. The bottom ends of the measured curves drop to zero due to the termination of the Dy-wire. Due to this effect and the uncertainty of

Funded by the European Union

Funded by the European Union. Views and opinions expressed are however those of the author(s) only and do not necessarily reflect those of the European Union or the European Atomic Energy Community ('EC-Euratom'). Neither the European Union nor the granting authority can be held responsible for them.

the measurement–calculation fitting (see (Ványi et al., 2021)), the axial positioning uncertainty of the measured points is estimated of about 3 mm. The uncertainty of the detected counts (due to Poisson statistics, positioning, collimator geometry etc.) is estimated to be about 0.03 in relative units.

The measured reaction rate profiles showed good agreement with the initial Serpent Monte Carlo simulations. However, the measured and calculated reflector hump heights differ in some cases, a difference which can probably be attributed to unknown local geometric irregularities or material inhomogeneities (for more details, see (Ványi et al., 2021)).

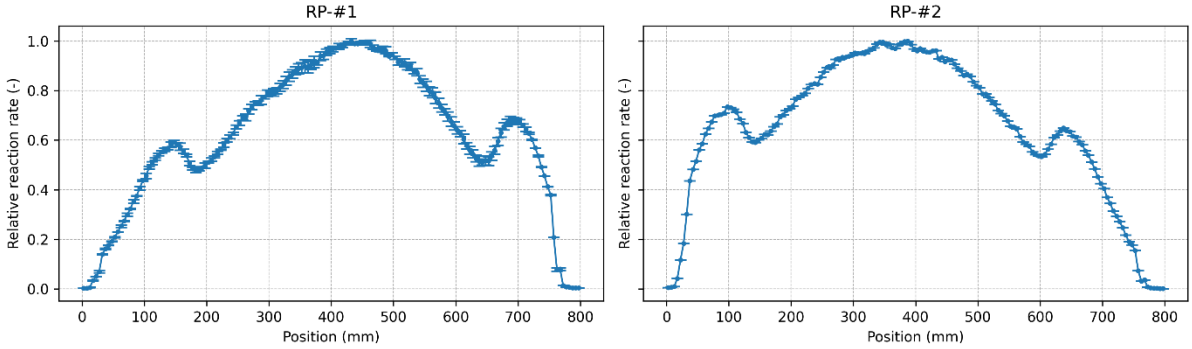

Figure 3-7: Evaluated relative reaction rate measurements RP-#1 and RP-#2

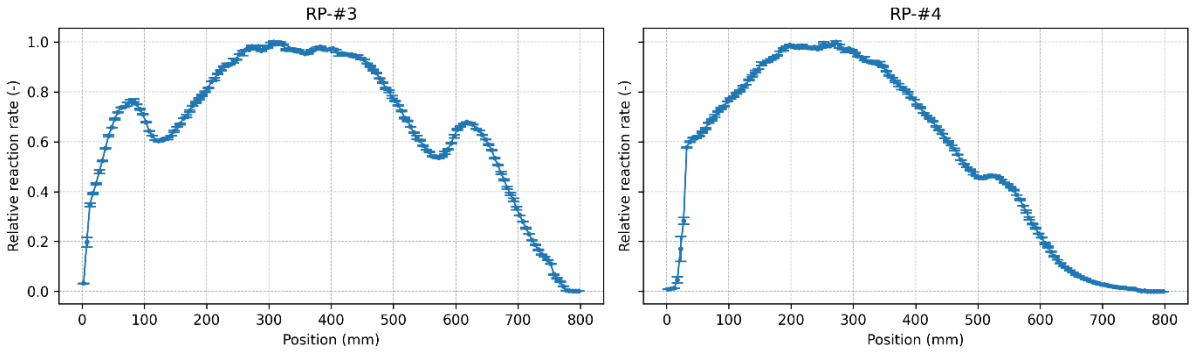

Figure 3-8: Evaluated relative reaction rate measurements RP-#3 and RP-#4

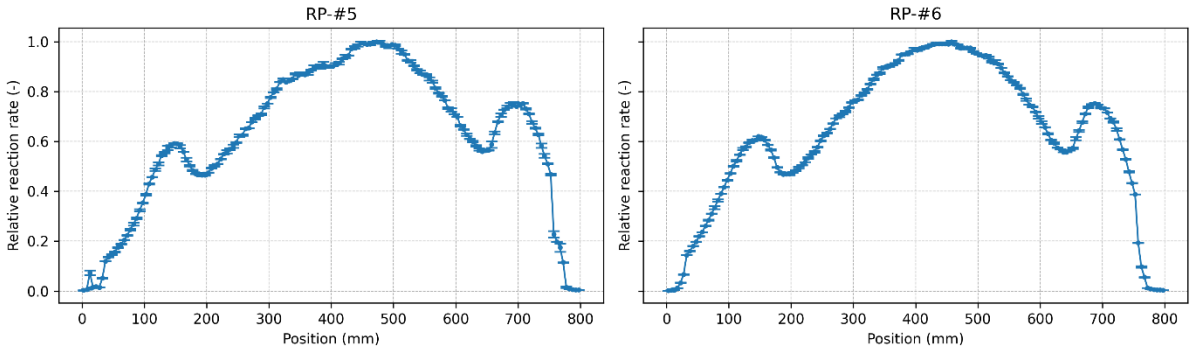

Figure 3-9: Evaluated relative reaction rate measurements RP-#5 and RP-#6

Funded by the European Union

Funded by the European Union. Views and opinions expressed are however those of the author(s) only and do not necessarily reflect those of the European Union or the European Atomic Energy Community ('EC-Euratom'). Neither the European Union nor the granting authority can be held responsible for them.

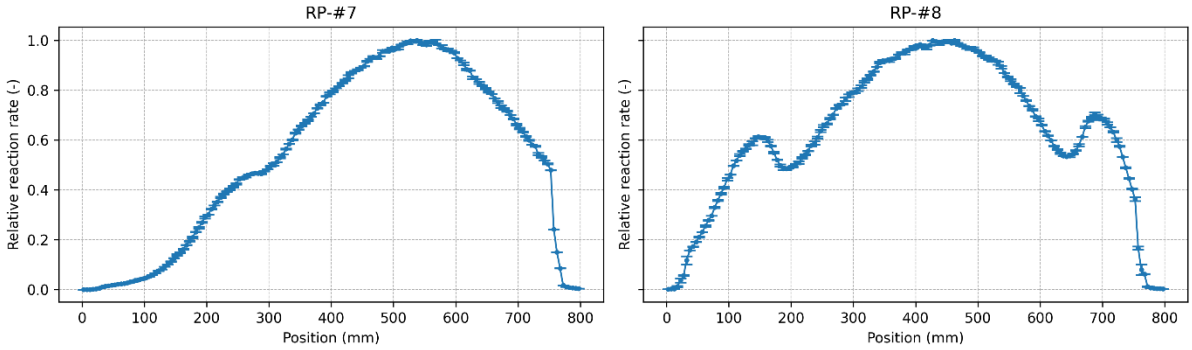

Figure 3-10: Evaluated relative reaction rate measurements RP-#7 and RP-#8

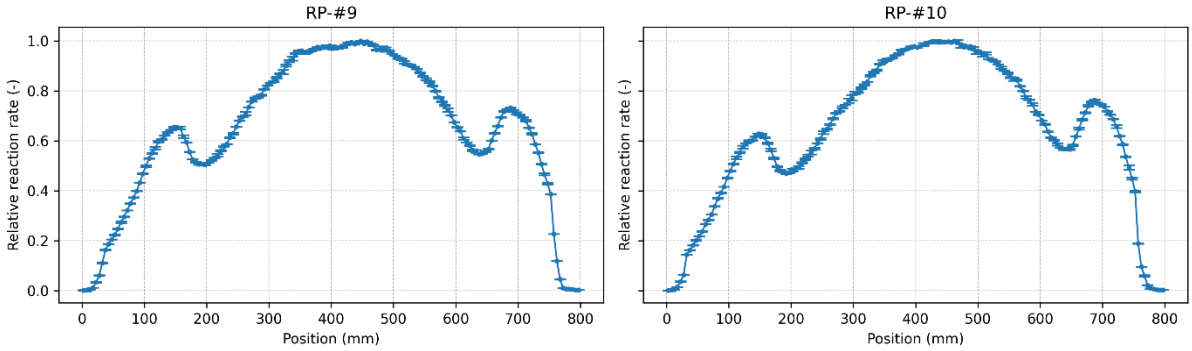

Figure 3-11: Evaluated relative reaction rate measurements RP-#9 and RP-#10

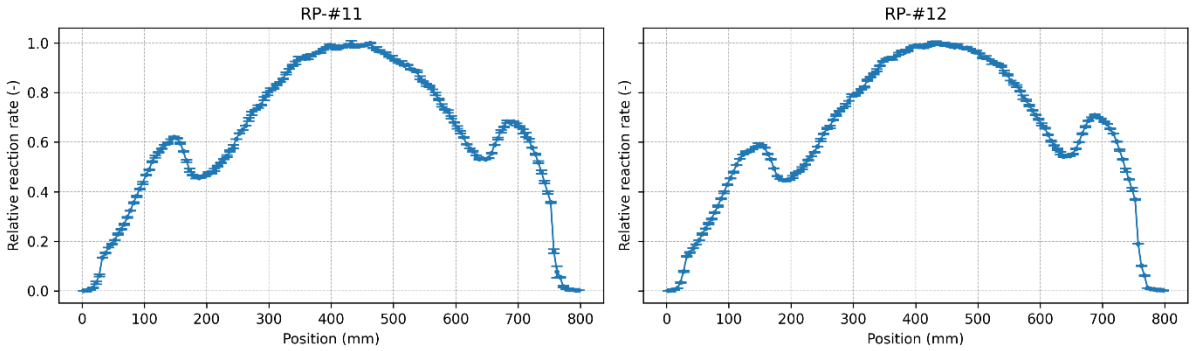

Figure 3-12: Evaluated relative reaction rate measurements RP-#11 and RP-#12

Funded by the European Union

Funded by the European Union. Views and opinions expressed are however those of the author(s) only and do not necessarily reflect those of the European Union or the European Atomic Energy Community ('EC-Euratom'). Neither the European Union nor the granting authority can be held responsible for them.

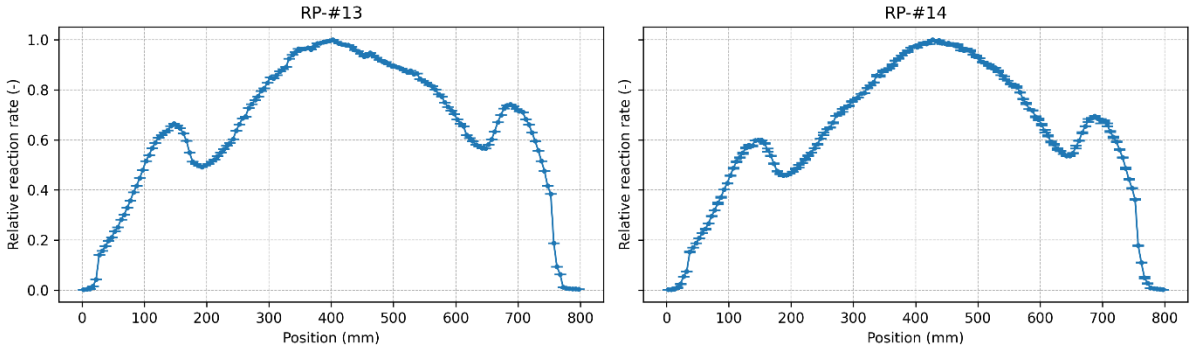

Figure 3-13: Evaluated relative reaction rate measurements RP-#13 and RP-#14

3.3.3. Vessel thermal hydraulics measurements

Comprehensive temperature measurements were carried out in the vessel of BME TR to characterize the flow conditions and the temperature field across various reactor transients. Over a two-week experimental campaign in May 2021, six long transients (≥1 hour) and eleven shorter transients (typically 20–30 minutes) were performed.

3.3.3.1. Temperature sensors

In total, thirteen thermocouples were utilised as instrumentation for the measurements. Twelve of these were of type K, class 1 precision, with exposed hot junction and kapton insulation along their 7-meter-long wire. One thermocouple was type J "legacy" sensor of class 1 precision and with an ungrounded hot junction (the adjective "legacy" refers to the circumstance that the equipment was inherited from earlier thermal measurements). For each measurement, the thermocouples were connected to a National Instrument NI-9213 card. The data card has sixteen thermocouple channels. The accuracy of the cold-junction compensation is typically 0.8 °C, but maximum 1.7 °C according to the hardware specification. In the NI LabVIEW 2020 software (version 20.0f1) a graphical interface was created to display a graph of the thermocouple signals and calculate mean temperature values along with the corresponding standard deviations for each connected sensor separately.

3.3.3.2. Equipment

The calibrated thermocouples were positioned on two long hollow aluminium rods. The first (central) rod was 5500 mm long, with an outer diameter of 25 mm and a wall thickness of 1.5 mm. The wall of the pipe was perforated so that the water could enter in order to ensure appropriate radiation protection. To the lower end of the rod a 115 mm long, 18 mm wide, 10 mm thick aluminium slab was screwed symmetrically, which had two 10 mm diameter holes at the opposite sides, for assembly positioning on two diagonal fuel assembly tips, and a 5 mm diameter hole approximately at a quarter point. This hole fixes the 70 mm long hollow needle, holding a thermocouple in position just above the level of the fuel rods. A type K thermocouple was positioned at the end of this needle in such a way that when the equipment was fixed on the assembly tips, the sensor was just above a sub-channel (see Figure 3-14). Five further type K thermocouples were fixed to the outer surface of the rod with aluminium wire 1000 mm, 1750 mm, 2500 mm, 3250 mm, 4000 mm above the core level (i.e. above the upper level of the graphite assemblies), with each sensor facing in the same direction and the junctions being about 10-15 mm from the rod surface. The rod was moved to different positions during the experiments.

Funded by the European Union

Funded by the European Union. Views and opinions expressed are however those of the author(s) only and do not necessarily reflect those of the European Union or the European Atomic Energy Community ('EC-Euratom'). Neither the European Union nor the granting authority can be held responsible for them.

Figure 3-14: The bottom part of the central thermocouple holder rod

The second (peripheral) rod was 7900 mm long and was assembled from shorter rods of different wall diameters and thicknesses. The equipment would be fixed in one single position next to the core (about 50 mm from the A4 graphite) for each measurement. Six type K thermocouples were positioned to the exterior so that the first sensor would be at the core level, while the rest of the five thermocouples would be 1000 mm, 1750 mm, 2500 mm, 3250 mm and 4000 mm above the core level (i.e. in the same elevations as those of the other rod) and facing in the same radially inward direction. An additional type J thermocouple was fixed 750 mm below the core level, facing approximately the middle of a recirculation window below the core. Figure 3-15 and Figure 3-16 show the experimental setup in the reactor vessel.

The upper ends of the sensor wires were connected to the NI-9213 card, which was applied to a computer that executed the LabVIEW measurement software and recorded the measured data to a hard drive.

Funded by the European Union

Funded by the European Union. Views and opinions expressed are however those of the author(s) only and do not necessarily reflect those of the European Union or the European Atomic Energy Community ('EC-Euratom'). Neither the European Union nor the granting authority can be held responsible for them.

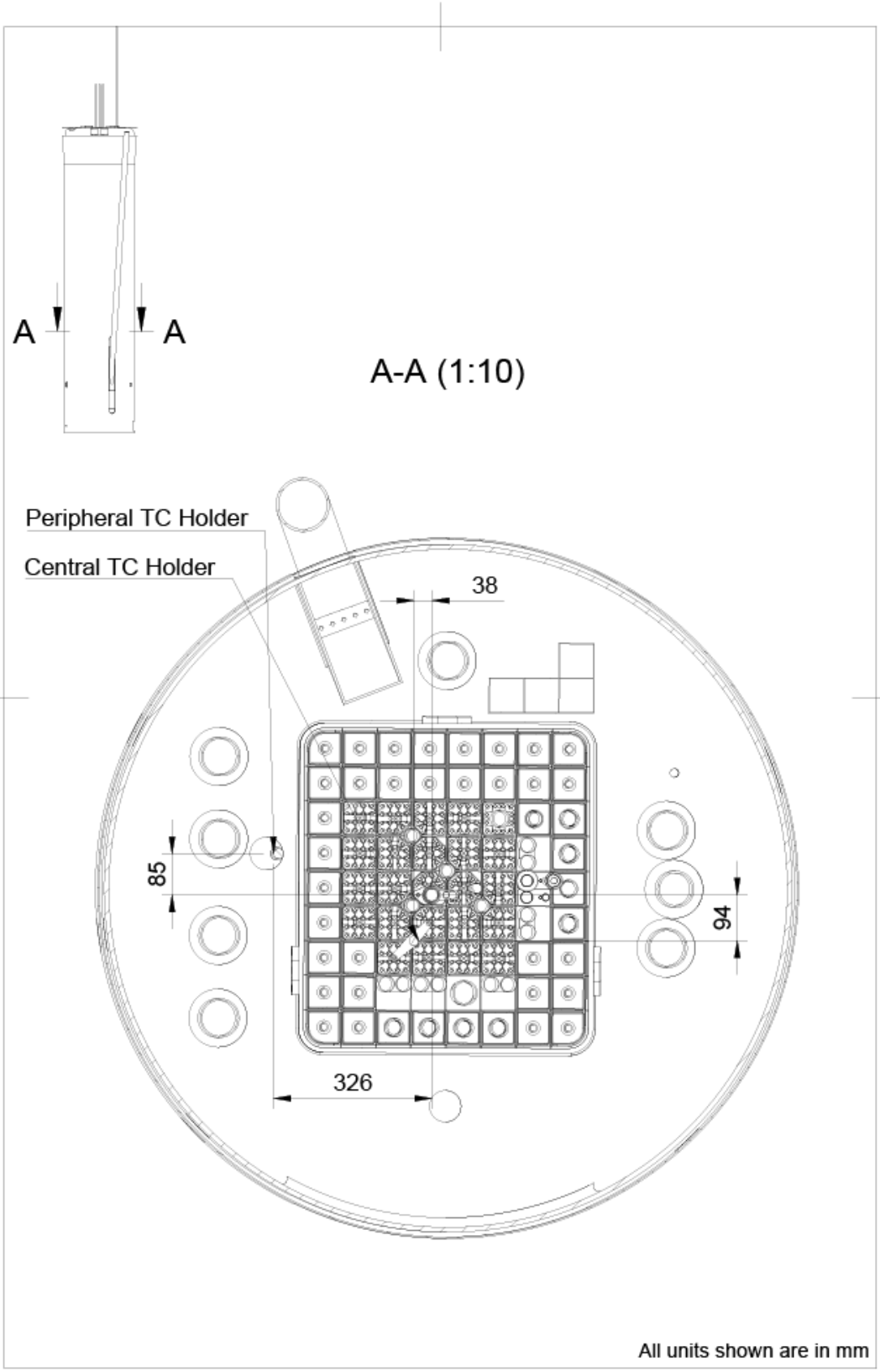

Figure 3-15: Experimental setup of the thermocouple holders (view from the top)

Funded by the European Union

Funded by the European Union. Views and opinions expressed are however those of the author(s) only and do not necessarily reflect those of the European Union or the European Atomic Energy Community ('EC-Euratom'). Neither the European Union nor the granting authority can be held responsible for them.

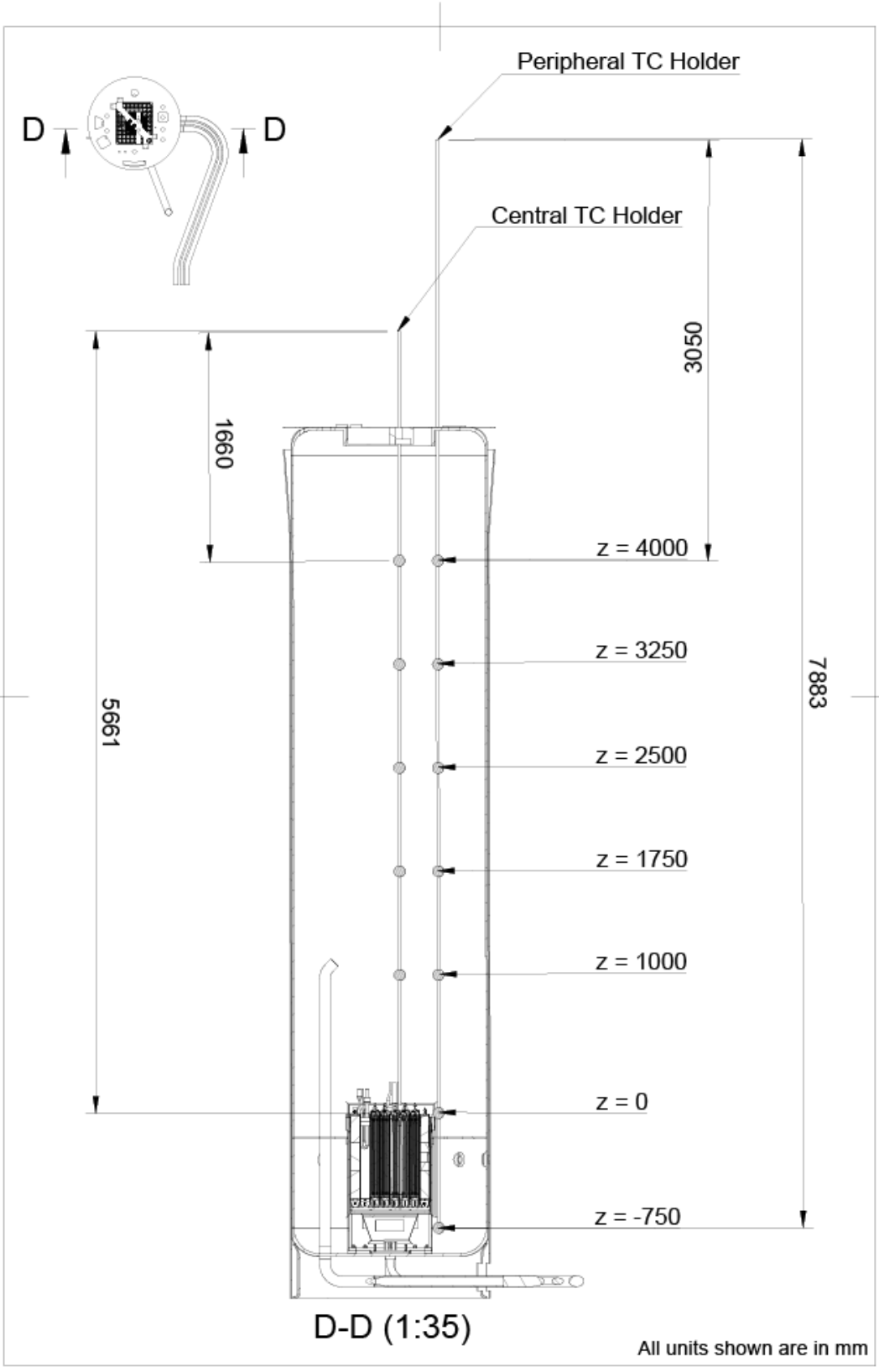

Figure 3-16: Experimental setup of the thermocouple holders (lateral view)

Funded by the European Union

Funded by the European Union. Views and opinions expressed are however those of the author(s) only and do not necessarily reflect those of the European Union or the European Atomic Energy Community ('EC-Euratom'). Neither the European Union nor the granting authority can be held responsible for them.

3.3.3.3. Transient description

Six longer and eleven shorter transients were performed using the equipment described in the previous subsections. Before each experiment, all the temperature measurements had to show the same values within at least 1.0 °C tolerance. Temperature disparities (i.e. vertical stratification) were minimised by either waiting or circulating water through the vessel by the primary circuit system. All of the experiments started and ended in 0 W power shutdown state of the reactor. The power of the reactor was logged every 30 seconds, while the NI-9213 card was set to a sampling rate of 75 Hz.

Table 3-5 summarises the relevant details of the transients. The "Needle position" column indicates the sub-channel that the needle of the shorter rod is facing (the first letter and number are the assembly identifiers, while the second number depicts the sub-channel number; the sub-channel numbering starts from the corner closest to the A1 position and continues from left to right, from top to bottom, see Figure 3-4). The position of the longer rod remained the same throughout the experiments. At "P_1-P_2-P_3" transient the reactor was started from 0 kW, operated 10 minutes at power level P_1, then 10 minutes at power level P_2 and finally 10 minutes at power level P_3. The values are expressed in kW, the power change times are not included in the irradiation time intervals (thus, a "P_1-P_2-P_3" type transient lasted more than 30 minutes).

The longer irradiations of different power levels were chosen to observe the main flow phenomena in the vessel and the evolution of the temperature field over time. The different short transients were executed in order to study the response of the system (through the temperature field) to sudden power changes.

Table 3-5: Summarizing table of the performed transients.

Transient ID	Needle position	Transient duration (min)	Description
TH-#1	E5/7	60	Constant 1 kW
TH-#2	E5/7	60	Constant 10 kW
TH-#3	E5/7	60	Constant 20 kW
TH-#4	E5/7	60	Constant 50 kW
TH-#5	F7/1	60	Constant 50 kW
TH-#6	E5/7	90	Constant 100 kW
TH-#7	B6/9	30	50-0-100 transient
TH-#8	D6/7	30	50-0-100 transient
TH-#9	D6/9	30	50-0-100 transient
TH-#10	D7/1	30	50-0-100 transient
TH-#11	D7/3	30	50-0-100 transient
TH-#12	E5/7	30	50-0-100 transient
TH-#13	E7/1	30	50-0-100 transient
TH-#14	F7/1	30	50-0-100 transient
TH-#15	E5/7	30	50-100-50 transient
TH-#16	E5/1	20	50-100 transient

Funded by the European Union

Funded by the European Union. Views and opinions expressed are however those of the author(s) only and do not necessarily reflect those of the European Union or the European Atomic Energy Community ('EC-Euratom'). Neither the European Union nor the granting authority can be held responsible for them.

TH-#17	E5/1	30	100-50-100 transient

The time to reach 10 kW from a shutdown state was typically 8–10 minutes, while to reach 100 kW it was 11–12 minutes. At the end of the transients, when the reactor was shut down by dropping the control and safety rods, the reactor power went below 1% of the previous power level within one minute. Figure 3-17 presents the logged power curves of Transients TH-#2, TH-#4 and TH-#6 (shifted to each other for better visibility).

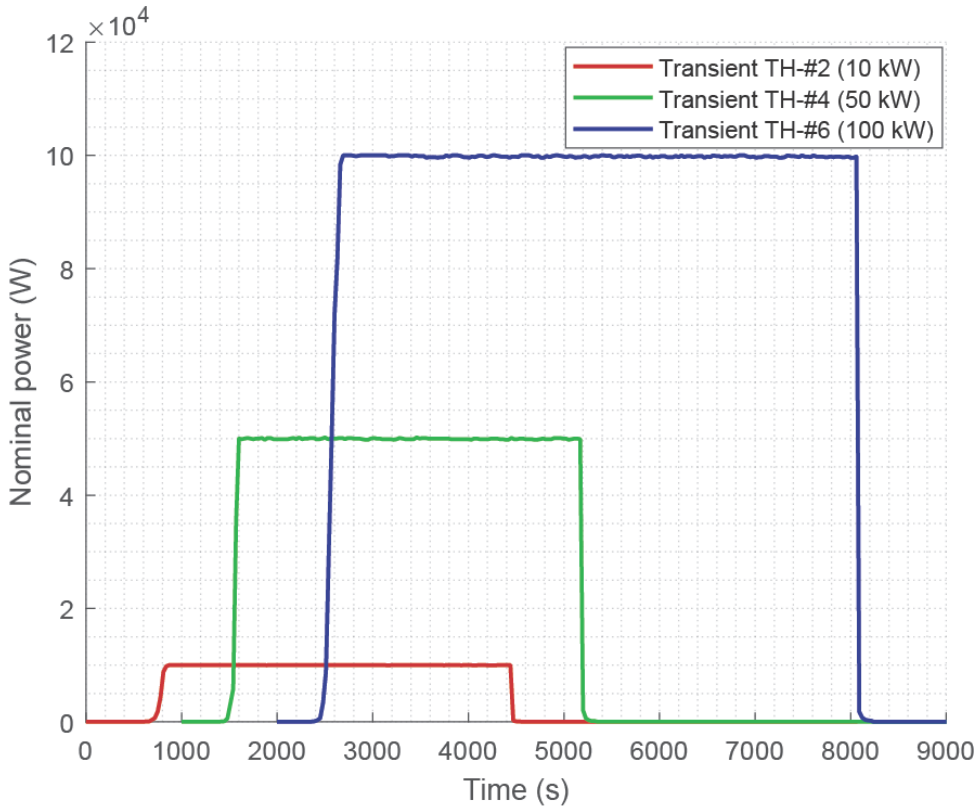

Figure 3-17: Logged power curves of transients TH-#2, TH-#4 and TH-#6

3.3.3.4. Results and discussion

The calibrated 75 Hz raw thermocouple data was collapsed into 1 Hz data by averaging over each 75 data point, but no other special treatment was applied.

In general, the measurement results were consistent with the preliminary expectations and the conventional, low-fidelity TRACE calculations (for more details see (Ványi, Hursin, Aszódi, et al., 2023)). The used type J thermocouple (peripheral, z = -750 mm) exhibited anomalous behaviour at the start of each measurement day, but subsequently stabilized and produced reliable readings.

Of the many findings, the following highlights are particularly noteworthy:

- Axial thermal stratification can be clearly observed in each measurement.
- While the reactor is at nominal power, the measured temperature is increasing with the altitude for the central sensors, while decreasing for the peripheral sensors.
- It takes considerable time before the recirculating warm water reaches the peripheral sensors at z = 0 mm and z = -750 mm. The recirculation time delay is clearly visible at the peripheral thermocouples of the long constant power transients (reactor power ≥ 10 kW).

Funded by the European Union

Funded by the European Union. Views and opinions expressed are however those of the author(s) only and do not necessarily reflect those of the European Union or the European Atomic Energy Community ('EC-Euratom'). Neither the European Union nor the granting authority can be held responsible for them.

- While at the top of the vessel, the mixing equalizes the water temperature. At lower elevations (e.g. 1750 mm. 3500 mm), there is considerable temperature difference between the sensors of the same altitude.
- Certain central thermocouples provide adequate data for velocity estimation using correlation techniques (see (Por et al., 2003) for technical details). Temperature disparities quickly disappear before and after the transient, enabling power estimation through calorimetric methods.

The measurement curves are shown below in sequential order from Figure 3-18 to Figure 3-34.

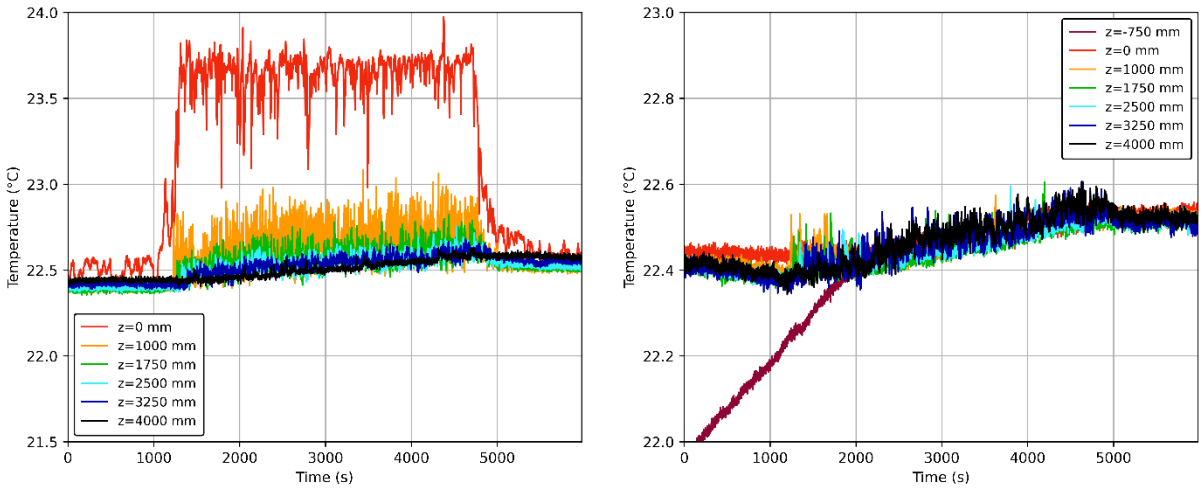

(a) Central thermocouples (b) Peripheral thermocouples

Figure 3-18: Measured temperatures during the TH-#1 transient (constant 1 kW, 60 minutes)

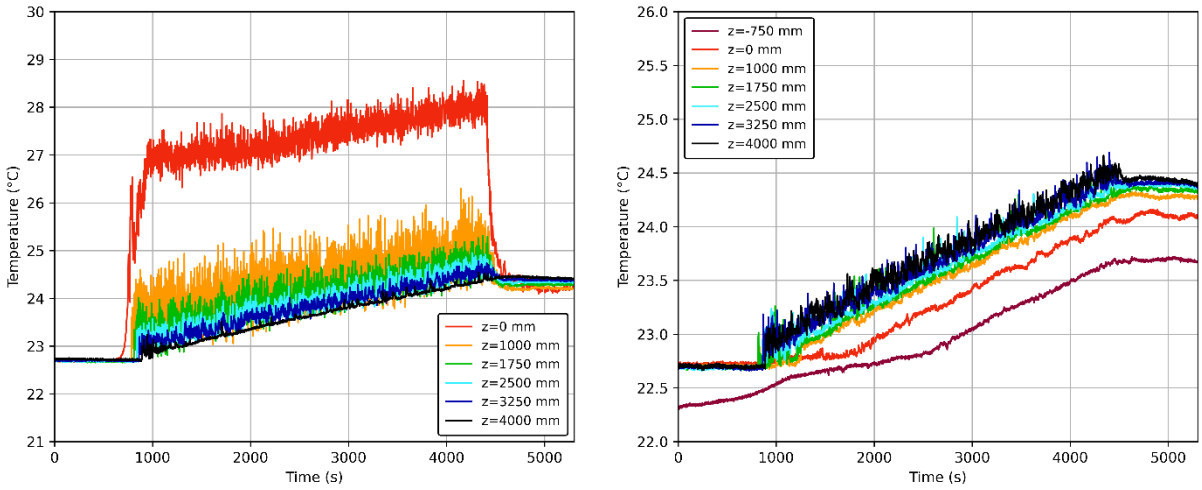

(a) Central thermocouples (b) Peripheral thermocouples

Figure 3-19: Measured temperatures during the TH-#2 transient (constant 10 kW, 60 minutes)

Funded by the European Union

Funded by the European Union. Views and opinions expressed are however those of the author(s) only and do not necessarily reflect those of the European Union or the European Atomic Energy Community ('EC-Euratom'). Neither the European Union nor the granting authority can be held responsible for them.

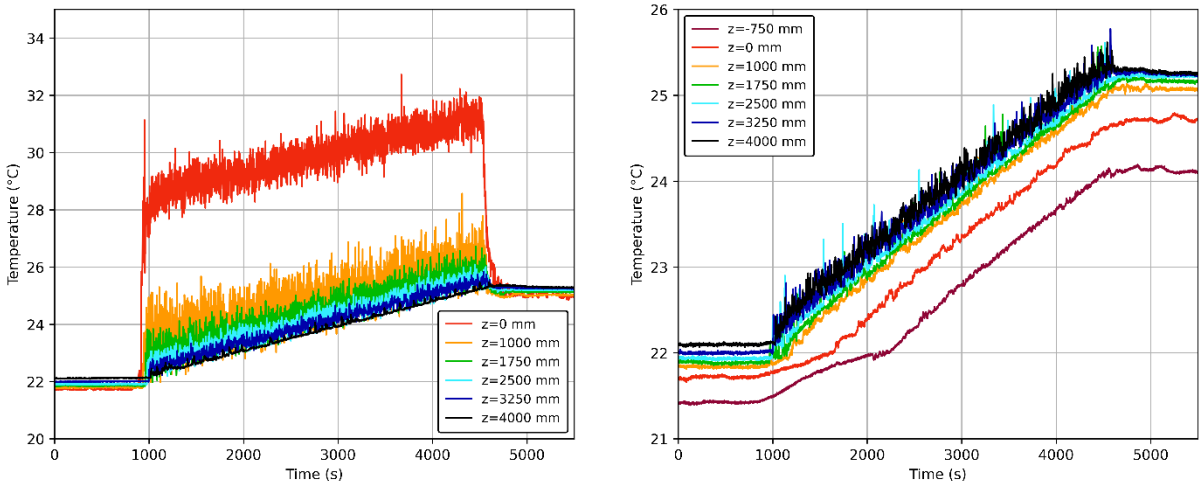

(a) Central thermocouples (b) Peripheral thermocouples

Figure 3-20: Measured temperatures during the TH-#3 transient (constant 20 kW, 60 minutes)

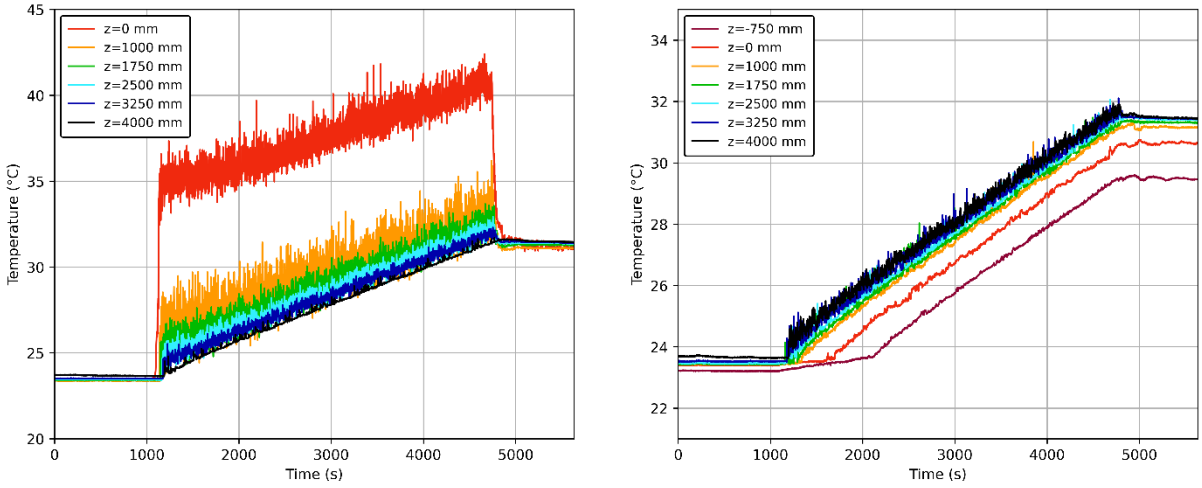

(a) Central thermocouples (b) Peripheral thermocouples

Figure 3-21: Measured temperatures during the TH-#4 transient (constant 50 kW, 60 minutes)

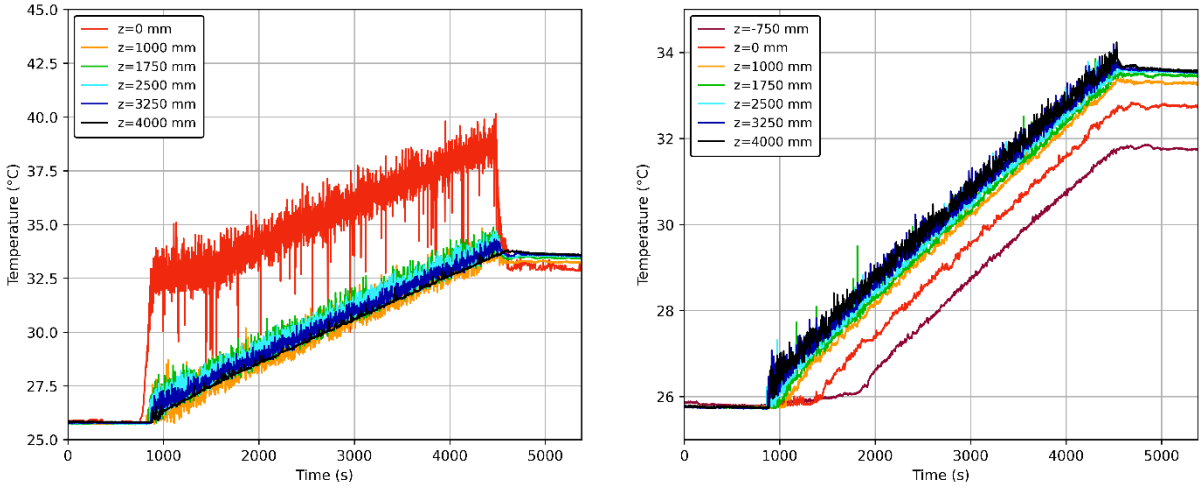

(a) Central thermocouples (b) Peripheral thermocouples

Figure 3-22: Measured temperatures during the TH-#5 transient (constant 50 kW, 60 minutes)

Funded by the European Union

Funded by the European Union. Views and opinions expressed are however those of the author(s) only and do not necessarily reflect those of the European Union or the European Atomic Energy Community ('EC-Euratom'). Neither the European Union nor the granting authority can be held responsible for them.

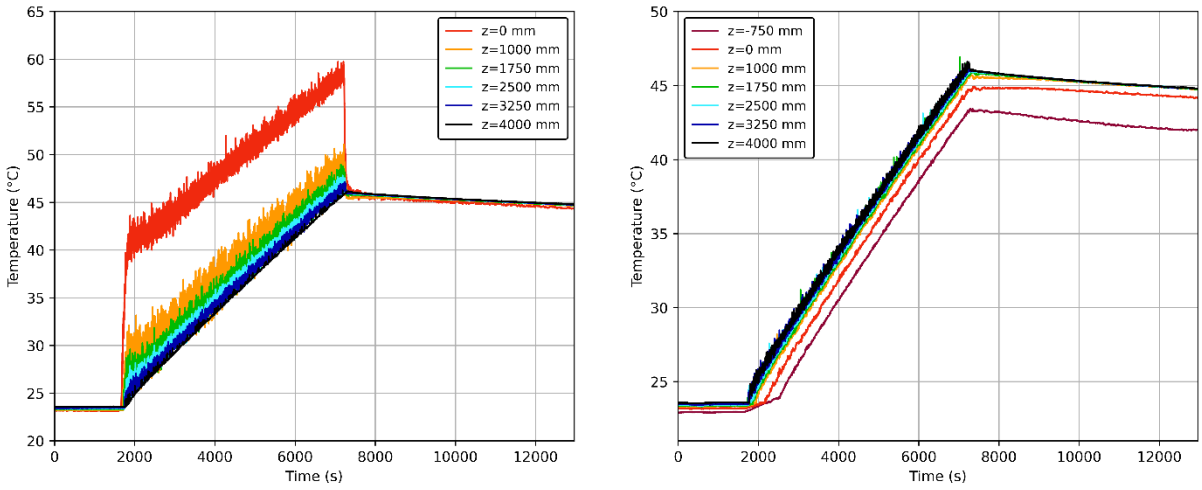

(a) Central thermocouples (b) Peripheral thermocouples

Figure 3-23: Measured temperatures during the TH-#6 transient (constant 100 kW, 90 minutes)

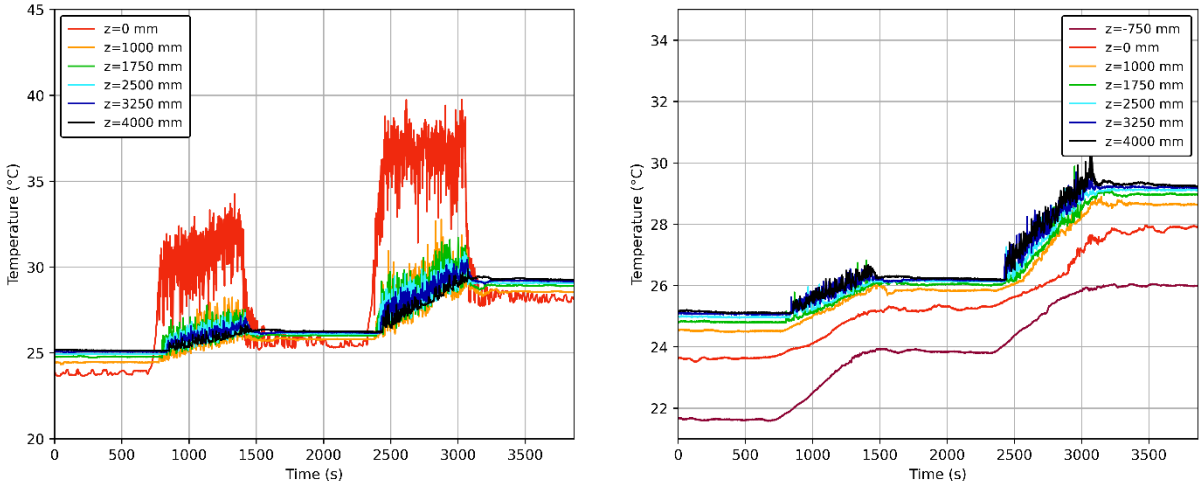

(a) Central thermocouples (b) Peripheral thermocouples

Figure 3-24: Measured temperatures during the TH-#7 transient (50-0-100 transient, 30 minutes)

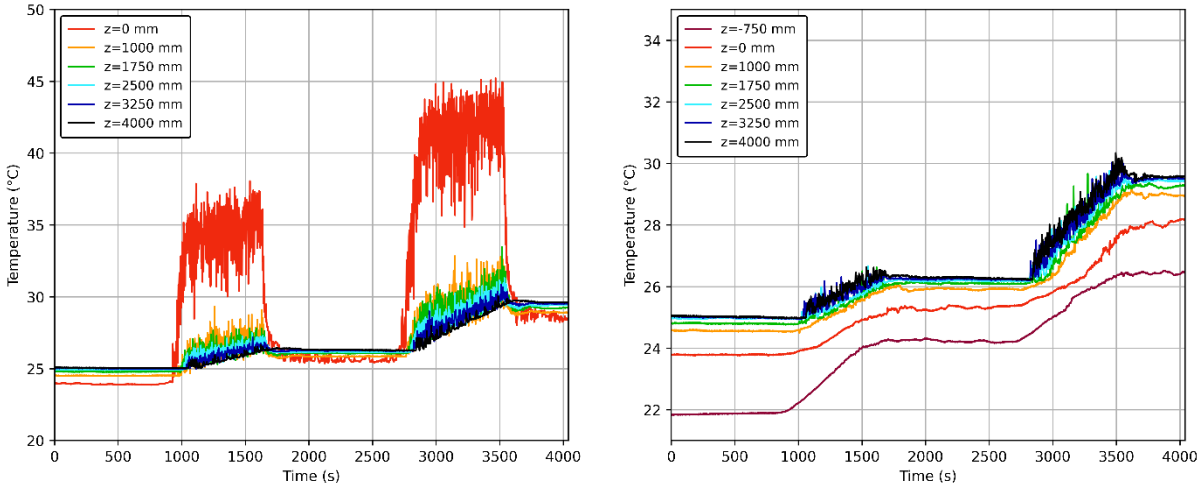

(a) Central thermocouples (b) Peripheral thermocouples

Figure 3-25: Measured temperatures during the TH-#8 transient (50-0-100 transient, 30 minutes)

Funded by the European Union

Funded by the European Union. Views and opinions expressed are however those of the author(s) only and do not necessarily reflect those of the European Union or the European Atomic Energy Community ('EC-Euratom'). Neither the European Union nor the granting authority can be held responsible for them.

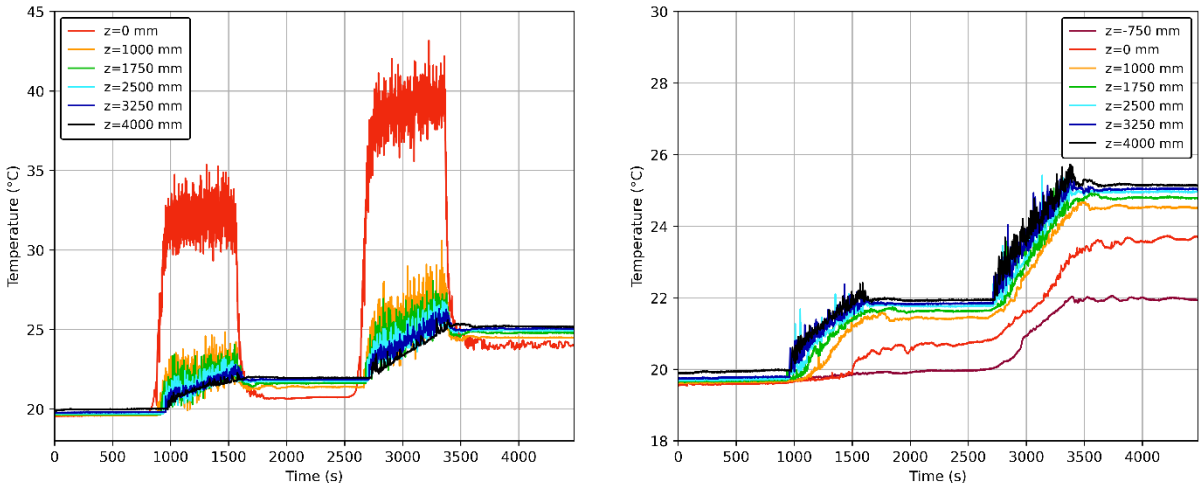

(a) Central thermocouples (b) Peripheral thermocouples

Figure 3-26: Measured temperatures during the TH-#9 transient (50-0-100 transient, 30 minutes)

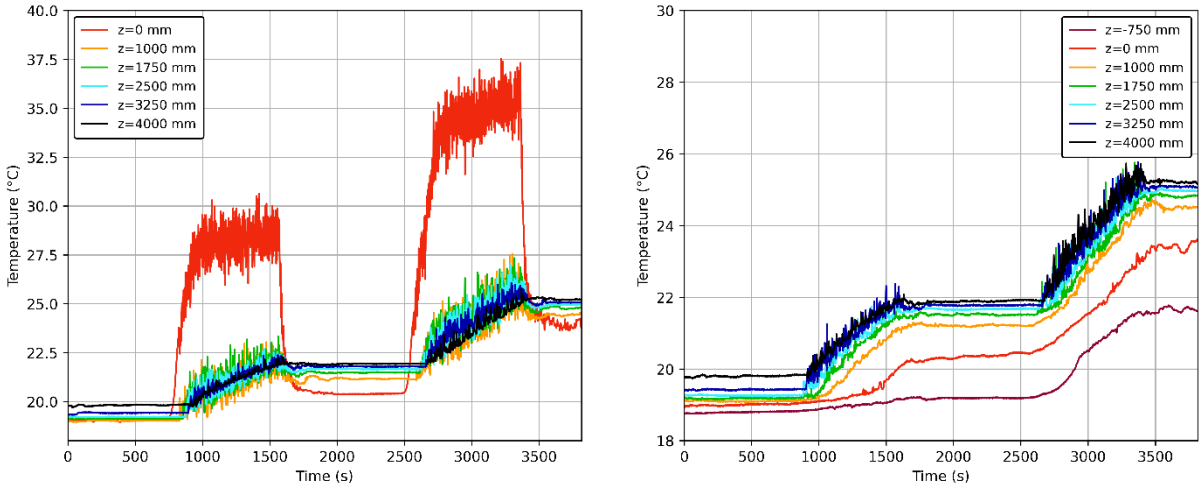

(a) Central thermocouples (b) Peripheral thermocouples

Figure 3-27: Measured temperatures during the TH-#10 transient (50-0-100 transient, 30 minutes)

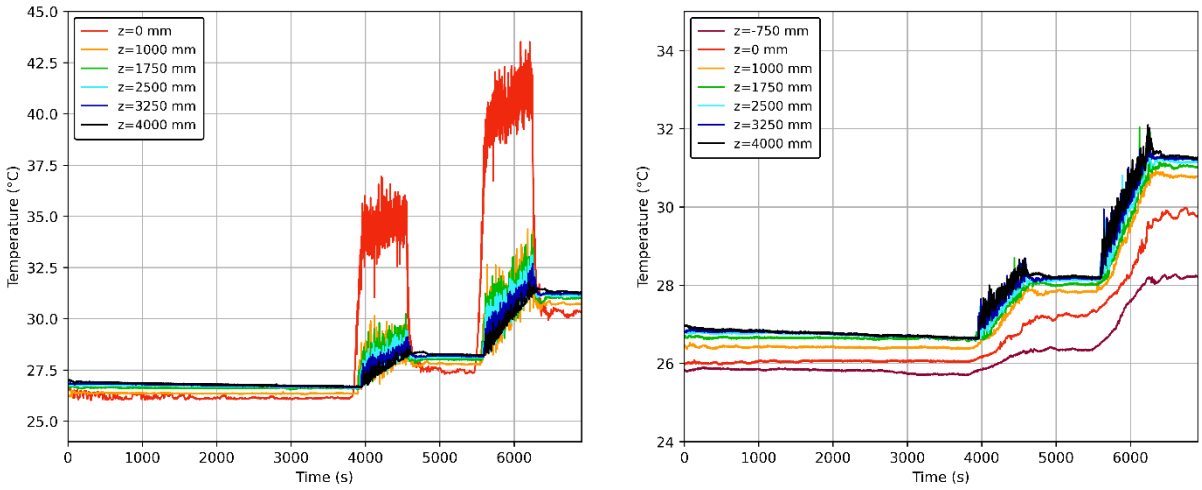

(a) Central thermocouples (b) Peripheral thermocouples

Figure 3-28: Measured temperatures during the TH-#11 transient (50-0-100 transient, 30 minutes)

Funded by the European Union

Funded by the European Union. Views and opinions expressed are however those of the author(s) only and do not necessarily reflect those of the European Union or the European Atomic Energy Community ('EC-Euratom'). Neither the European Union nor the granting authority can be held responsible for them.

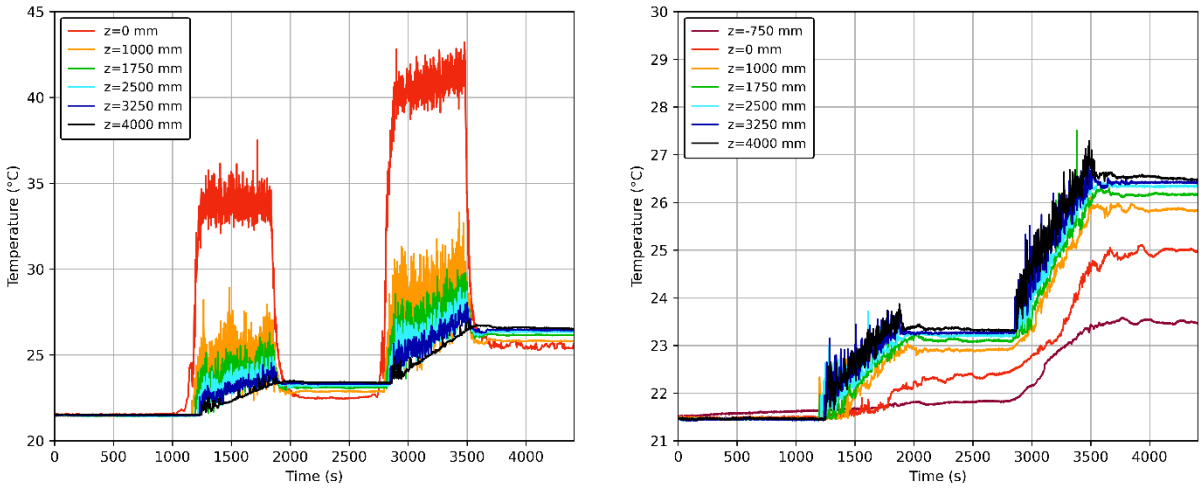

(a) Central thermocouples

(b) Peripheral thermocouples

Figure 3-29: Measured temperatures during the TH-#12 transient (50-0-100 transient, 30 minutes)

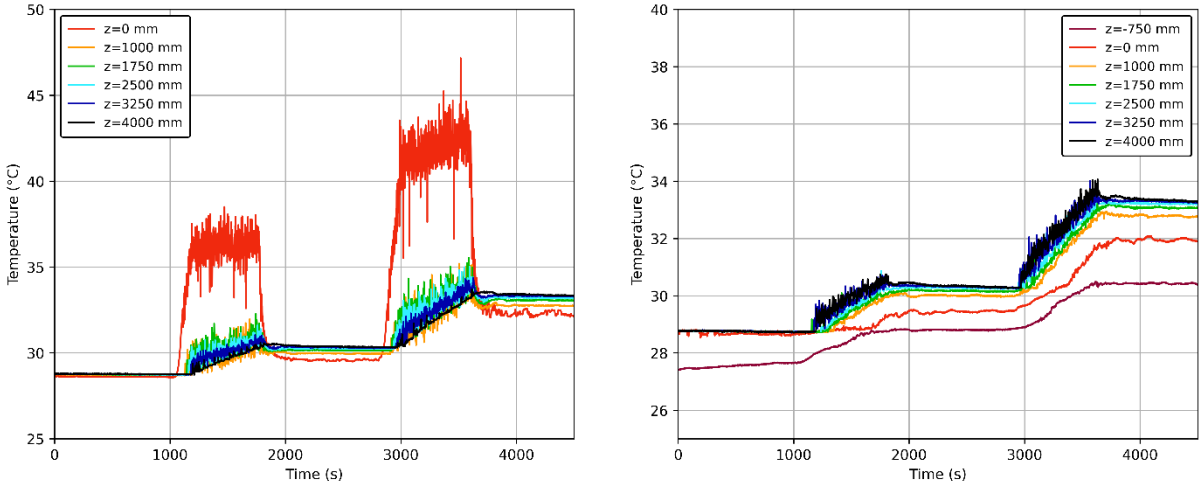

(a) Central thermocouples

(b) Peripheral thermocouples

Figure 3-30: Measured temperatures during the TH-#13 transient (50-0-100 transient, 30 minutes)

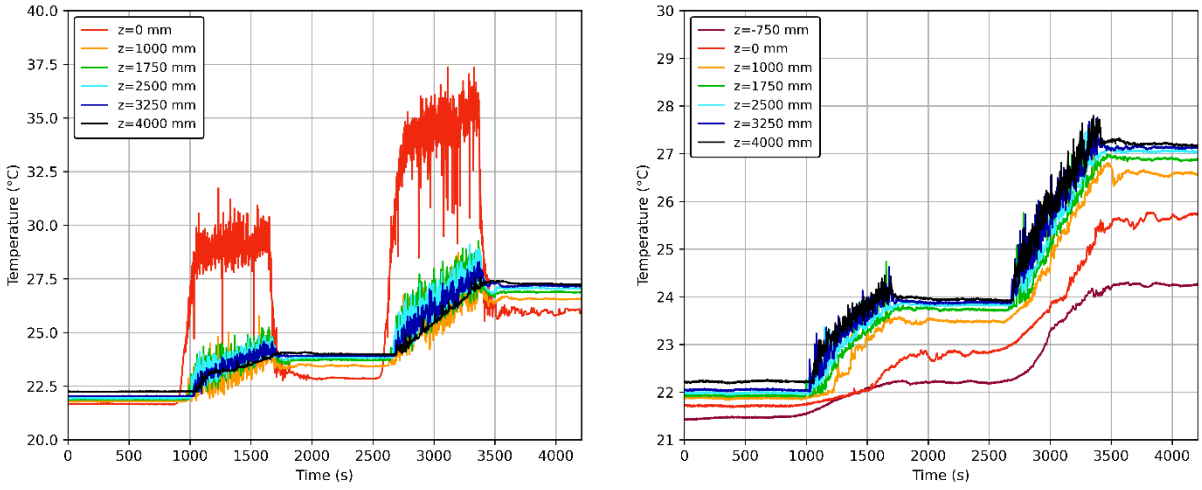

(a) Central thermocouples

(b) Peripheral thermocouples

Figure 3-31: Measured temperatures during the TH-#14 transient (50-0-100 transient, 30 minutes)

Funded by the European Union

Funded by the European Union. Views and opinions expressed are however those of the author(s) only and do not necessarily reflect those of the European Union or the European Atomic Energy Community ('EC-Euratom'). Neither the European Union nor the granting authority can be held responsible for them.

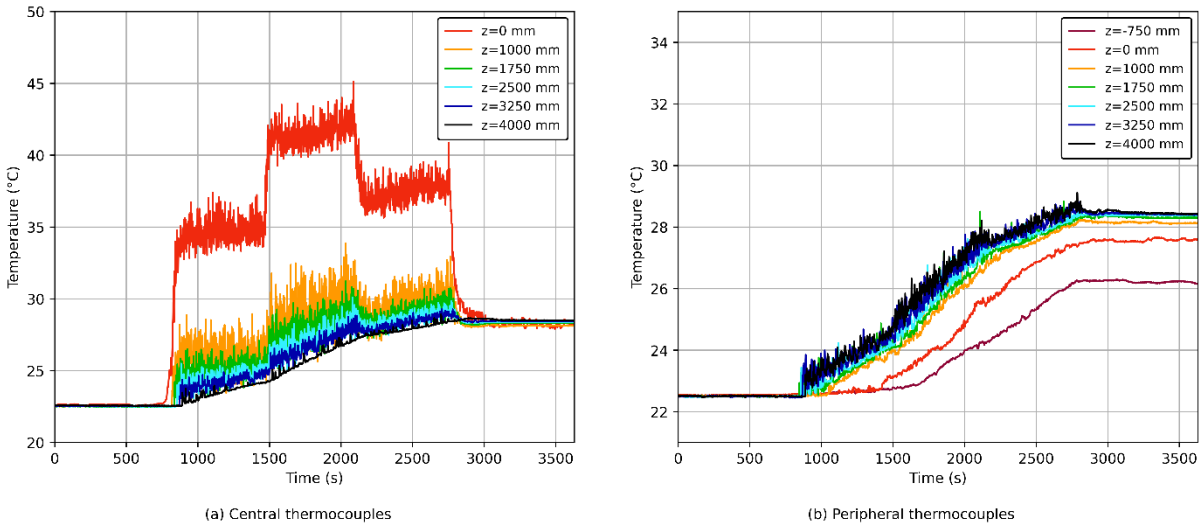

Figure 3-32: Measured temperatures during the TH-#15 transient (50-100-50 transient, 30 minutes)

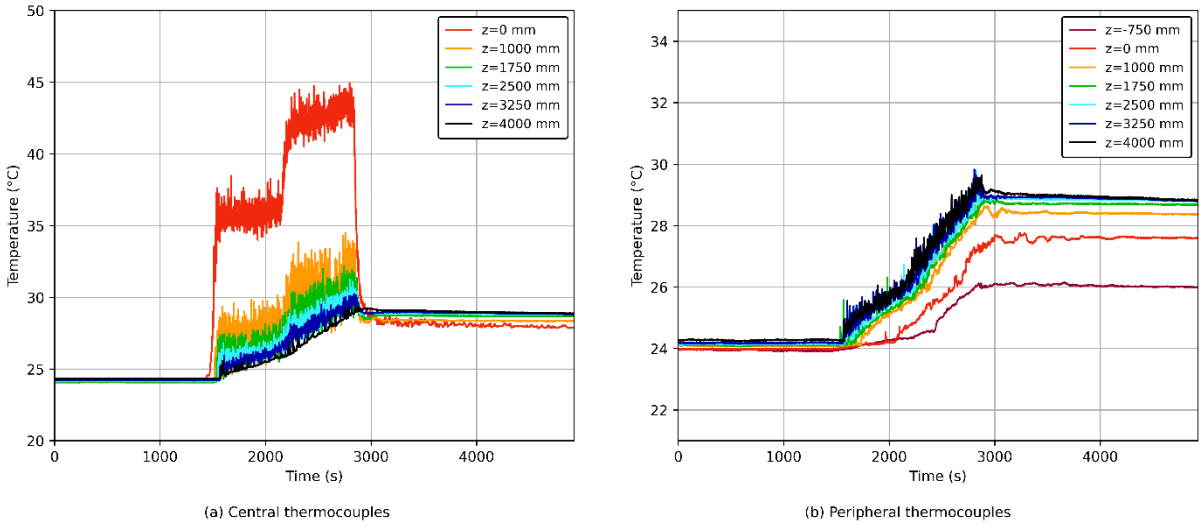

Figure 3-33: Measured temperatures during the TH-#16 transient (50-100 transient, 20 minutes)

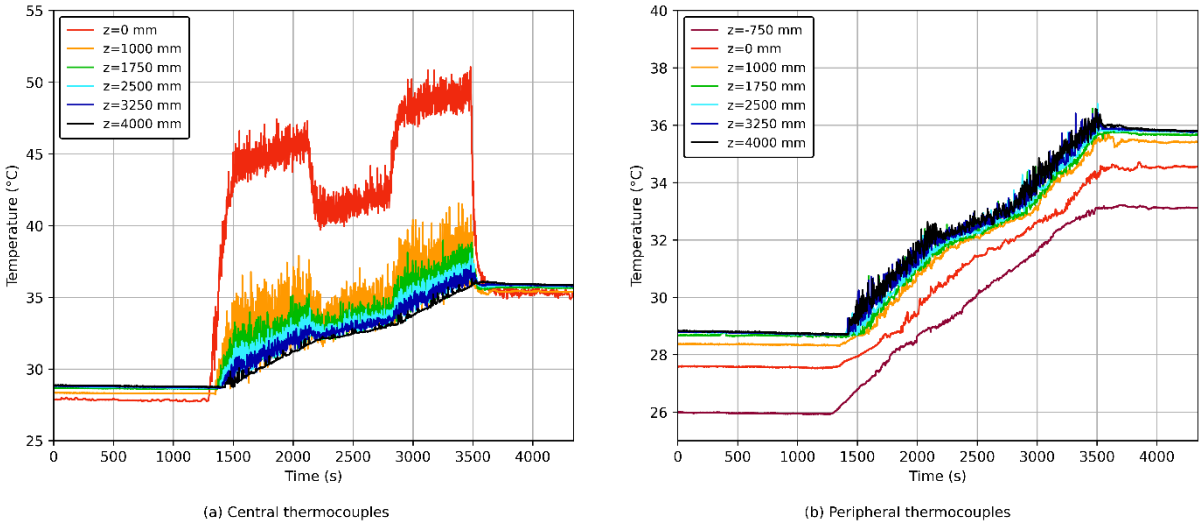

Figure 3-34: Measured temperatures during the TH-#17 transient (100-50-100 transient, 30 minutes)

Funded by the European Union

Funded by the European Union. Views and opinions expressed are however those of the author(s) only and do not necessarily reflect those of the European Union or the European Atomic Energy Community ('EC-Euratom'). Neither the European Union nor the granting authority can be held responsible for them.

3.3.4. Multi-physics measurements

In June 2022, a two-week experimental program was conducted at the Training Reactor of BME, during which a series of reactor transient experiments were performed. The objective of these measurements was to characterize the reactor's thermal feedback under various transient scenarios. To this end, multiple thermocouples were installed at different fuel assembly outlets, while the signals from an ex-core neutron detector were recorded simultaneously.

3.3.4.1. Temperature measurements

In total, sixteen identical type K thermocouples were used for temperature measurements during the experiments. The thermocouples were of class 1 precision, with exposed hot junction and had kapton insulation along their seven-meter-long wire. The sensors connected to a National Instrument NI-9213 high-density thermocouple input module, which was connected to a computer. The data card had sixteen thermocouple channels, all of which were used during the experiments. According to the hardware specification, the cold-junction compensation of the device is typically 0.8 °C but maximum 1.7 °C. For control, data acquisition and display purposes, a graphical interface was created in the National Instrument LabVIEW 2020 software (version 20.0f1). The program displayed in graph and logged to file the thermocouple signals. The same interface was used to display and log the data of the neutronic measurement (see Subsection 3.3.4.2).

All the sensors were first intercalibrated in air and water at different temperatures. For the purpose of absolute calibration, the thermocouples were placed in both boiling water and melting ice-water mixture as well. Based on the calibration measurements. the relative and absolute precisions of the sensors were conservatively estimated to be 0.2 °C and 0.5 °C, respectively.

As the reactor can only be instrumented from the top, through a water layer of 5000 mm, thermocouple holder and positioning equipment had to be designed and manufactured. The equipment consisted of a 6000 mm long, hollow aluminium rod (diameter: 20 mm, wall thickness: 2 mm, material: aluminium alloy AW-6060), a connecting cross-shaped aluminium plate (thickness: 5 mm, material: aluminium alloy AW-6060) and four medical stainless-steel needles fixed perpendicularly to the plate (see Figure 3-35). In total, four whole identical thermocouple holders were manufactured and used simultaneously for each experiment.

Funded by the European Union

Funded by the European Union. Views and opinions expressed are however those of the author(s) only and do not necessarily reflect those of the European Union or the European Atomic Energy Community ('EC-Euratom'). Neither the European Union nor the granting authority can be held responsible for them.

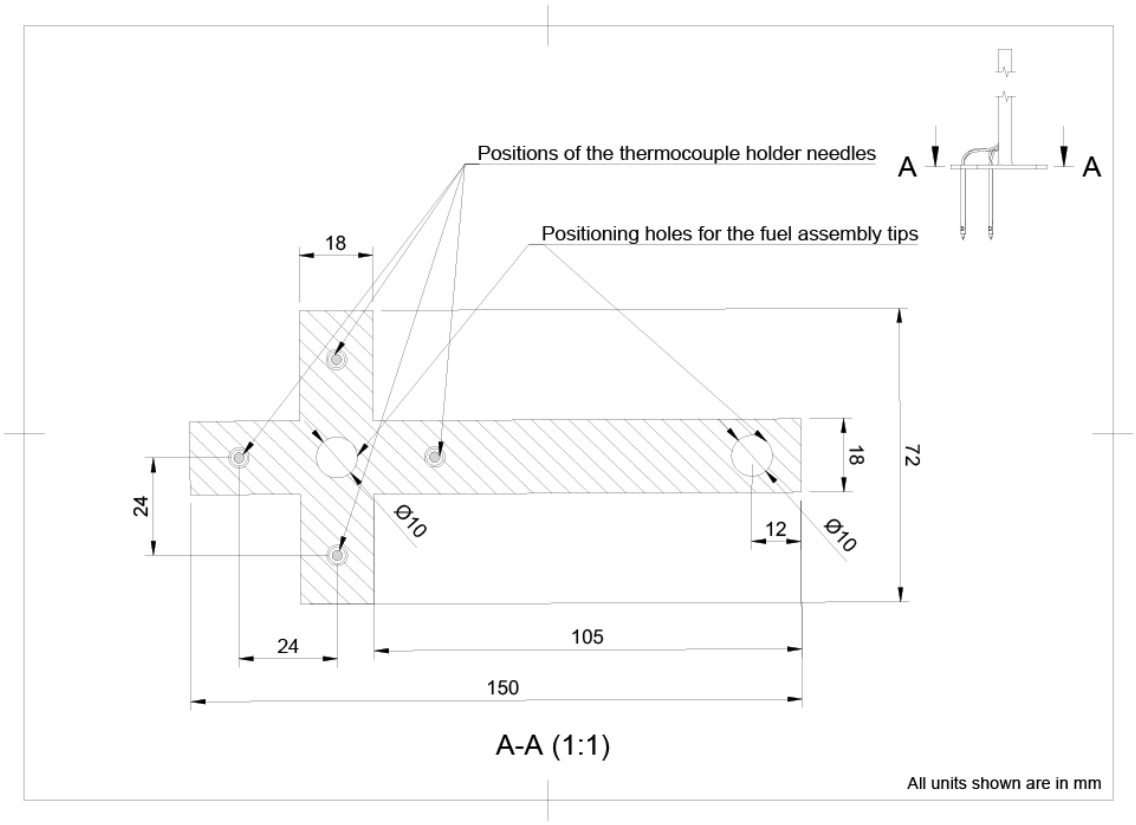

Figure 3-35: Drawing of the cross-shaped plate part of the thermocouple holders

The walls of the long pipes were perforated for radiation protection reasons. Seven holes were drilled on the cross-shaped plate: one for fixing the pipe to the plate with an aluminium screw, two for positioning the equipment on two diagonal fuel assembly tips and four others for the needle positioning of the temperature sensors. The geometry of the cross was designed so that when the holder is fixed and placed above a regular EK-10 fuel assembly, the four needles are centred above the four corner sub-channels. Four thermocouples were pulled through each main pipe, and each of them inserted into a single specific needle and fixed, so that the hot junctions of the sensors were about 5 mm below the bottom of the needles. The lengths of the needles were chosen so that when the equipment is fixed, the bottom of the thermocouple hot junction is at the same axial level as the top of the fuel pins. Figure 3-36 shows a fixed experimental setup of the thermocouple holders.

Funded by the European Union

Funded by the European Union. Views and opinions expressed are however those of the author(s) only and do not necessarily reflect those of the European Union or the European Atomic Energy Community ('EC-Euratom'). Neither the European Union nor the granting authority can be held responsible for them.

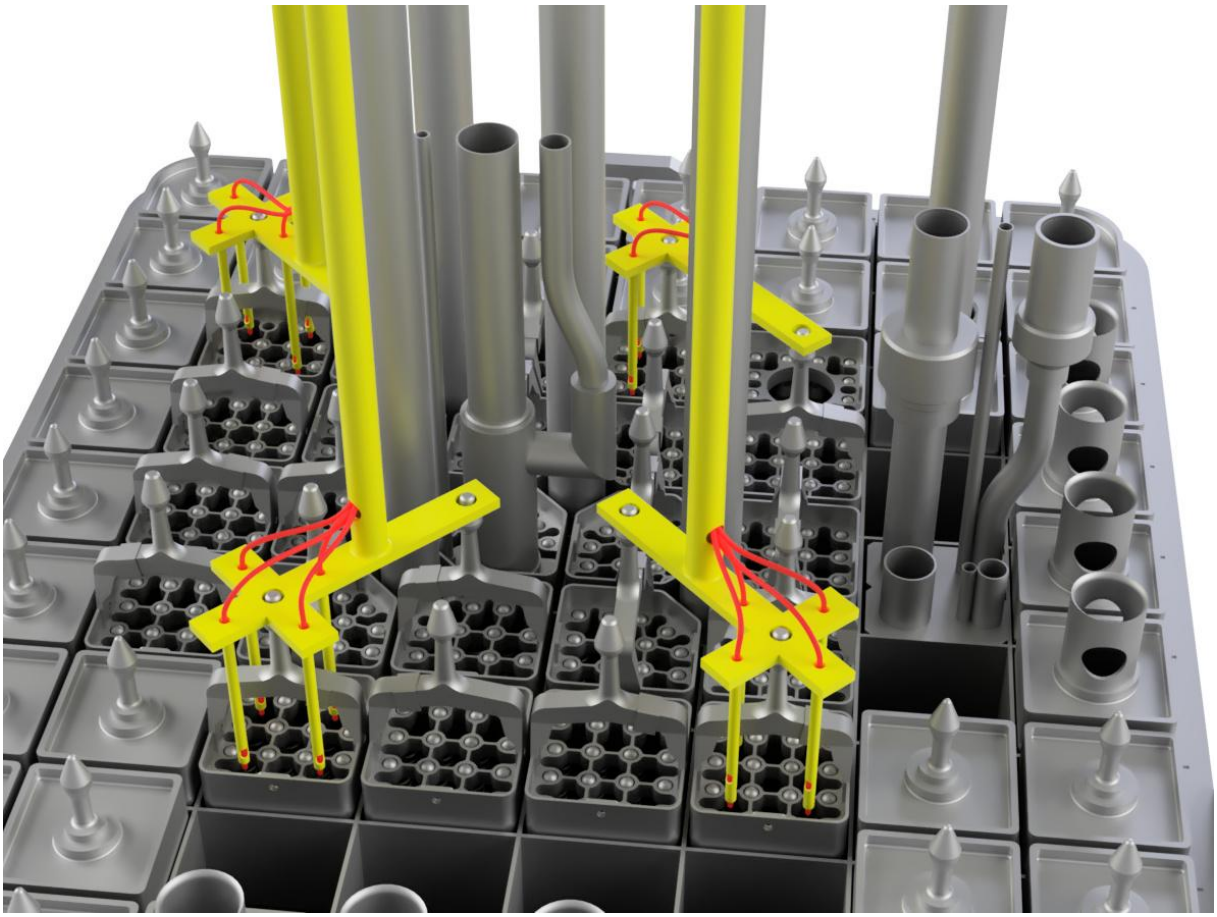

Figure 3-36: Experimental setup of the thermocouple holders (CAD model)

3.3.4.2. Neutronic measurements

The Training Reactor has five built-in neutron detector measurements, which are housed in separate air-filled protecting tubes around the reactor core. Two of the measurements are type CFUL08 fission chambers used in pulse mode (internal notation: I1 and I2), while the rest are type KNK-53M boron-lined, gamma-compensated ionization chambers operated in current mode (internal notation: E4, E5 and E6). During the experiments, the signal of the E5 ionization chamber was sampled and recorded, which has the clearest and most reliable signal based on operational experiences. The radial position of the E5 protecting tube is about 140 mm left and 35 mm above the centre of graphite assembly A1 in Figure 3-4. The axial position of the detector is not known precisely.

The detector is connected to a built-in signal processing device that consists of a pico-ammeter, a main processor along with test, communication and display units. During the experiments, the chamber current was sampled through this unit with the help of a LabVIEW interface. The sampled signal was displayed simultaneously with the thermocouple data and logged separately to file.

3.3.4.3. Transient description

In 9 workdays, 11 successful experiments were performed. Each transient started in a near-critical state and ended in another near-critical or shutdown state. In the case of experiments that started from a cold state, each thermocouple had to have the same reading within 0.3 °C tolerance. In order to start with a homogenized coolant temperature distribution, sufficient time was allowed between the experiments, during which the primary coolant circulating was utilized, to mix the coolant to a sufficient degree.

Funded by the European Union

Funded by the European Union. Views and opinions expressed are however those of the author(s) only and do not necessarily reflect those of the European Union or the European Atomic Energy Community ('EC-Euratom'). Neither the European Union nor the granting authority can be held responsible for them.

The chamber current of the E5 neutron detector was sampled with the rate of 10 Hz, while the sampling frequency of the thermocouples was 75 Hz throughout the experiments.

During the measurements, two experimental thermocouple setups were used. In the first one (Setup #1), the holder rods were fixed on the following assembly tips: E3–F4, B3–C4, C7–D6, F7-–E6, with the sensors being inserted to the first mentioned assembly (this setup corresponds to the one shown in Figure 3-36). In the second one (Setup #2), the sensor holder rods were fixed on the following assembly tips: E3–F4, B4–C3, C6–D7, F6–E7, with the thermocouples being inserted into the first mentioned assembly. Unfortunately, the F4–E3 switch could not be administered, because there was not enough space between the sensor holder plate and the nearby vertical irradiation channels.

Three main types of transients were performed:

- Reactivity insertion to cold state: The reactor was operated in automatic mode at 5 W nominal power for at least 10 minutes, so the delayed-neutron precursor nuclei would reach their equilibrium concentration. Then, the reactor was switched to manual mode and reactivity was inserted to the system by withdrawing one of the control rods to a specified position. The supercritical reactor was monitored until a new critical state was reached.
- Reactivity insertion to hot state: The reactor was operated in automatic mode at a specific power level above 5 kW for at least 10 minutes, so the delayed-neutron precursor nuclei would reach their equilibrium concentration. Then, the reactor was switched to manual mode and reactivity was inserted to the system by withdrawing one of the control rods to a specified position. The supercritical reactor was monitored until a new critical state was reached.
- Long irradiation: The reactor was operated in automatic mode at a certain power level for a specified longer period of time. In the case of these transients, the manual control rod was set z_{MAN} = 600 mm after the irradiation power was reached. Following the irradiation, one of the control rods was dropped and the reactor was monitored until a shutdown state was reached.

Table 3-6 and Table 3-7 present the main characteristics of the performed transients.

Table 3-6: Summary of the performed transients (CI: cold insertion, HI: hot insertion, LI: long irradiation)

Transient ID	Setup #	Type	Duration (s)	Power (W)	
				Initial	Final
FB-#1	1	CI	4040	5	4325
FB-#2	1	CI	1550	5	45938
FB-#3	1	CI	2150	5	21991
FB-#4	1	HI	1290	21991	55519
FB-#5	1	HI	520	10012	91385
FB-#6	1	LI	5400	101948	103668
FB-#7	2	CI	2140	5	21440
FB-#8	2	HI	1270	21440	55519
FB-#9	2	CI	2950	5	11994

Funded by the European Union

Funded by the European Union. Views and opinions expressed are however those of the author(s) only and do not necessarily reflect those of the European Union or the European Atomic Energy Community ('EC-Euratom'). Neither the European Union nor the granting authority can be held responsible for them.

FB-#10	2	CI	1270	5	47166
FB-#11	2	LI	5400	101948	103422

Table 3-7: Summary of the control rod positions of the performed transients (CI: cold insertion, HI: hot insertion, LI: long irradiation)

Transient ID	Setup #	Type	Initial control rod positions		Final control rod positions	
			z_{AUT} (mm)	z_{MAN} (mm)	z_{AUT} (mm)	z_{MAN} (mm)
FB-#1	1	CI	346	450	346	460
FB-#2	1	CI	558	380	558	420
FB-#3	1	CI	300	482	350	482
FB-#4	1	HI	350	482	400	482
FB-#5	1	HI	382	450	600	450
FB-#6	1	LI	381	600	402	600
FB-#7	2	CI	300	496	350	496
FB-#8	2	HI	350	496	400	496
FB-#9	2	CI	372	450	372	470
FB-#10	2	CI	589	381	589	421
FB-#11	2	LI	378	600	397	600

3.3.4.4. Results and discussion

Theoretically, the measured chamber current of detector E5 is proportional to the nominal thermal core power of the reactor, which is based on the neutronic detector E6 and logged automatically every 30 s. In practice, the two detectors are located in different positions and might have different gamma compensation. Nevertheless, based on the measured critical states, a coefficient was determined that transforms the measured chamber current into nominal power. The uncertainty of this power data is estimated to be 3%, which does not include the actual unknown gamma compensation bias of the detectors and the accuracy of the reactor power calibration. The overall conservatively estimated uncertainty of the presented power curves might be as high as 6%.

By averaging over 75 data points, the 75 Hz measured raw temperature data were collapsed into 1 Hz data. The signals of thermocouples fixed over a given assembly were averaged. In the presented graphs, the 1 Hz assembly temperature data were further smoothed with a moving average algorithm over a 30-second time window to help the readability of the presented results. The absolute precision of the thermocouples was estimated to be 0.5 °C.

In the presented power data large sudden changes can be seen at certain power levels (e.g. approximately at 2100 W below, in Figure 3-37). These are due to the change of the measurement method within the pico-ammeter corresponding to neutron detector E5.

Funded by the European Union

Funded by the European Union. Views and opinions expressed are however those of the author(s) only and do not necessarily reflect those of the European Union or the European Atomic Energy Community ('EC-Euratom'). Neither the European Union nor the granting authority can be held responsible for them.

In general, the measurement results were consistent with the preliminary experimental expectations. However, the first series of conventional, low-fidelity coupled TRACE/PARCS simulations failed to reproduce the measurements (for more details see (Ványi, Hursin, & Czifrus, 2023)).

The measurement curves are shown below in sequential order from Figure 3-37 to Figure 3-47.

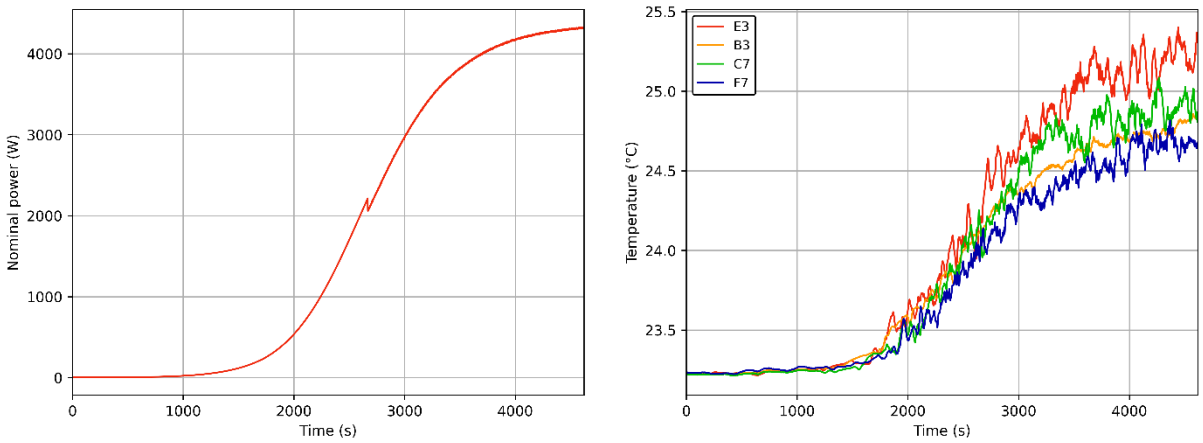

(a) Nominal power (b) Temperature measurements

Figure 3-37: Evaluated power and temperature curves of transient FB-#1

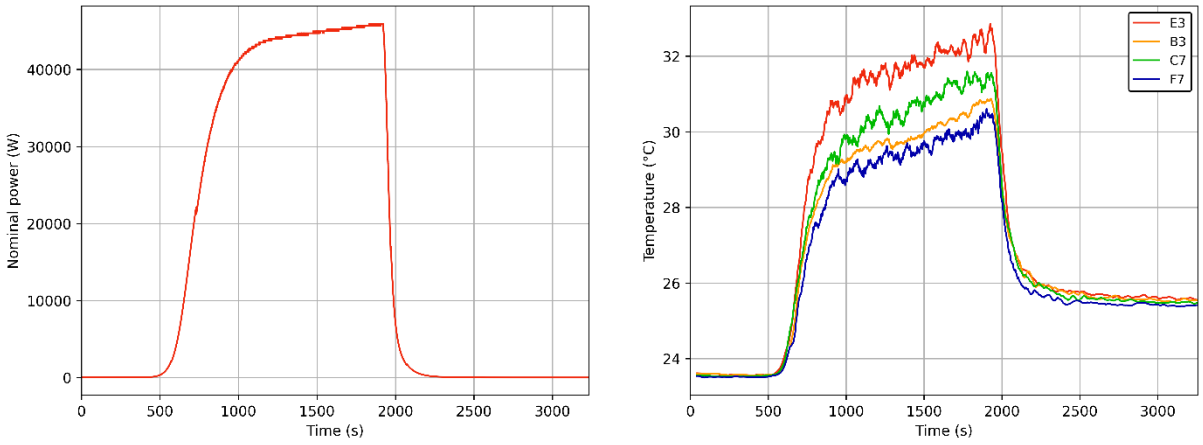

(a) Nominal power (b) Temperature measurements

Figure 3-38: Evaluated power and temperature curves of transient FB-#2

Funded by the European Union

Funded by the European Union. Views and opinions expressed are however those of the author(s) only and do not necessarily reflect those of the European Union or the European Atomic Energy Community ('EC-Euratom'). Neither the European Union nor the granting authority can be held responsible for them.

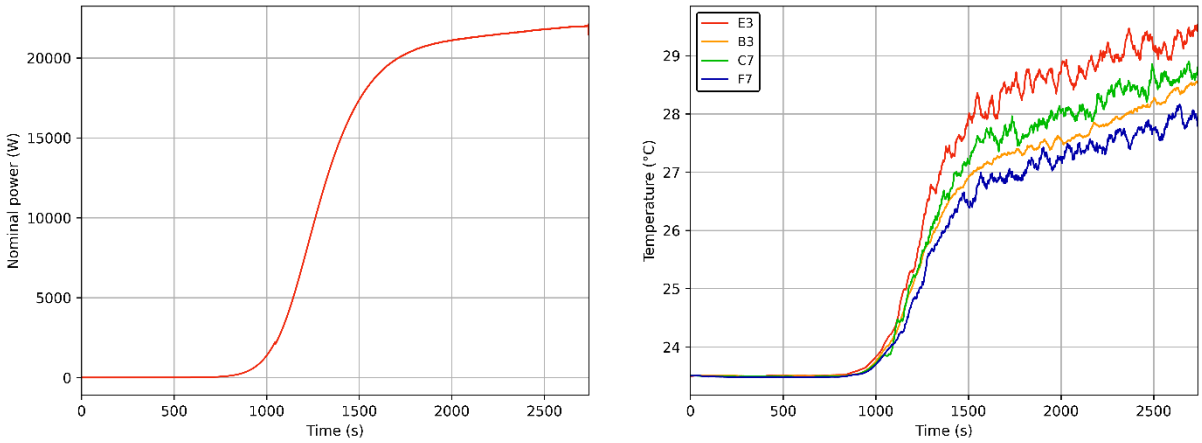

(a) Nominal power (b) Temperature measurements

Figure 3-39: Evaluated power and temperature curves of transient FB-#3

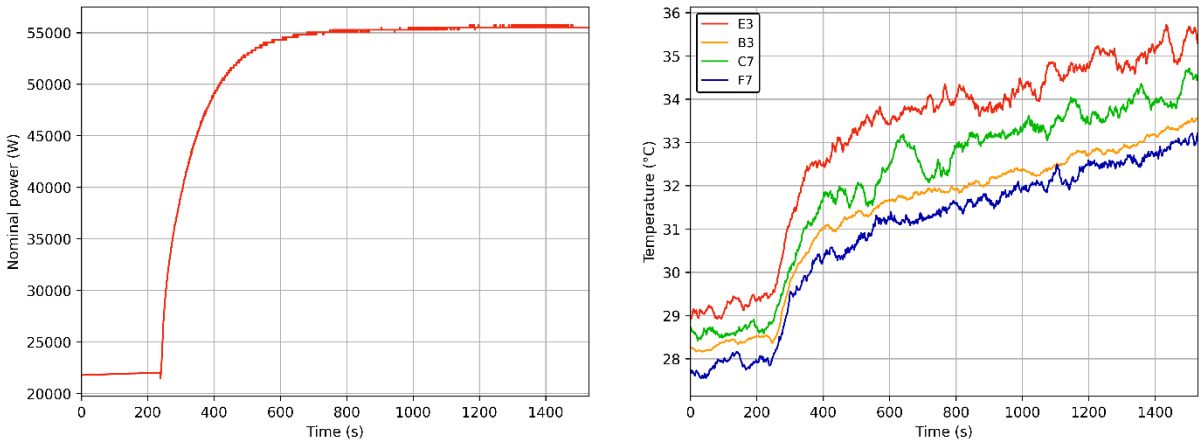

(a) Nominal power (b) Temperature measurements

Figure 3-40: Evaluated power and temperature curves of transient FB-#4

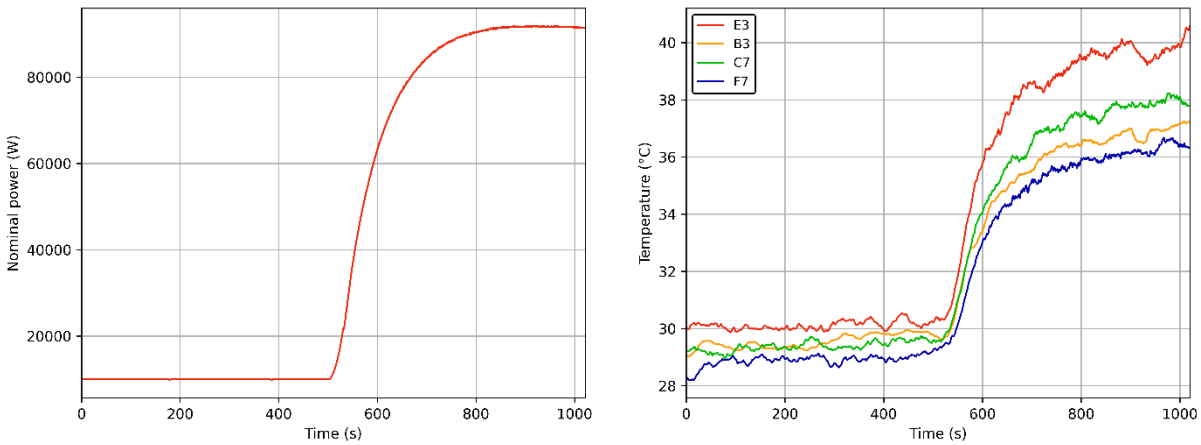

(a) Nominal power (b) Temperature measurements

Figure 3-41: Evaluated power and temperature curves of transient FB-#5

Funded by the European Union

Funded by the European Union. Views and opinions expressed are however those of the author(s) only and do not necessarily reflect those of the European Union or the European Atomic Energy Community ('EC-Euratom'). Neither the European Union nor the granting authority can be held responsible for them.

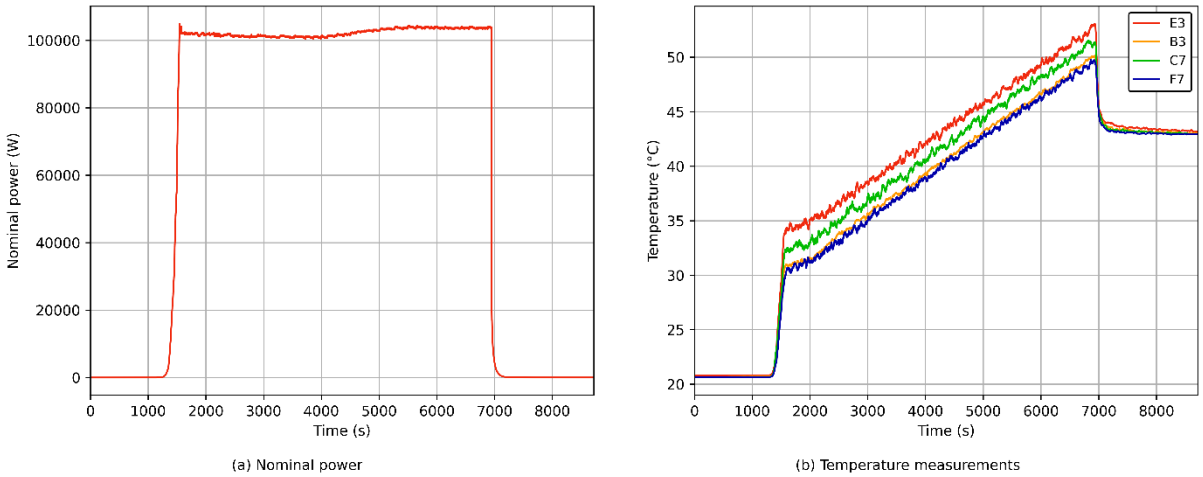

(a) Nominal power (b) Temperature measurements

Figure 3-42: Evaluated power and temperature curves of transient FB-#6

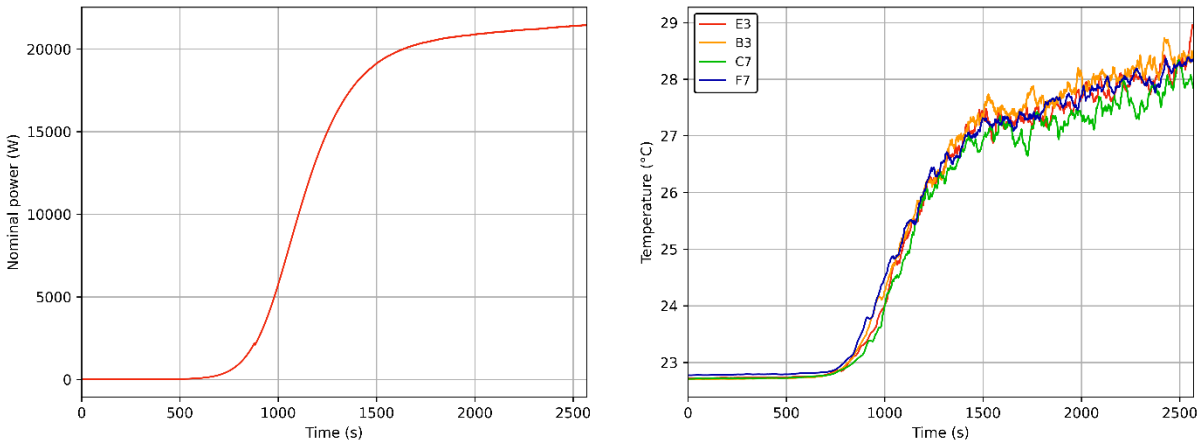

(a) Nominal power (b) Temperature measurements

Figure 3-43: Evaluated power and temperature curves of transient FB-#8

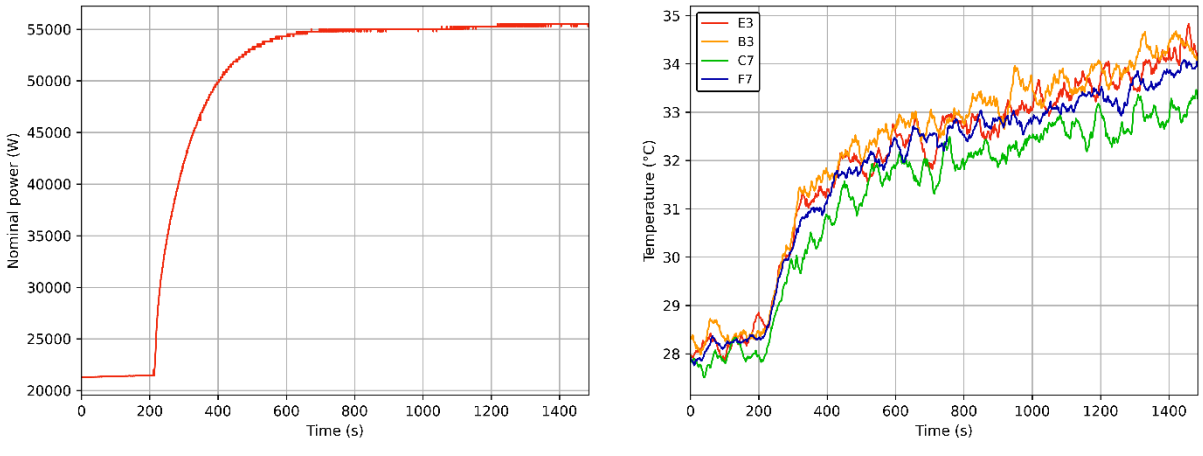

(a) Nominal power (b) Temperature measurements

Figure 3-44: Evaluated power and temperature curves of transient FB-#8

Funded by the European Union

Funded by the European Union. Views and opinions expressed are however those of the author(s) only and do not necessarily reflect those of the European Union or the European Atomic Energy Community ('EC-Euratom'). Neither the European Union nor the granting authority can be held responsible for them.

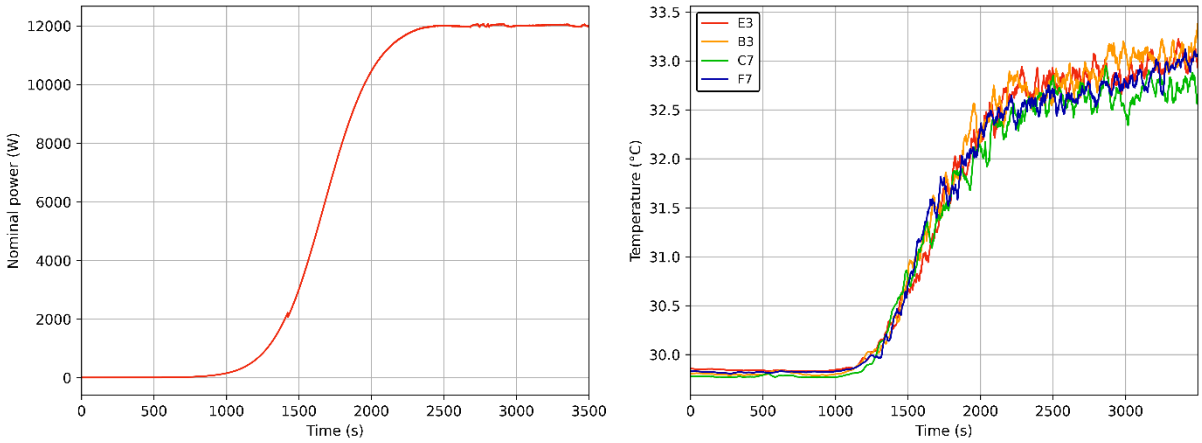

(a) Nominal power (b) Temperature measurements

Figure 3-45: Evaluated power and temperature curves of transient FB-#9

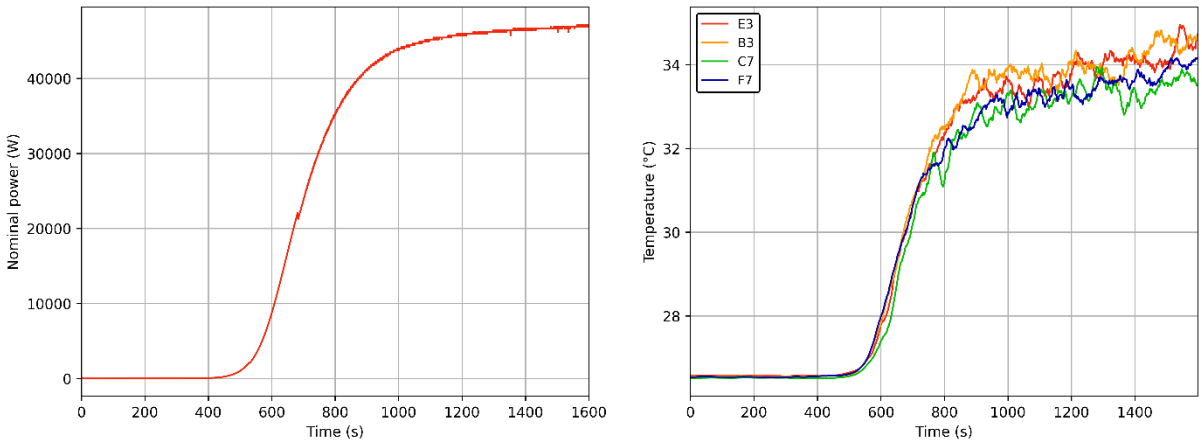

(a) Nominal power (b) Temperature measurements

Figure 3-46: Evaluated power and temperature curves of transient FB-#10

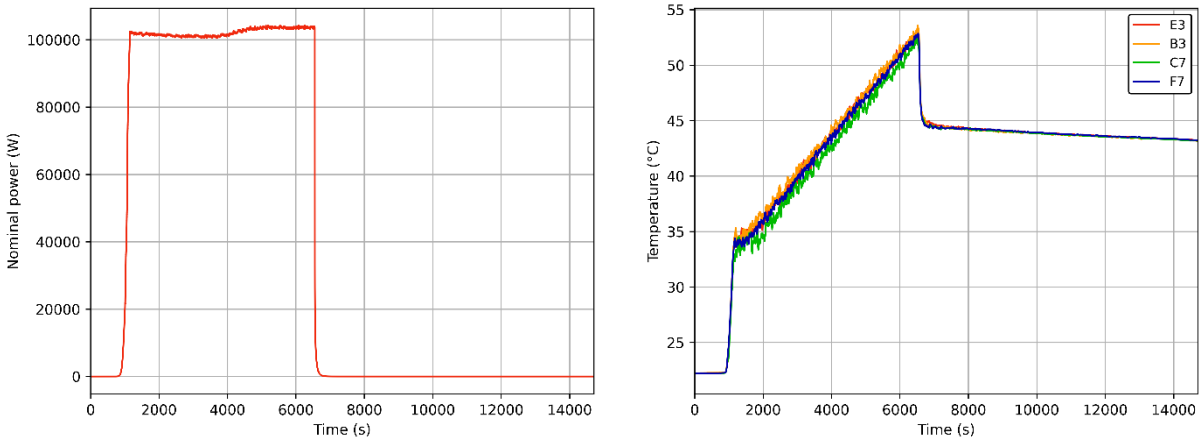

(a) Nominal power (b) Temperature measurements

Figure 3-47: Evaluated power and temperature curves of transient FB-#11

Funded by the European Union

Funded by the European Union. Views and opinions expressed are however those of the author(s) only and do not necessarily reflect those of the European Union or the European Atomic Energy Community ('EC-Euratom'). Neither the European Union nor the granting authority can be held responsible for them.

4. Budapest Research Reactor

The construction of the Budapest Research Reactor (BRR) started on 25.03.1956, and the first critical commissioning took place on 25.03.1959. A second reconstruction started in 1986 and lasted until 1990. Critical upgrading was carried out on 12.12.1992. The reactor received its operating licence on 25.11.1993. The power is 10 MW, beryllium is used as a reflector, and the coolant and moderator are light water. In the meantime, the 36% U-235 fuel was replaced with LEU fuel. The last authority review and a further reconstruction started in 2020, resulting in the reactor being granted a provisional operating licence until 2033. The purpose of the reactor is to serve scientific research as a neutron source for material science research and its applications in applied research and development.

4.1. Facility overview

The BRR took its current form and design between 1980 and 1990. The reactor is of the vessel type, which is classified as VVRSZ-M10 in the Hungarian designation system. A characteristic feature of these reactors is that the ion-exchanged light water used as moderator is also a coolant. The cooling water flows from the top down through the active zone i.e. the core, which contains WWR-M2 fuel elements containing uranium oxide fuel with 19.75% enrichment, in an aluminium matrix. The reactor is controlled with 14 manually operated shim control rods for xenon and burnup management and 3 automatic safety rods, containing B_4C neutron absorber, as well as a single automatic i.e. Regulating rod made of stainless steel for fine reactor power control. The facility is designed for research and isotope production. The reactor has a thermal power of 10 MW, with an absolute maximum thermal neutron flux of $1.24 \cdot 10^{14} cm^{-2} s^{-1}$.

4.1.1. Primary circuit

The primary circuit removes the heat generated during reactor operation from the active zone and transfers it to the secondary circuit through two heat exchangers connected in parallel. The coolant in the primary circuit is circulated by three service and one stand-by main circulating pump in normal operation, while two stand-by pumps (one service and one stand-by) are available in case of emergency. The stainless-steel primary circuit piping is connected to the aluminium alloy piping through a transition bore in each flange joint to prevent electrochemical corrosion. A similar connection is made to the gravity emergency cooling system tank. This provides the coolant flow for a limited period in the event of a malfunction in the primary pumps system, removing the decay heat until one of the standby pumps starts.

4.1.2. Secondary circuit

The system is closed circuit. The heat generated in the reactor is transferred through water-water counter current heat exchangers to the secondary circuit, which cools off via the Heller-rotary cooling tower where the heat is transferred to the environment through the closed water circuit finned tubes of the cooling tower. Here too, the cooling water is circulated by four circulating pumps, three of which are in continuous operation, and one is on standby. The pressure in the secondary circuit is higher than that in the primary circuit, ensuring that no active water is released to the environment.

4.1.3. The reactor vessel and its surroundings

The reactor vessel is made of aluminium with a vertical axis and a circular section with an open lid with the reactor zone located on the bottom of the vessel. The heating elements, which can be placed in different configurations in the core, are surrounded by a beryllium reflector to increase the neutron flux. A fraction of neutrons is transported to the ten channels in the horizontal plane of symmetry formed in the vertical centre of the reactor zone. Vertical irradiation channels are also available in the tank, making the reactor suitable for irradiations with high neutron fluxes in the core.

Funded by the European Union

Funded by the European Union. Views and opinions expressed are however those of the author(s) only and do not necessarily reflect those of the European Union or the European Atomic Energy Community ('EC-Euratom'). Neither the European Union nor the granting authority can be held responsible for them.

The Reactor vessel is an open-top vessel located inside the Reactor block i.e. a heavy concrete biological shielding with 4 cast iron rings at the top of the tank. There is an air gap between the vessel and the concrete. The reactor vessel is 2300 mm in diameter, made of 16 mm thick R-AlMg2.5 alloy and 5686 mm high. The tank contains approximately 20 m^3 of desalinated, de-ionized water.

The reactor vessel is bounded on the top by the reactor cover, which consists of two cast iron discs arranged eccentrically one inside the other.

4.1.4. Reactor zone

4.1.4.1. Zonal basket

The zonal basket (Figure 4-1) is a cylinder rolled from sheet metal and post-machined by chipping. Inside it is the zonal grid support, fixed by a welded joint. The hexagonal opening of the zone grid holder is fitted with the zone grid, which is provided with holes for the orientation of the heating bundles and for the passage of cooling water.

The zone grid is not fixed to the zone grid holder. Its position relative to each other is determined by the support and the hexagonally machined shoulder.

A beryllium shell (puttony) assembled from components, is bolted to the approximately 140° sector of the outer surface of the zonal basket, covering the tangential and cold neutron channels as well as the beryllium around the horizontal channel I. The zonal basket is open at the beryllium envelope location, 135° arc 434 mm wide, for the mounting of the beryllium elements. The backbone of the beryllium casing is formed by the lower and upper casing planes with welded edges.

The upper envelope is perforated to allow for cooling water to flow through. The two ends of the enclosure are bounded by a flanged breast plate and back plate and a side plate and back plate.

The enclosure elements are fastened together by M8 screws, while the assembled beryllium enclosure is connected to the zone tank by M12 flange screws.

The 4 Ø135 mm ducts and the 3 Ø95 mm ducts are also connected to the zone tank with M12 flange screws.

The upper part of the zonal basket is welded with a rolled flange made of "L" profile bars. Cut-outs in the lower part of the zone box provide space for the cooling water discharge pipe. the overflow pipe and the welded joint of the casing pipe. The zone box is secured by a removable screw to the 4 lugs welded to the embossed bottom.

After the positioned channel slots have been made. the following channels are located between the zone basket and the reactor vessel shell:

- 3 radial channels (Nominal Diameter (NA) 100mm) I., II., III.
- 2 radial channels (NA 100mm) (fast neutron) IV., V.
- 3 radial channels (NA 60mm) VI., VII., VIII.
- 1 tangential channel (NA 100mm)
- 1 cold neutron channel.

Funded by the European Union

Funded by the European Union. Views and opinions expressed are however those of the author(s) only and do not necessarily reflect those of the European Union or the European Atomic Energy Community ('EC-Euratom'). Neither the European Union nor the granting authority can be held responsible for them.

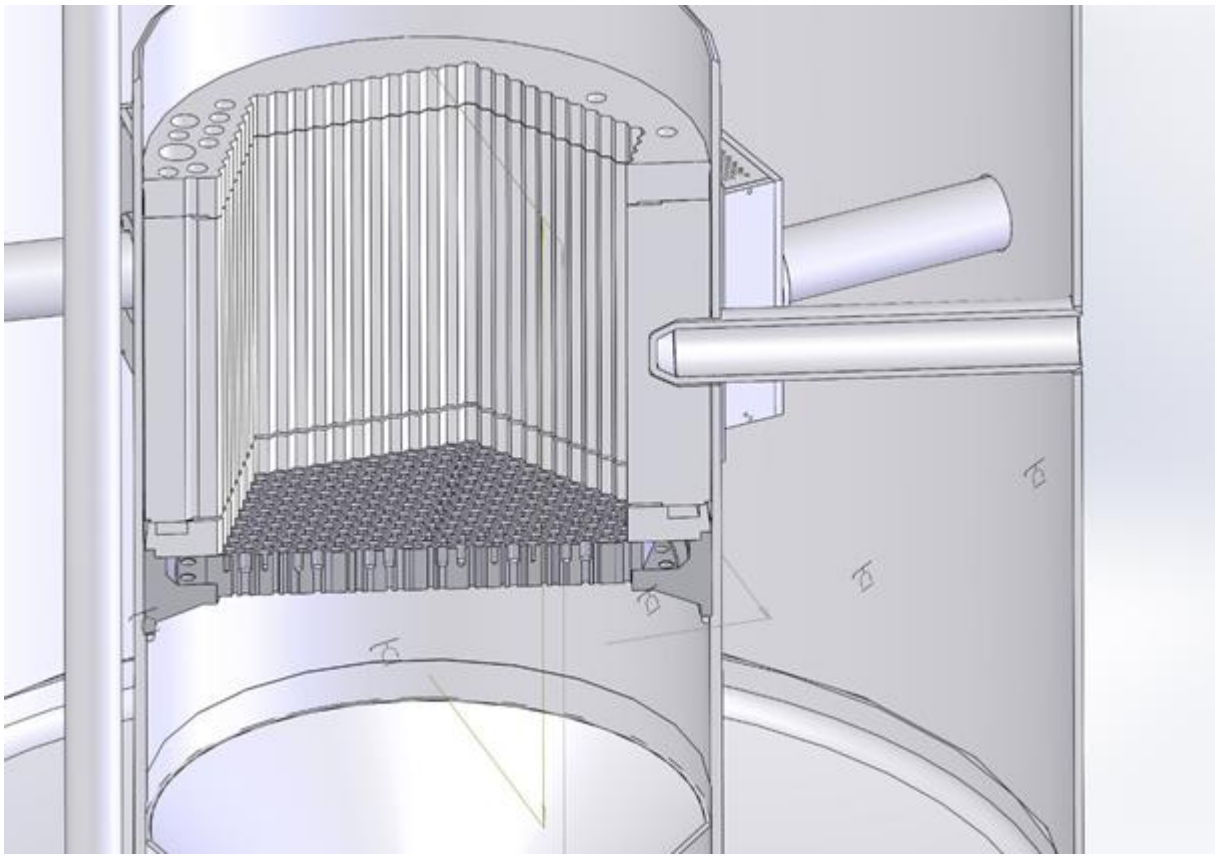

Figure 4-1: Drawing of the interior of BRR with the zone basket. the core and the horizontal neutron channel.

4.1.4.2. Fuel

The zone is equipped with VVR-M2 type single and triple fuel elements. Each fuel element consists of 3 concentric elements, two of which are cylindrical, these are the internal elements, and one hexagonal, this is the external element (Figure 4-2). The distance between the elements is provided by stepped spacers on the head and foot sections. The design of the fuel element head allows it to be moved safely with the manipulation tool (Figure 4-3). The positioning of the fuel elements in the zone grid is ensured by the foot part and at the height of the head by the design of the head. The triple fuel element consists of three individual fuel stacks, one with a central gripping head and three with legs, as shown in Figure 4-3 and Figure 4-4. The characteristic parameters of the fuel elements are given in Table 4-1 .

Table 4-1: The characteristic parameters of the fuel elements

Data	VVR-M2 LEU
Enrichment [%]	19.75± 0.25
Cover material	reactor grade aluminium
Cover thickness [mm]	0.75
Element thickness [mm]	2.5
Fissile material composition	UO_2+Al mixture
Fissile material thickness in the element [mm]	0.98

Funded by the European Union

Funded by the European Union. Views and opinions expressed are however those of the author(s) only and do not necessarily reflect those of the European Union or the European Atomic Energy Community ('EC-Euratom'). Neither the European Union nor the granting authority can be held responsible for them.

Number of elements in the bundle	3
Nominal active length [mm]	600
Heat transfer surface per unit volume [cm^2/cm^3]	3.67
^{235}U concentration in the active zone [g/liter]	78.6
^{235}U concentration in the fissile material [g/cm^3]	0.65
^{235}U per 1 m^2 fuel element surface [g/m^2]	216
Cooling surface area of a bundle [m^2]	0.232
Average ^{235}U content per batch [g]	50
Volume fraction of water in the cell [%]	54.2
H/U ratio in the cell	183

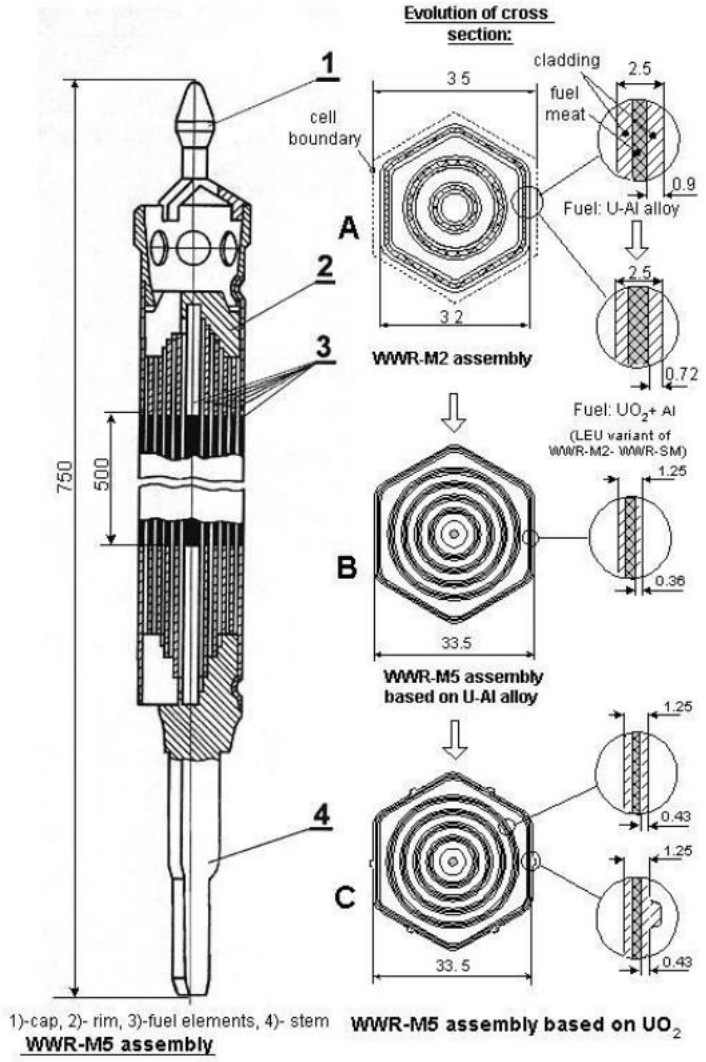

Figure 4-2: Schematic view of the WWR-M2 and WWR-M5 fuel assemblies.

Funded by the European Union

Funded by the European Union. Views and opinions expressed are however those of the author(s) only and do not necessarily reflect those of the European Union or the European Atomic Energy Community ('EC-Euratom'). Neither the European Union nor the granting authority can be held responsible for them.

Figure 4-3: A VVR-M2 type triple fuel element.

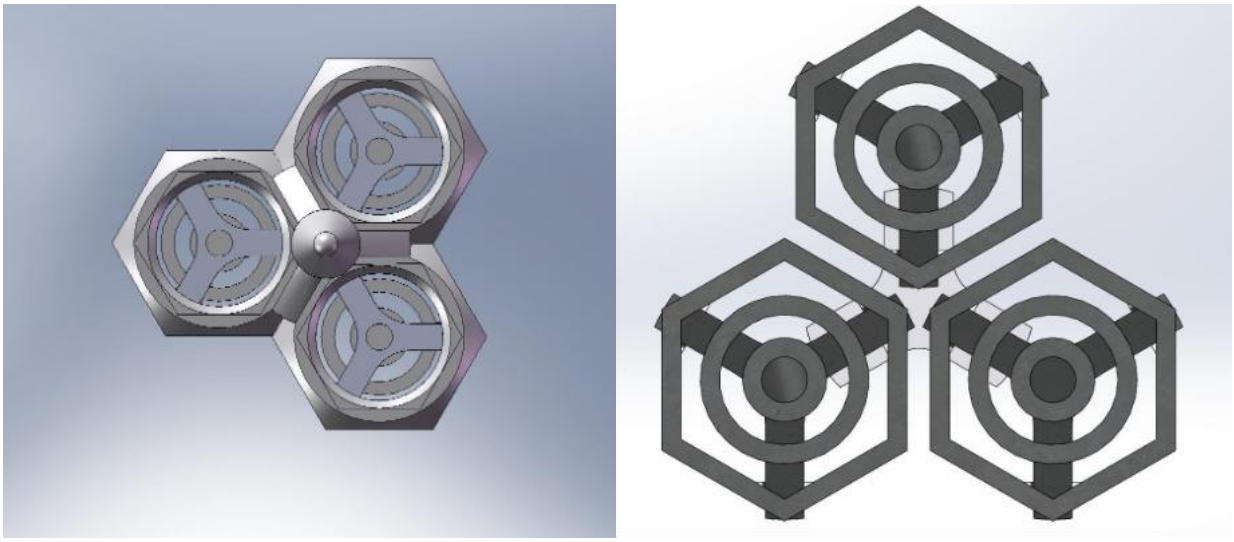

Figure 4-4: Cross-cut view of the tripe WWR-M2 fuel element.

Funded by the European Union

Funded by the European Union. Views and opinions expressed are however those of the author(s) only and do not necessarily reflect those of the European Union or the European Atomic Energy Community ('EC-Euratom'). Neither the European Union nor the granting authority can be held responsible for them.

4.1.4.3. Zone layout

The structure of the zone is illustrated in Figure 4-5.

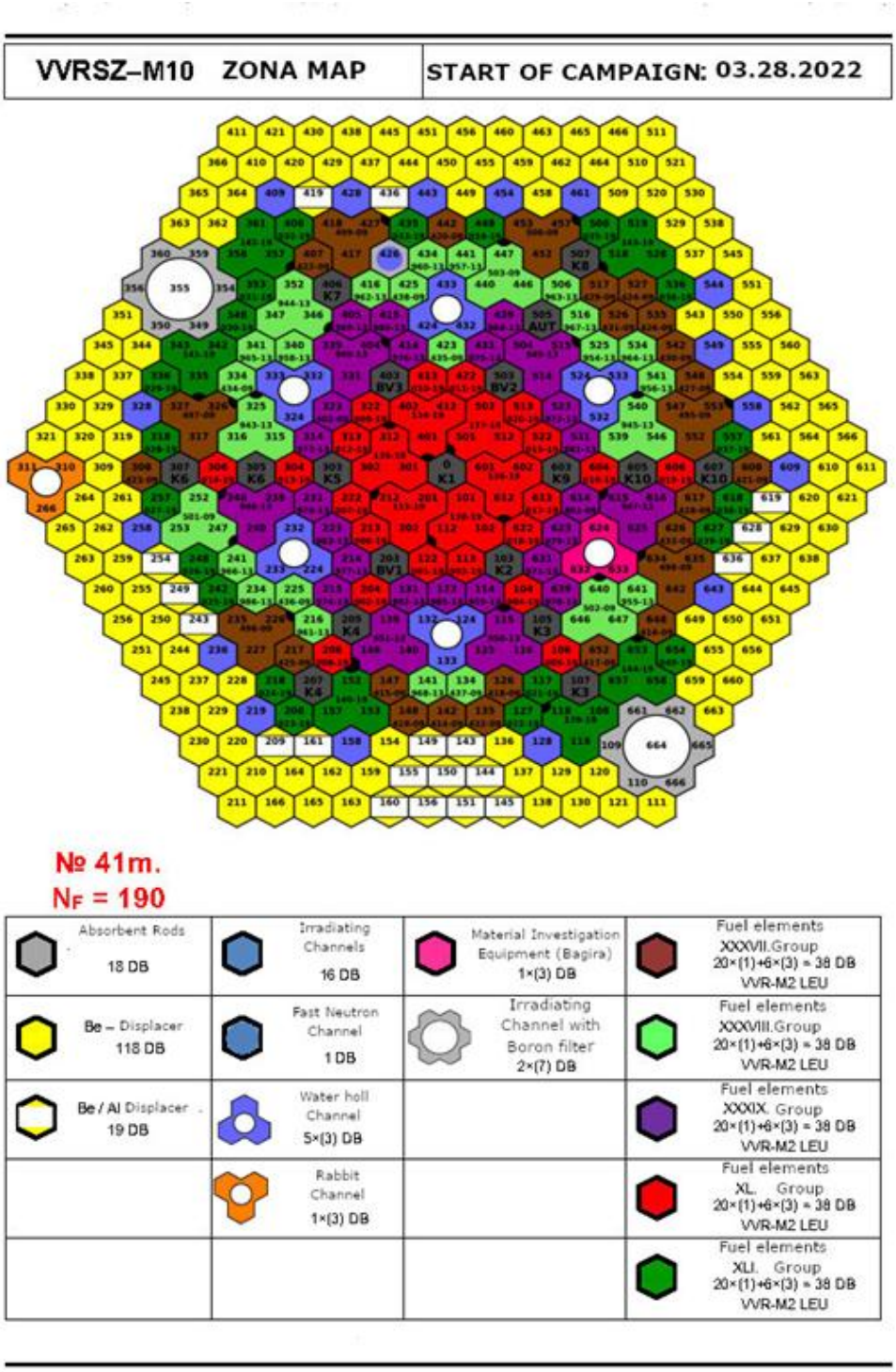

Figure 4-5: The reactor zone map.

Funded by the European Union

Funded by the European Union. Views and opinions expressed are however those of the author(s) only and do not necessarily reflect those of the European Union or the European Atomic Energy Community ('EC-Euratom'). Neither the European Union nor the granting authority can be held responsible for them.

4.1.4.4. Beryllium

The grid supporting the active zone contains 397 hexagonal cells with a 35 mm pitch, surrounded by a reflector made of metal-beryllium segments. Within the reflector shroud, beryllium elements with the same geometry as the fuel elements are placed in some cells, which allows for easy replacement of the beryllium elements subject to the highest burn-up (4×10^{22} n/cm^2 integral fast-neutron flux is the limit at which they need to be replaced).

4.1.4.5. Beryllium reflector

The beryllium reflector (Figure 4-6) consists of 17 interlocking elements. The dimensions of each element were determined by the nuclear requirements of the reflector, the manufacturing capabilities and their mounting location.

The reflector elements are divided in such a way that they can be mounted radially on the ends of the channels extending into the zone basket. Aluminium segments are bolted to the lower plane of each beryllium element. The aluminium segments orient the beryllium in position within the zone basket.

The top plane of the beryllium reflector is sealed by an aluminium ring, which has been modified to create a large diameter silicon irradiation site. The ring is fixed to the beryllium elements by screws. The ring orients the reflector to match the inner diameter of the zonal basket.

The beryllium elements surrounding the cold neutron channel and the tangential channel are in a beryllium enclosure mounted on the zone tank. Channels for water cooling are formed on the surface of the beryllium elements. The elements are provided with threads at accessible locations for mounting and gripping.

The beryllium reflector elements must be installed in a particular installation sequence.

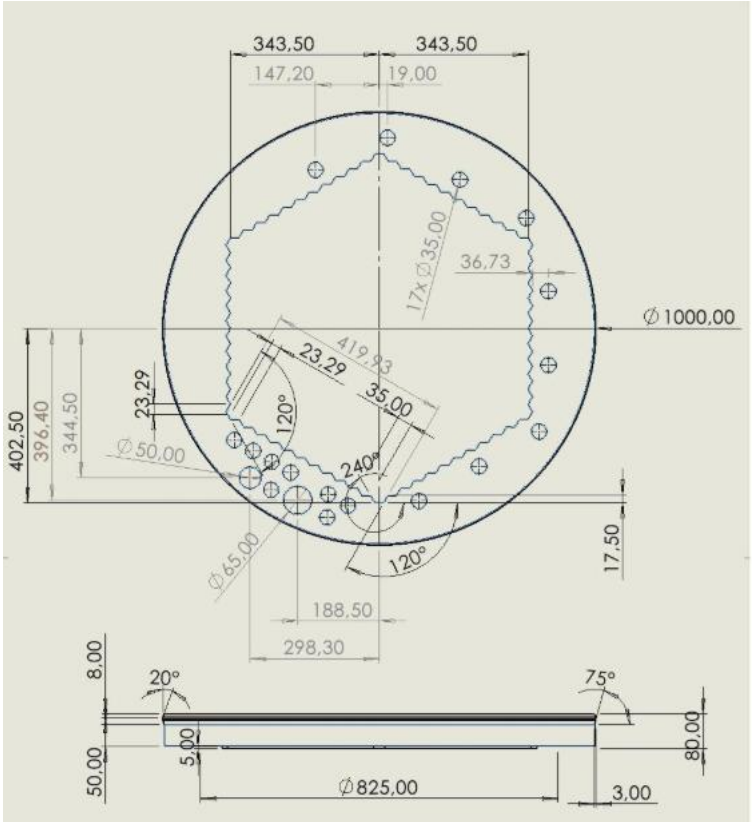

Figure 4-6: The beryllium reflector around the core.

Funded by the European Union

Funded by the European Union. Views and opinions expressed are however those of the author(s) only and do not necessarily reflect those of the European Union or the European Atomic Energy Community ('EC-Euratom'). Neither the European Union nor the granting authority can be held responsible for them.

4.1.4.6. Vertical channels

The active zone can accommodate 51 vertical irradiation channels. 46 are currently in use. These are:

- 13 irradiation channels
- 1 fast neutron channel
- 5 x (3) water hole channels
- 1 x (3) pieces of tube mail
- 1 x (3) material testing channels
- 2 x (7) Boron filtered irradiation channels

4.1.4.7. Horizontal (Radial) channels

Starting from the centre of the Zone (Figure 4-7). ten horizontal channels are arranged radially around the reactor. These are:

- 3 radial channels (NA 100) I., II., III.
- 2 radial channels (NA 100) (fast) IV., V.
- 3 radial channels (NA 60) VI., VII., VIII.
- 1 tangential channel (NA 100) IX.
- 1 cold neutron channel. (Tangential channel NA 100) X.

They continue through the reactor wall and into the heavy concrete biological shielding surrounding the reactor vessel. Each horizontal channel terminates in a channel lock that rotates along its horizontal axis. Detailed dimensions are available via the core CAD drawing.

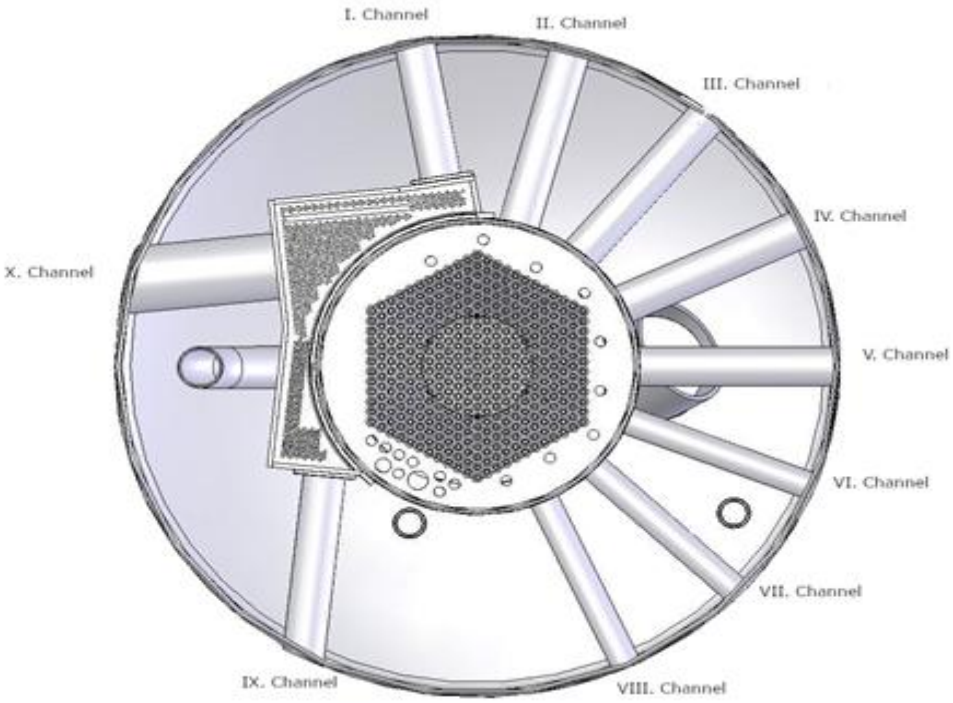

Figure 4-7: Arrangement of horizontal channels around the core.

4.1.4.8. Regulating and Safety Protection (absorbent) rods

The absorber rods are identical in both material and construction to those used before the reconstruction, which occurred between 1986-1992, with 17 rods of neutron absorbing material of 50 - 150 µm natural boron carbide pressed to a density of ~1.6 g/cm3 and 25 mm in diameter, about 100 mm longer than the uranium section of the fuel elements. In this way, at the lower end of the rod the boron carbide charge extends 5 cm

Funded by the European Union

Funded by the European Union. Views and opinions expressed are however those of the author(s) only and do not necessarily reflect those of the European Union or the European Atomic Energy Community ('EC-Euratom'). Neither the European Union nor the granting authority can be held responsible for them.

above the uranium charge of the fuel element at the top and bottom (the upper and lower end positions of the absorbent rods are shown in Figure 4-8).

The boron carbide is enclosed in an aluminium tube, hermetically sealed by electron beam welding, with a bayonet-locking head at one end to connect it to the intermediate piece that moves the rod.

The automatic power control rod is identical in construction to the one described above, however steel is used as a neutron absorber throughout the rod's diameter.

The guide tubes of the safety rods and control rods are filled with water. The individual positions of the control and safety rods are shown in Figure 4-8.

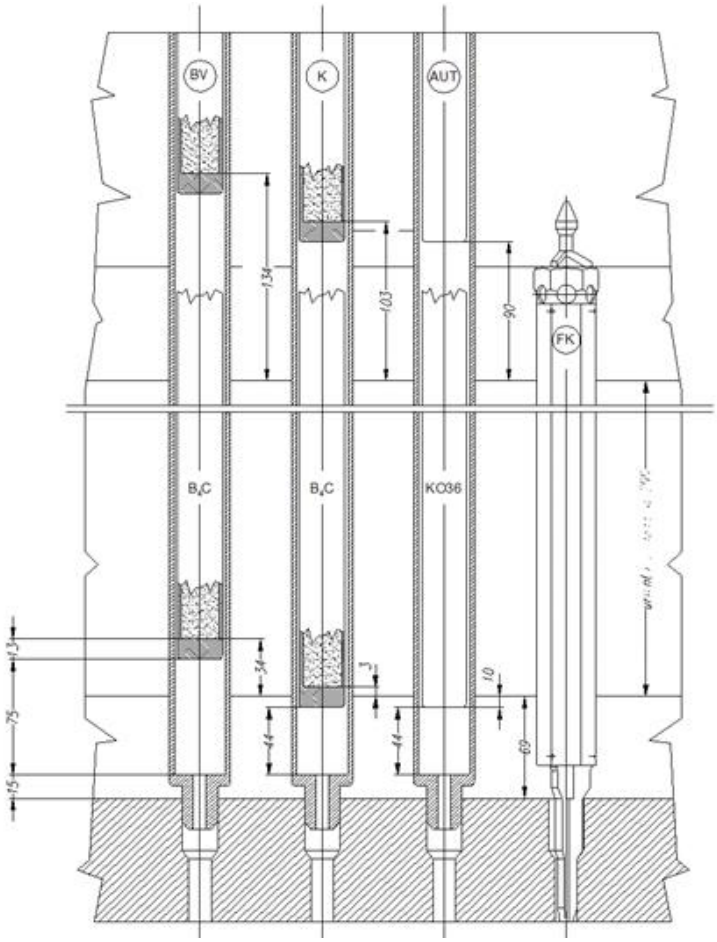

Figure 4-8: The vertical positions of the control and safety rods.

Table 4-2: Grouping and value of control rods before and after modification of core loading #41m.

No. 41m. End of cycle 14				No 41m. Beginning of cycle 15		Relative uncertainty [%]	
Position	Rod	Aut. Min. 1	10 MW1	Aut. Min. 2	10 MW2	Aut. min	10 MW
0	K1	2.808	2.777	2.808	2.808	0.0	-1.1
103	K2	2.111	2.146	2.087	2.123	1.2	1.1
105/107	K3	1.493	1.573	1.411	1.519	5.8	3.5

Funded by the European Union

Funded by the European Union. Views and opinions expressed are however those of the author(s) only and do not necessarily reflect those of the European Union or the European Atomic Energy Community ('EC-Euratom'). Neither the European Union nor the granting authority can be held responsible for them.

205/207	K4	2.511	2.345	2.386	2.262	5.2	3.7
303	K5	2.628	2.451	2.652	2.470	-0.9	-0.8
305/307	K6	1.976	1.845	1.980	1.863	-0.2	-1.0
406	K7	1.170	0.955	1.183	0.977	-1.1	-2.2
507	K8	1.205	0.964	1.213	0.982	-0.7	-1.8
603	K9	2.160	2.124	2.160	2.120	0.0	0.2
605/607	K10	1.698	1.688	1.662	1.681	2.2	0.5
203/503/403	BV (1+2+3)	6.907	6.741	6.939	6.827	-0.5	-1.3
505	AUT	0.680	0.561	0.689	0.572	-1.3	-2.0
0	K1	2.808	2.777	2.808	2.808	0.0	-1.1
103	K2	2.111	2.146	2.087	2.123	1.2	1.1
105/107	K3	1.493	1.573	1.411	1.519	5.8	3.5
205/207	K4	2.511	2.345	2.386	2.262	5.2	3.7
505	AUT	0.680	0.561	0.689	0.572	-1.3	-2.0

auto. min.1: Cold, non-toxic condition, inner curtain **0** cm, outer curtain: **49.90** cm
10 MW1: Warm start condition, inner curtain: **21.20** cm, outer curtain: **60** cm
auto. min.2: Cold. non-toxic condition, inner curtain: **0** cm,outer curtain: **51.10** cm
auto. min.2: Warm start condition, inner curtain: **22.20** cm, outer curtain: **60** cm

where non-toxic conditions imply that the reactor was not operational for roughly 40 h prior to the experiment, so no significant reactivity effects due to xenon and samarium poisoning are present.

Table 4-3: Reactivity data after modification

Date	Rod position [cm]											Reactivity reserve [$]
	K1	K2	K3	K4	K5	K6	K7	K8	K9	K10	AUT	
Nov. 29th, 2022	18.8	18.8	70	70	18.8	70	70	70	18.8	70	30	7.68

4.1.5. Composition of materials

To determine the material composition of the fuel elements, the files generated by the KIKO3D program (Keresztúri et al., 2003) are used in the BREKI program, which produces the KIKOBURN.out inventory file. This contains the data of all the fuel elements included in the campaigns so far.

Funded by the European Union

Funded by the European Union. Views and opinions expressed are however those of the author(s) only and do not necessarily reflect those of the European Union or the European Atomic Energy Community ('EC-Euratom'). Neither the European Union nor the granting authority can be held responsible for them.

4.2. Experiments

4.2.1. Experiment 1: Axial Flux measurement in the fast channel of BRR

4.2.1.1. Introduction

Regular axial-flux experiments are conducted using neutron activation analysis (Section 2.1) at only 3 positions in the irradiation channels, primarily to characterise the thermal neutron flux over the full 60 cm length of the fuel elements in a fast-flux irradiation channel (number 426 in Figure 4-5) decided to measure continuous axial flux for the complete 60 cm length of the fuel elements in a fast-flux irradiation channel. To squeeze the water out of the channel would provide better measurement of fast flux component for modelling.

4.2.1.2. Quantity of interest. measurement technique. measurement procedure. Etc

Our primary interest is to develop high quality models for calculation of the neutron flux in the irradiation channels with the highest possible accuracy. This may give a good validation possibility to high fidelity models for power reactors.

Since the measurement circumstances are more complicated in a 10 MW research reactor than in the low-power teaching reactors, squeezing the water out of the irradiation channel cannot be done with one 60 cm long cylindrical sealed container; we had to use a maximum of 20 cm long sealed Al containers to place the activation wires in them. Furthermore, to sink the container under the water lead weight must be put at the bottom of it. To be able to remove the containers from the working reactor, proper handle must be built on top of the container, as shown in Figure 4-9a. Figure 4-9b showcases the photo of the three Al frames with the Fe wires. The weights of the frames and the Fe wires are handwritten. These frames were then placed in sealed Al tubes with 20 cm total length each. The length of the wires was about 16.2 cm. The AlAu(110 pm) wires with a diameter of 0.1 mm were also placed in the Al frames. The Fe wires were high-purity iron 99.99% with a diameter of 0.1 mm.

a)

b)

Figure 4-9: a) Demonstration sealable tube with handle for irradiation samples on the right. On the left, a lead disk is shown, which helps to sink the sealable tube in the water. In b), on the right, the Al frames with Fe wires are shown.

The wires' characteristics are summarised in Table 4-4.

Funded by the European Union

Funded by the European Union. Views and opinions expressed are however those of the author(s) only and do not necessarily reflect those of the European Union or the European Atomic Energy Community ('EC-Euratom'). Neither the European Union nor the granting authority can be held responsible for them.

Table 4-4: Characteristics of the neutron activation wires.

Wire	Mass (g)	dMass	Mass Al	Diame-ter (cm)	Number of atoms(a) 54Fe / Al/ cm	Rel unc %	Number of atoms(b) 58Fe/Au/cm	Rel unc %
Fe-1	0.072	0.0003		0.025	2.436E+18	1.08%	2.1894E+18	1.08
Fe-2	0.0714	0.0003		0.025	2.436E+18	1.08%	2.1712E+18	1.08
Fe-3	0.0734	0.0003		0.025	2.436E+18	1.08%	2.2320E+18	1.08
AlAu-1	0.0149	0.0003	0.014898	0.02	1.893E+19	2.25%	5.0111E+15	2.27
AlAu-2	0.0149	0.0003	0.014898	0.02	1.893E+19	2.25%	5.0111E+15	3.01
AlAu-3	0.0145	0.0003	0.014498	0.02	1.893E+19	2.30%	4.8766E+15	3.01

The irradiation of the three pairs of wires in three containers lasted 58, 60 and 62 minutes for the tubes numbered 3, 2 and 1, respectively, on the 5th of November 2025. Of course, the bottom tube, number 1, spent more time in the fast channel number 426 (see Figure 4-5). After the activation periods, the tubes were transferred to the reactor's hot chamber. After a few days' decay period, the wires were taken to the measurement station.

In the meantime, the acquisition system was set up using the 13% efficient HPGe detector of the low-level counting system in the Neutron Guide Hall of the BRR. For scanning the activated wires, a programmable moving table has been purchased and configured to perform automated experiments in conjunction with a DSA2001 Multi Channel Analyser. Photos of the setup are shown in Figure 4-10.

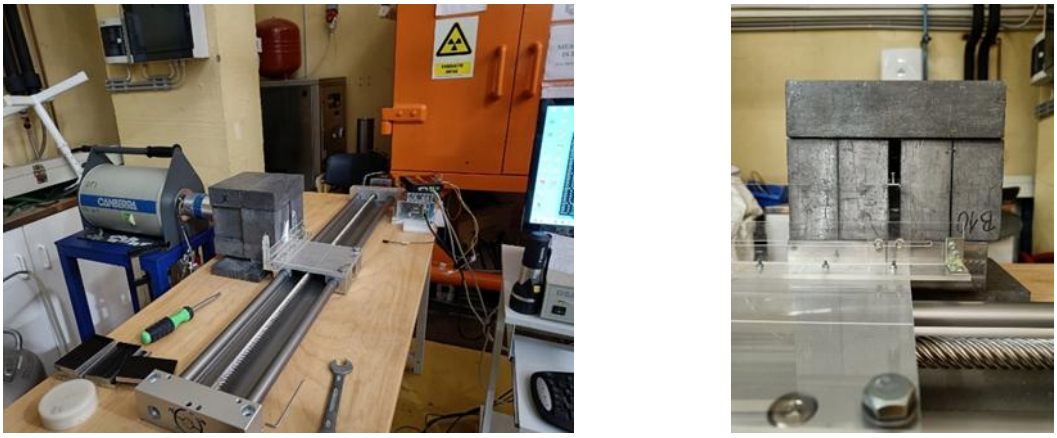

Figure 4-10: (Left) HPGe detector with lead shielding, moving table with measuring frame, (right) and 10 mm slit in lead collimator in front of the HPGe.

Using this setup, sixteen gamma spectra were acquired by applying 1 cm steps from the lower end of the wire in the fast activation channel 426. Altogether 48 gamma spectra were acquired in 1 or 1.5 hours. In addition to these measurements, calibration experiments were performed with ^{60}Co, ^{133}Ba, ^{152}Eu and ^{226}Ra sources, and a long room background spectrum was taken. These spectra were evaluated using the in-house developed Hypermet PC gamma spectrum fitting software (Fazekas et al., 1997). An example of the activated and room background spectra is shown in Figure 4-11.

Funded by the European Union

Funded by the European Union. Views and opinions expressed are however those of the author(s) only and do not necessarily reflect those of the European Union or the European Atomic Energy Community ('EC-Euratom'). Neither the European Union nor the granting authority can be held responsible for them.

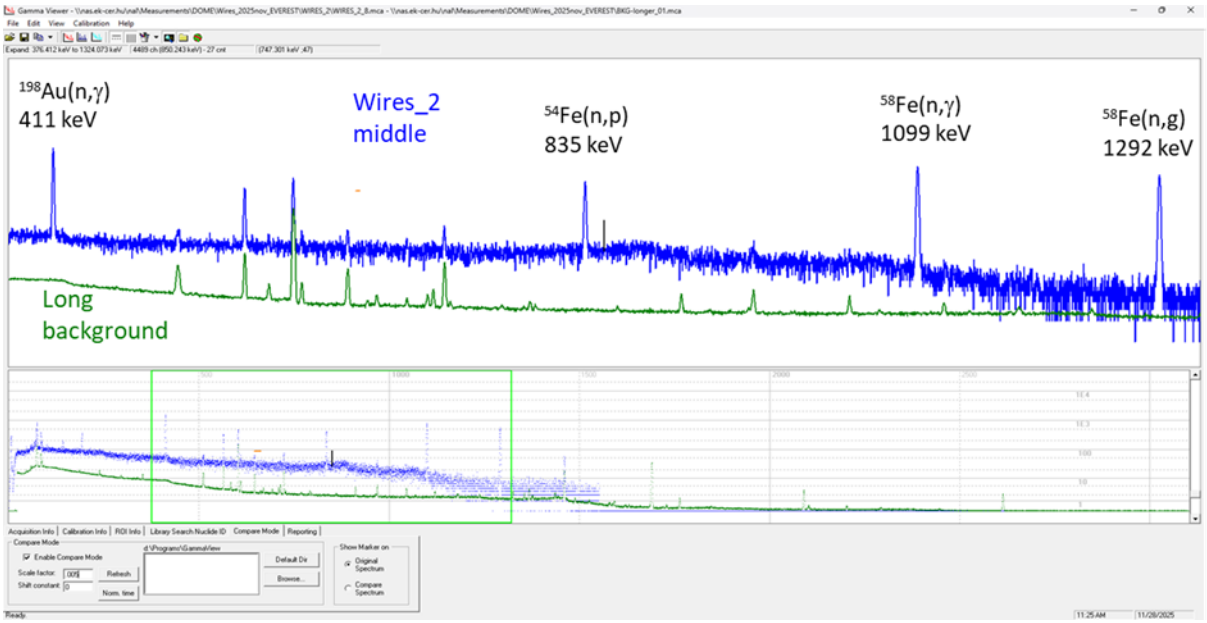

Figure 4-11: Example spectra with labelled gamma-peaks from the activated wires with the reactions that produced the emitting daughter isotopes

The evaluations of the peak-area tables were performed in Excel files using VBA macros to automate repetitive tasks. The measured peak area T carries the information on the number of daughter atoms created in the neutron reaction that acted on the parent atoms. In the case of the natural Fe wire, the ^{54}Fe(n,p)^{54}Mn and the ^{58}Fe(n,γ)^{59}Fe reactions provide sufficiently long-lived daughter nuclei. In case the AlAu(110 ppm±2) wire, only the ^{197}Au(n,γ)^{198}Au reaction yielded measurable activity in our case.

Since the 1 cm-wide slit in the Pb shielding is not perfect, we must remove it for every measured position to provide the number of atoms in the measured section and make the correction absolute. Of course, it depends on the measure of activation for each section that we are trying to determine, thus it leads to a set of linear equations that must be solved. This process is still under development.

Figure 4-12 shows some preliminary results of the daughter creation rate without the above-mentioned corrections. The iron wire was broken during the tube opening process on the set of 3 wires; thus, its activity dropped to 0 above the 54 cm position. The fitting function is a cosine with an amplitude, a scaled position and a shift in its argument. In the fit, only the amplitudes were changed from curve to curve; the other two parameters were constant with a 3 cm shift to the left, and the maximum became around 27 cm.

Funded by the European Union

Funded by the European Union. Views and opinions expressed are however those of the author(s) only and do not necessarily reflect those of the European Union or the European Atomic Energy Community ('EC-Euratom'). Neither the European Union nor the granting authority can be held responsible for them.

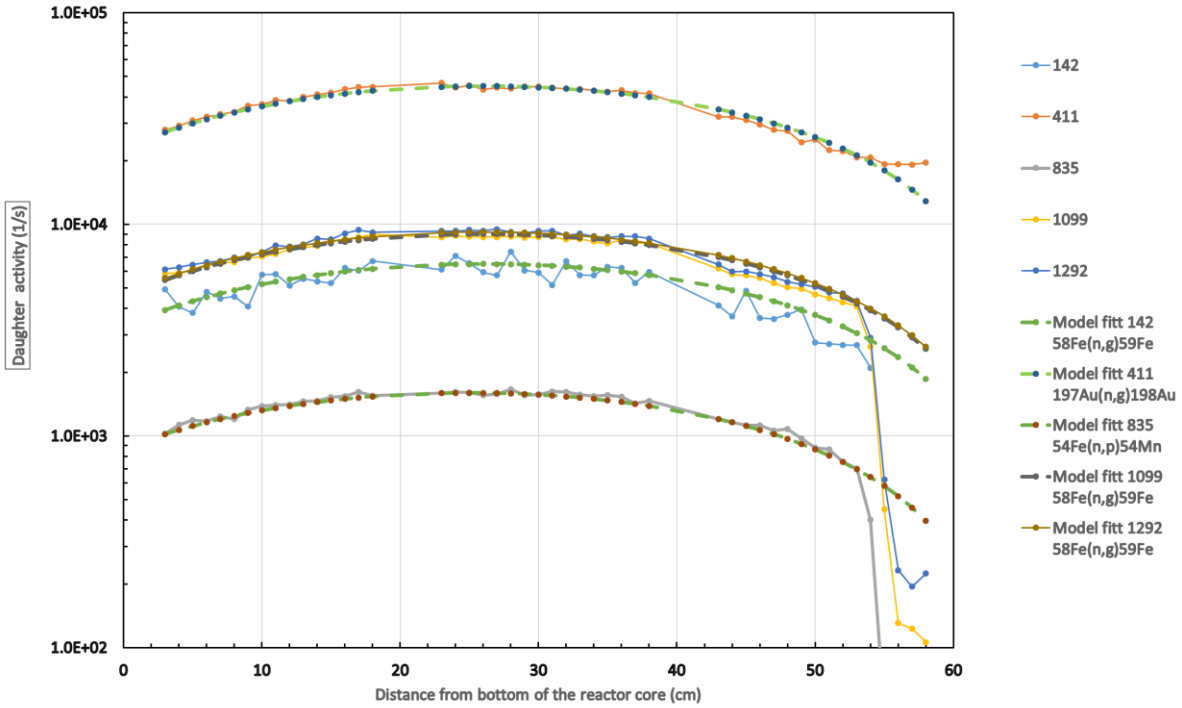

Figure 4-12: Daughter creation rate without corrections

Calculations were performed using an MCNP model for the possible changes that must be made. Figure 4-13 presents the result of efficiencies at several energies, including five shown in Figure 4-12.

The spatial integral of the efficiency provides a better view for the imperfect nature of the Pb slit and the amount of the needed correction (see Figure 4-13). Before we go to the explanation it is important to note the presented curve can be mirrored on the Y axes to the negative distances on the horizontal axes. We are interested in obtaining the detected peak area only in the (–0.5 cm, 0.5 cm) region, but we detect the total that includes the rest of the length of the wire. Furthermore, the activity along the wire length is changing, which is not known yet. Thus, the solution of the correction for the imperfect slit should involve the solution of a linear equation system. It should contain the unknown activity of the wire pieces. It can be modelled with 1 cm pieces in which we are interested in.

Funded by the European Union

Funded by the European Union. Views and opinions expressed are however those of the author(s) only and do not necessarily reflect those of the European Union or the European Atomic Energy Community ('EC-Euratom'). Neither the European Union nor the granting authority can be held responsible for them.

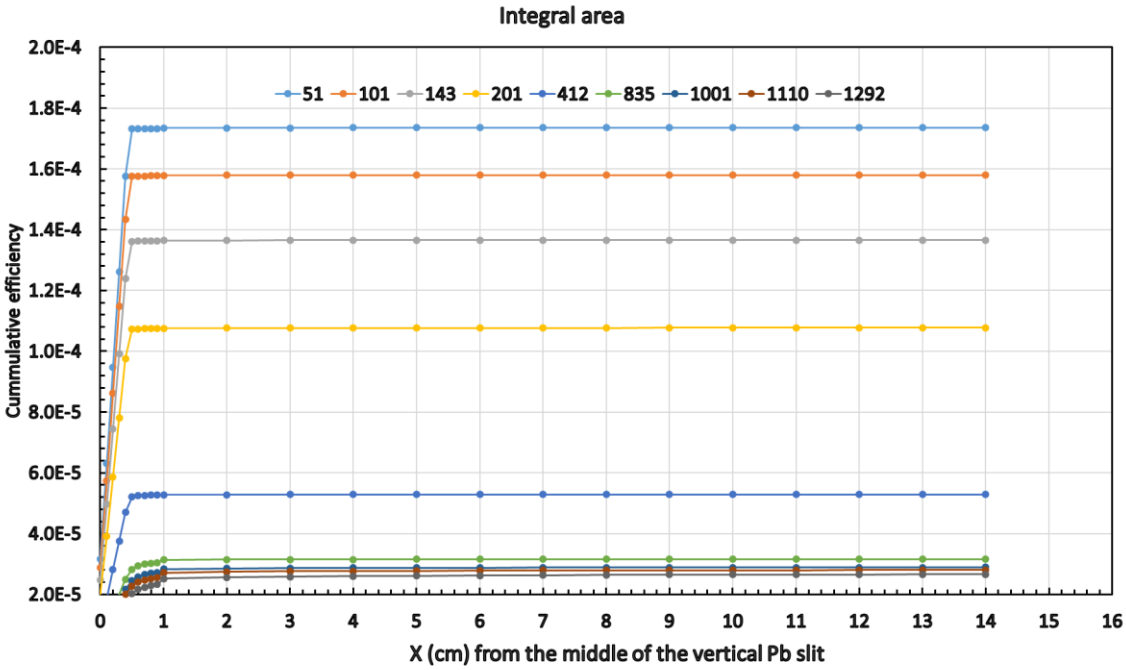

Figure 4-13: Cumulative efficiency vs. distance from the slit centre.

Nevertheless, it is also worthwhile to look the model geometry, showcased in Figure 4-14, for study of full energy peak efficiency at different position of the source.

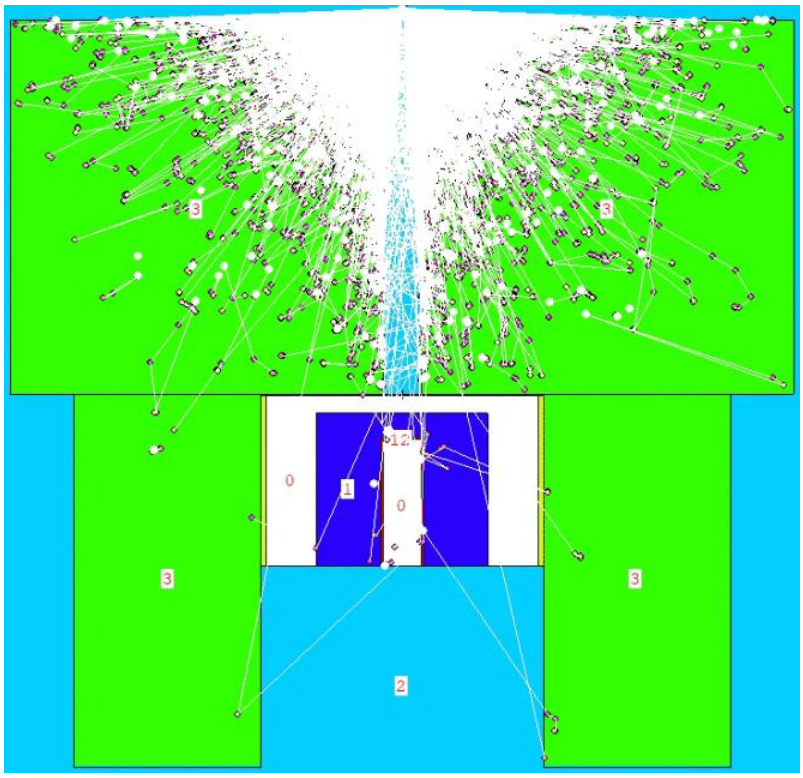

Figure 4-14: Particle tracks of 1292 keV gamma rays middle-toped from a source at middle-top of the white area. The detector is in dark blue, while the lead shielding is in green, the light blue is air, and the white is vacuum.

Funded by the European Union

Funded by the European Union. Views and opinions expressed are however those of the author(s) only and do not necessarily reflect those of the European Union or the European Atomic Energy Community ('EC-Euratom'). Neither the European Union nor the granting authority can be held responsible for them.

5. JSI TRIGA reactor

5.1. Facility overview

The JSI TRIGA Mark II reactor is a pool-type research reactor with the maximum steady-state reactor power of 250 kW cooled by natural convection. The reactor core is placed inside a 6.25 m high open tank with a diameter of 1.98 m. The core is submerged some 4.9 m below the water level as shown in Figure 5-1 and is surrounded by a graphite reflector, as shown in Figure 5-2. The reactor pool is lined with aluminium liner, and is surrounded by a heavy concrete biological shielding, which also allows for access to several ex-core irradiation facilities:

- Horizontal irradiation ports, with inner diameter of 15 cm:
  - Tangential irradiation port, which passes the core within the graphite reflector tangentially.
  - Thermal irradiation port, passing through a large graphite Thermal Column.
  - Radial Beam Irradiation port, extending radially outwards from the core's reflector
  - Radial piercing port, extending from the core, through the graphite reflector outwards
- A larger empty Thermalizing Column room – the Dry Chamber facility, used for irradiation of larger assemblies.

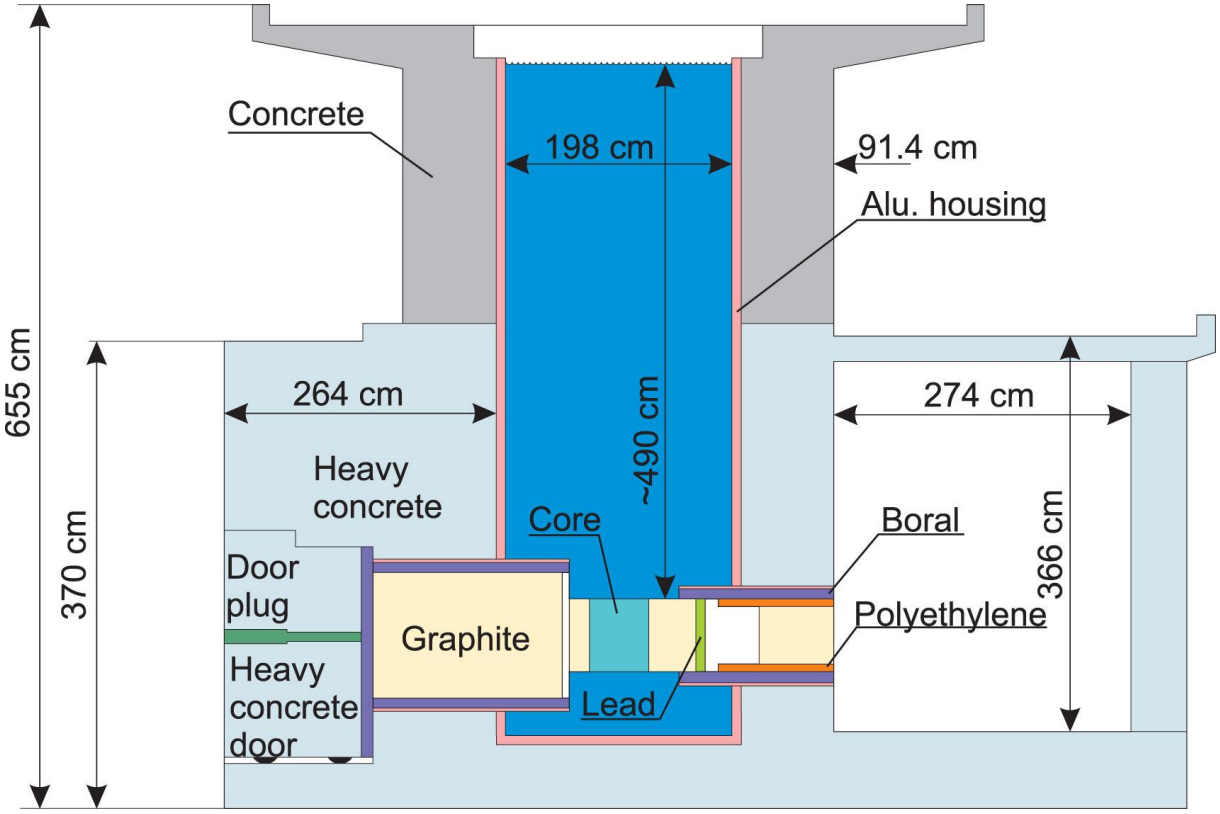

Figure 5-1: Side view of the JSI TRIGA reactor and irradiation ports.

Funded by the European Union

Funded by the European Union. Views and opinions expressed are however those of the author(s) only and do not necessarily reflect those of the European Union or the European Atomic Energy Community ('EC-Euratom'). Neither the European Union nor the granting authority can be held responsible for them.

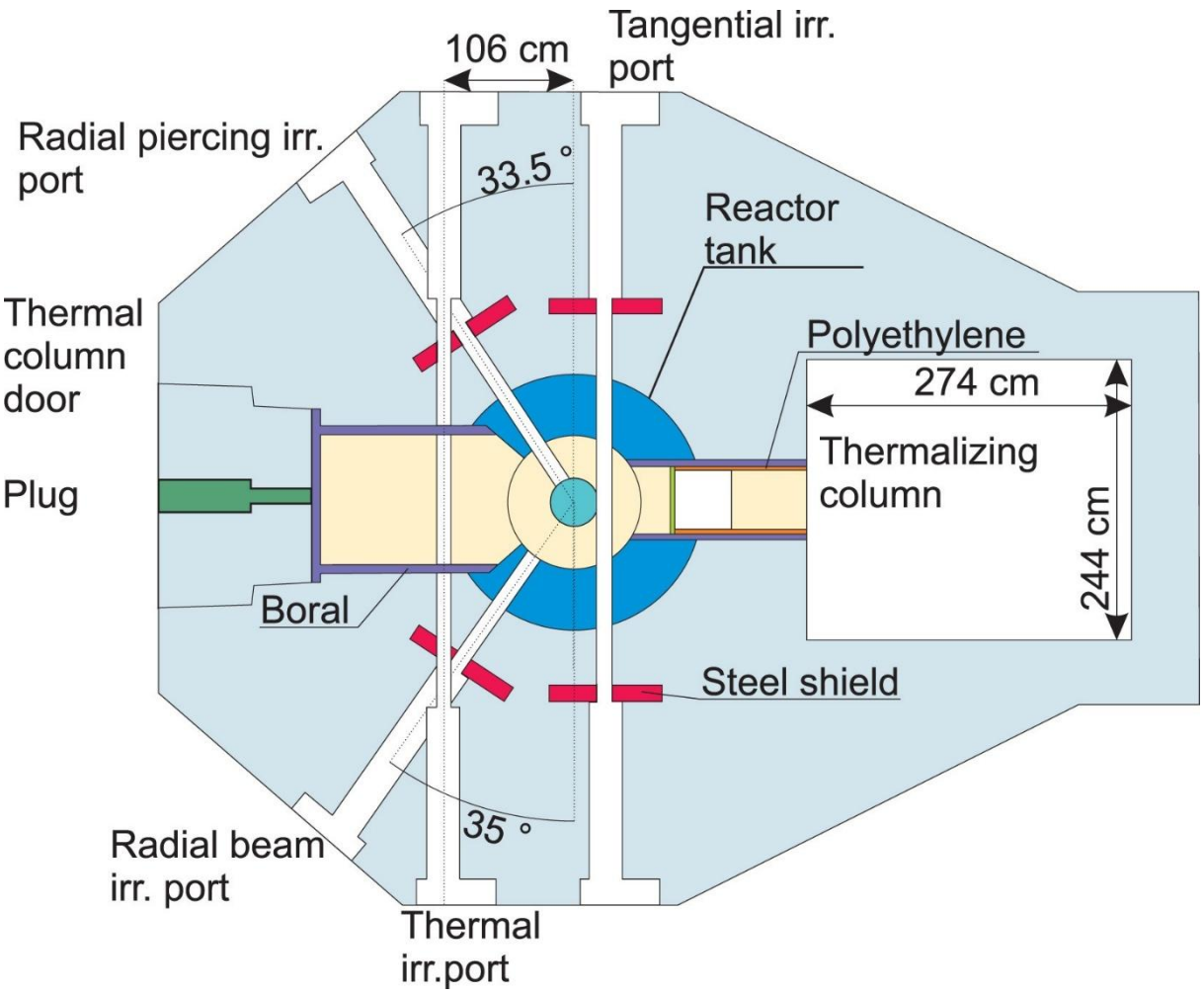

Figure 5-2: Top view of the JSI TRIGA reactor.

The reactor core consists of 91 in-core positions arranged in concentric rings (A-F), which can be filled either with a neutrons source, an irradiation position channels or a fuel element (Figure 5-3), schematically shown in Figure 5-4.

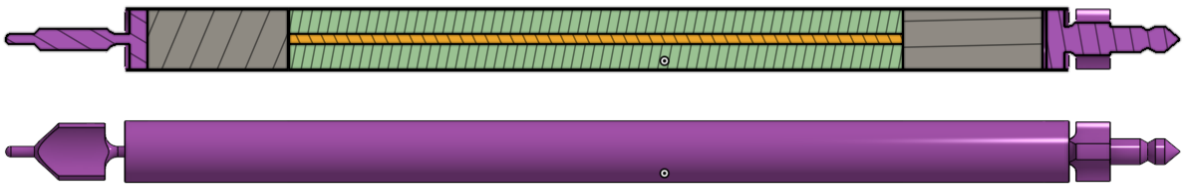

Figure 5-3: CAD drawing of the JSI TRIGA fuel element. Left: bottom pin, Right: top pin.

Funded by the European Union

Funded by the European Union. Views and opinions expressed are however those of the author(s) only and do not necessarily reflect those of the European Union or the European Atomic Energy Community ('EC-Euratom'). Neither the European Union nor the granting authority can be held responsible for them.

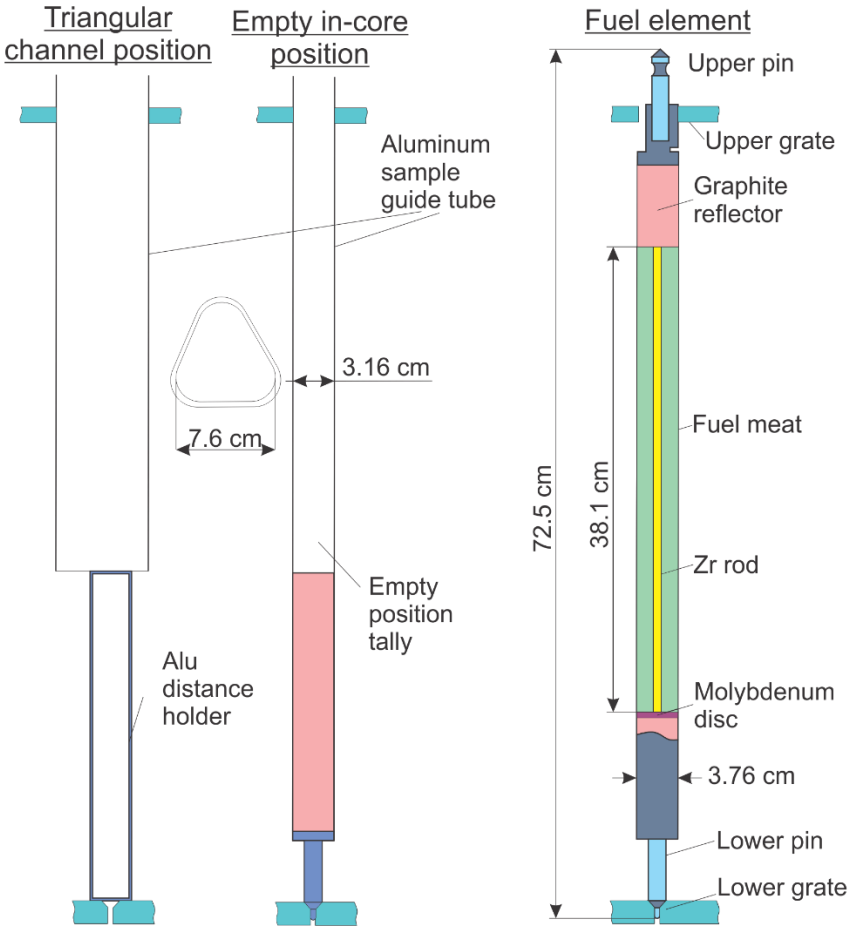

Figure 5-4: Schematic view of the JSI TRIGA fuel element, as well as standard and Triangular in-core irradiation positions.

Four positions are taken by the control rods, where 3 are equipped with a fuel follower i.e. top part of the rod has a B_4C neutron absorber, and the bottom is equipped with U-ZrH fuel, which displaces the neutron absorber as the rod is withdrawn from the core. The fourth control rod does not have a fuel-follower, but is equipped with a rapid ejection system using compressed air enabling reactor's pulse operation. Both control rod types are schematically shown in Figure 5-5.

Six positions in rings D and E are separated by two top-grid inserts and can be merged together to constitute two triangular openings. In-between the fuel positions, there is also an arrangement of holes ranging from 6 to 10 mm in diameter, for insertion of instrumentation and small samples. The fuel elements are held in position the bottom and top aluminium grid plates (Figure 5-8). It should be noted that the core configuration is changed on various occasions including individual experimental campaigns. An example of in-core fuel and measurement positions with relevant radii in cm shown in Figure 5-6.

Funded by the European Union

Funded by the European Union. Views and opinions expressed are however those of the author(s) only and do not necessarily reflect those of the European Union or the European Atomic Energy Community ('EC-Euratom'). Neither the European Union nor the granting authority can be held responsible for them.

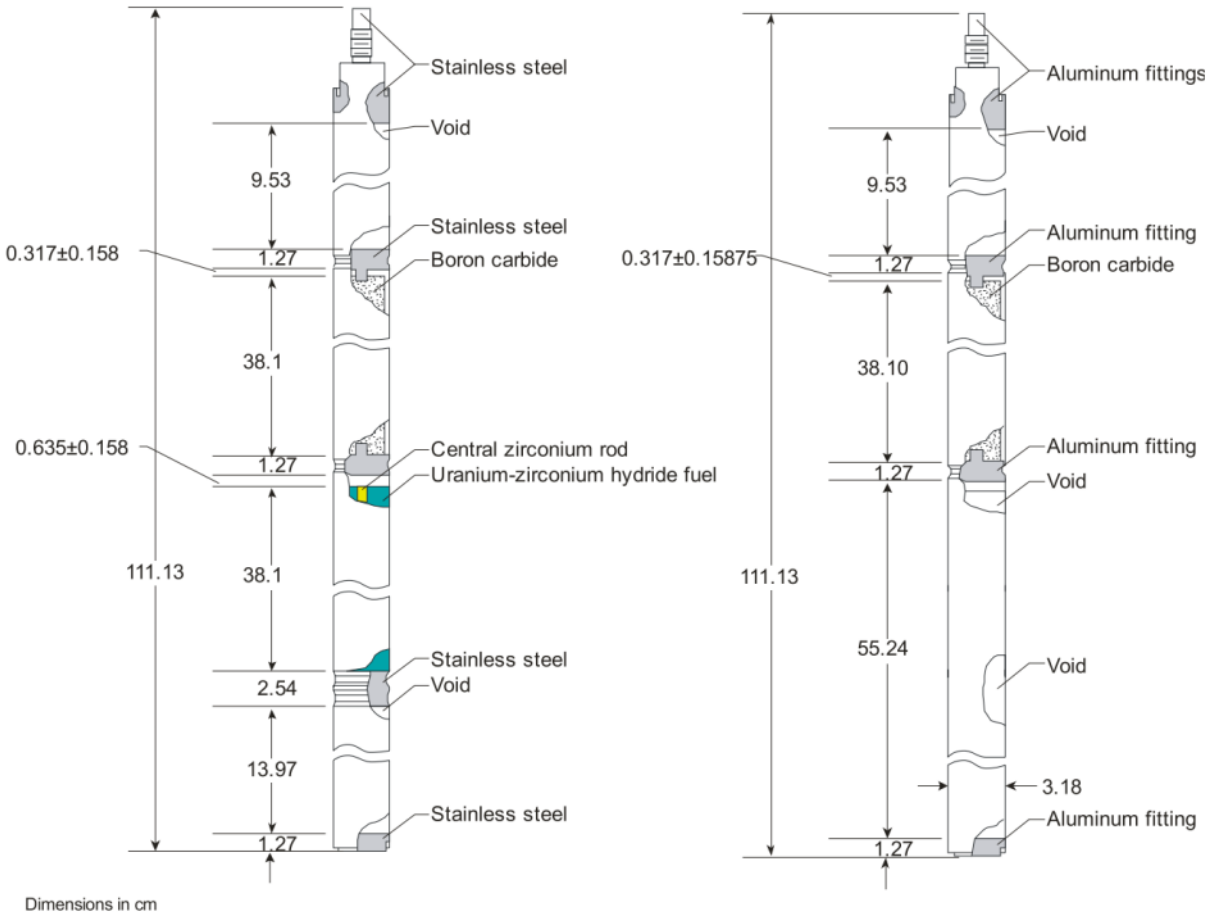

Figure 5-5: JSI TRIGA reactor control rods. Left: control rod with fuel follower. Right: a control rod without the fuel follower. Measurements are in cm.

The core is surrounded by a thick graphite reflector, equipped with a cylindrical channel, which holds the Carousel irradiation facility with 40 individual irradiation positions evenly spaced around the core, which can be rotated to the desired position. The graphite extends from the reflector outwards into two directions, leading to the Thermal and Thermalizing column and the Dry chamber irradiation facilities, as shown in Figure 5-1 and Figure 5-7.

Funded by the European Union

Funded by the European Union. Views and opinions expressed are however those of the author(s) only and do not necessarily reflect those of the European Union or the European Atomic Energy Community ('EC-Euratom'). Neither the European Union nor the granting authority can be held responsible for them.

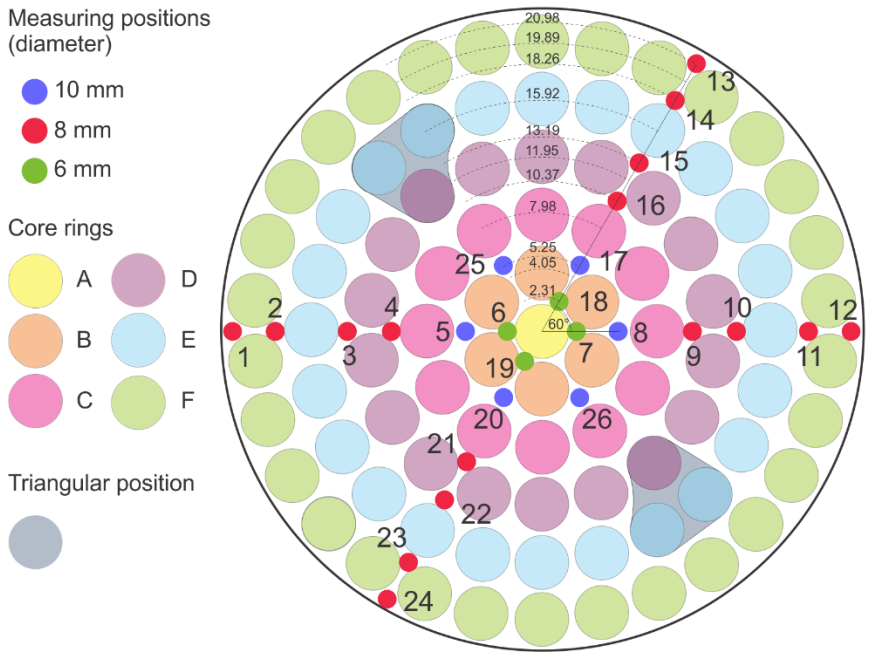

Figure 5-6: The schematic of the JSI TRIGA core loading positions and measuring positions (MPs) along with their distances from centre and numbers.

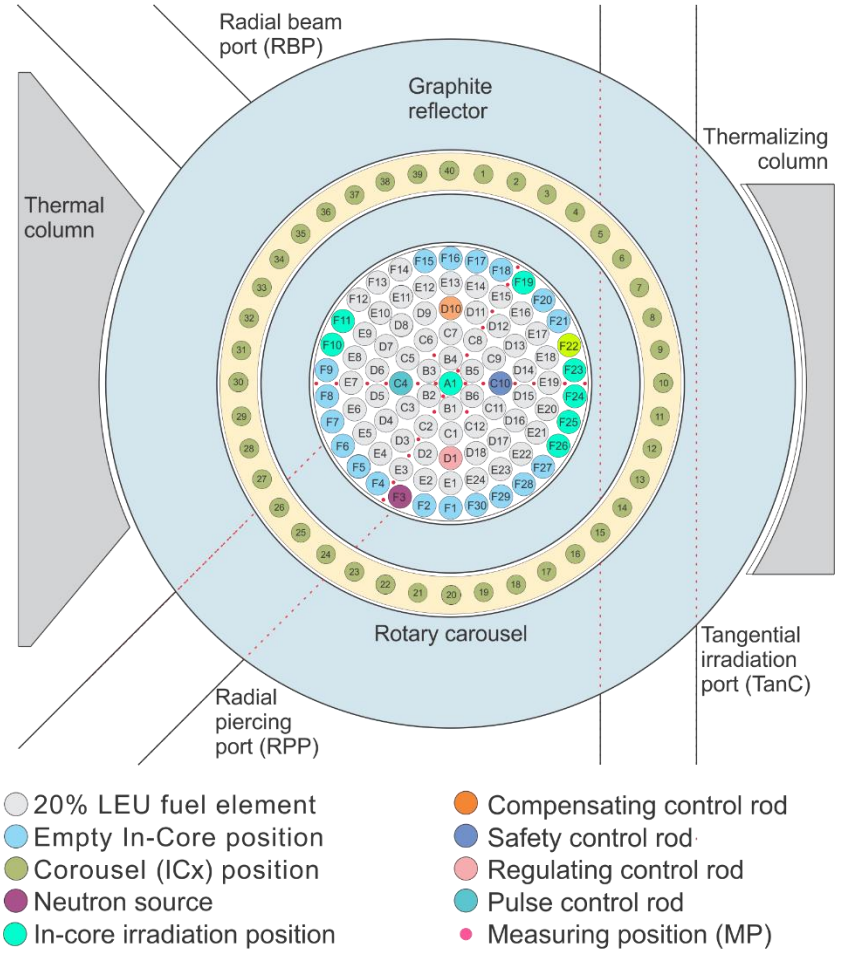

Figure 5-7: Typical reactor core configuration with the graphite reflector and the Rotary carousel facility; schematics of immediate horizontal irradiation facilities, as well as thermal and thermalizing column graphite stacks.

Funded by the European Union

Funded by the European Union. Views and opinions expressed are however those of the author(s) only and do not necessarily reflect those of the European Union or the European Atomic Energy Community ('EC-Euratom'). Neither the European Union nor the granting authority can be held responsible for them.

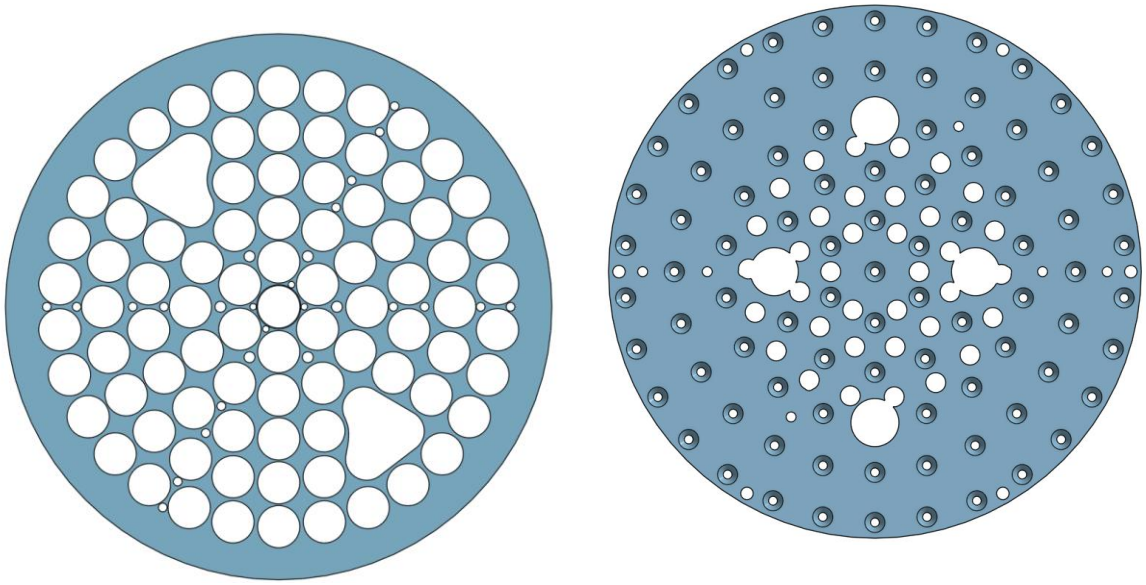

Figure 5-8: Top (left) and bottom (right) core grids made of Al6061 alloy, thickness of 0.75 inch or 1.905 cm. Distance between the plate bottom surfaces is 26.25 inches or 66.675 cm.

A detailed CAD drawing of the core structure, graphite reflector, carousel and horizontal irradiation ports: Piercing and Tangential port are shown in Figure 5-9. Detailed CAD drawing of the entire facility are available on request.

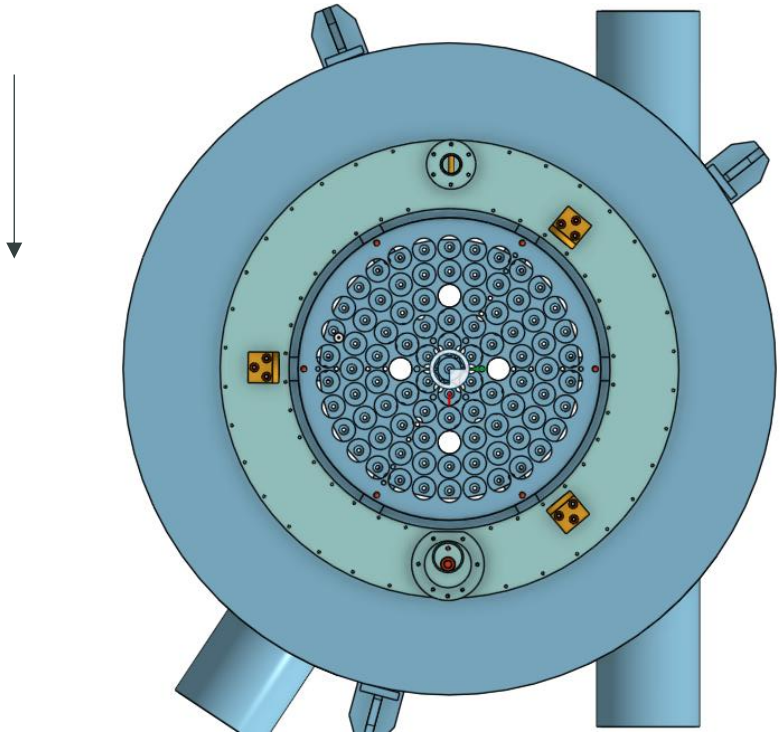

Figure 5-9: Detailed CAD drawing of the core, reflector, carousel and the tangential and piercing irradiation port, with the arrow pointing in the north direction.

Funded by the European Union

Funded by the European Union. Views and opinions expressed are however those of the author(s) only and do not necessarily reflect those of the European Union or the European Atomic Energy Community ('EC-Euratom'). Neither the European Union nor the granting authority can be held responsible for them.

5.2. Reactor power determination and calibration

The reactor power in the JSI TRIGA reactor is measured by a number of boron and ionization chambers, which are located just outside of the graphite reflectors, and are not located symmetrically, leading to power readout defects, described by (Kaiba et al., 2015). Moreover, in order to relate the reactor power to the detector response, a calorimetric method is commonly utilized. As per the reactor vendor - General Atomics (GA) - calibration procedure is performed by sampling the water from the reactor platform at uniform interval, to obtain the slope of the rising water temperature. from which the reactor power can be deduced. In order to reduce the uncertainty due to the heat transfer from the water to the outside world, this sort of calibration is performed at a reduced power level of roughly 60 kW and an adiabatic approximation is considered. In case that the response of the detector is not sufficient, the detector is moved closer to the reactor core. The reactor power deduced this way has an uncertainty between 15% - 20%, which is acceptable for common purposes, but not for benchmark quality experiments.

This is why an improved method based on the calorimetric method with electrical heaters has been introduced. where the injected heating power is well known and where both flux-tilts and heat conduction trough the reactor body are considered, leading to a reduced uncertainty of 2% (Štancar & Snoj, 2017). While this method is extremely accurate, it is very cumbersome in the sense that it requires several days for preparation and execution and cannot be routinely performed.

It should be noted that we've observed time dependence on the validity of these calibration factors, i.e. the factors that relate the detector signal to reactor power change in time. It is therefore advisable to perform a thorough thermal power calibration before any experiment, requiring the knowledge of the neutron flux with high accuracy.

During past experiments, we observed a noticeable water level increase (up to a cm) in the reactor pool water level due to volumetric thermal expansion, when the external cooling was turned off. This method is very robust, as it is not dependent on the point of measurement, flux redistribution and other factors, and was suggested in the past (Jones & Elliot, 1974). We're currently developing a capacitance-based water-level detector, which will be permanently installed on the edge of the reactor tank for continuous measurements, allowing to identify detector response changes and drift trends. Similar systems are used in the nuclear industry, for instance for water level monitoring inside pressurizers [17].

5.3. Experiments

5.3.1. Axial profile measurements of ^{197}Au(n.γ)^{198}Au

5.3.1.1. Introduction

A measurement of thermal axial neutron flux profiles in various measurement positions has been performed utilizing the ^{197}Au(n,γ) ^{198}Au reaction, in order to validate the JSI TRIGA neutron transport model in MCNP (Rising et al., 2025) in absolute terms (Radulović et al., 2014). The absolute reaction rates were scaled according to the reactor power and corrected for the flux redistribution effects. Simulations were performed with different nuclear data libraries, which have shown to have little effect. The agreement between measurements and simulations is within the uncertainty.

5.3.1.2. Detector setup & measurements

To measure the axial distribution of the ^{197}Au(n,γ) ^{198}Au reaction rates, a set of custom aluminium probes were designed and manufactured in-house, specifically to fit into 8 mm and 10 mm diameter MP positions. The probes consist of two parts: an internal aluminium rod with the diameter of 5 mm, with holes drilled trough the side in 1cm intervals, allowing for the placement of the dosimeter wires made of Al-0.1% Au obtained from IRMM (material code IRMM-530M) with diameter of 1 mm and 5 mm length. The external sleeve with the

Funded by the European Union

Funded by the European Union. Views and opinions expressed are however those of the author(s) only and do not necessarily reflect those of the European Union or the European Atomic Energy Community ('EC-Euratom'). Neither the European Union nor the granting authority can be held responsible for them.

outer diameter of 7.5 mm covers the inner aluminium rod, locking the dosimeter samples in place. The sleeve is equipped with the thread in the top, locking the inner rod in place, while allowing for the insertion of the probe inside the core using a rope. A detailed technical drawing and a few photos of the manufactured probes can be seen in Figure 5-10.

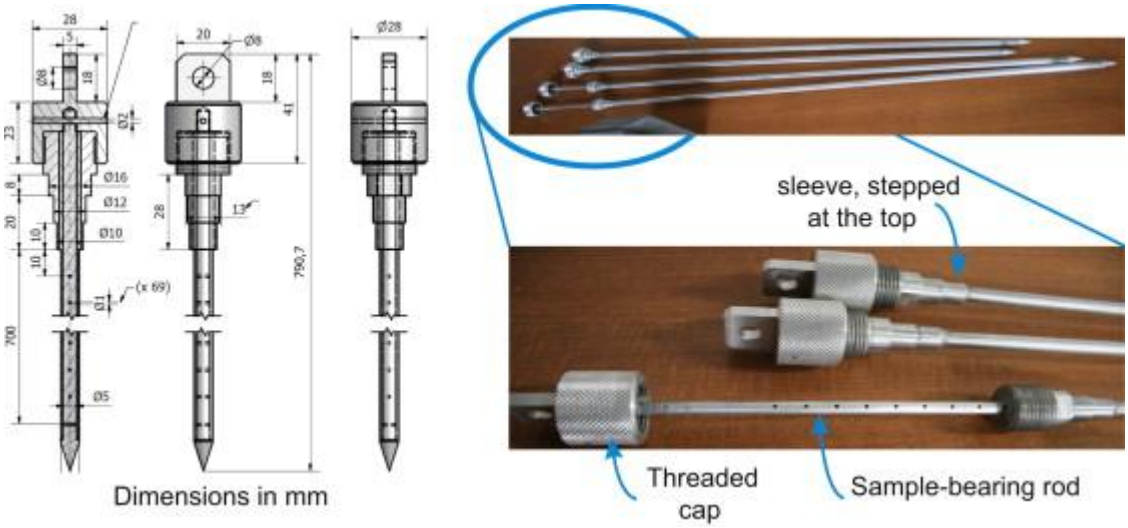

Figure 5-10: Aluminium probes used in the experiments - technical drawings and photographs.

The irradiations were performed on two different occasions, where each time two probes were inserted into their respective positions. Each of the probes carried 69 wire samples, which have been precisely weighted prior to irradiation. The irradiations were performed for the duration of 1 h at full reactor power – 250 kW. The positions of the probes during the two irradiations are shown in Figure 5-11, and the core configuration no. 190, as shown on Figure 5-12.

A few hours after the irradiation, the samples were extracted from the probes and counted using a HPGe detector Ortec® GEM40P4-PLUS-S and Ortec® Maestro software. The recorded spectra were analysed with the Hyperlab 2005 software. The saturated activities of the 198Au radionuclide in the samples, which corresponded to the $^{197}Au(n,\gamma)^{198}Au$ reaction rates, were determined from the fitted peak areas about 411.8 keV, timing information, the sample masses and the self-shielding factors, which were determined using the MATSSF code (Trkov et al., 2009).

Modelling reconstruction of this particular experiment was also performed, and the modelling results are also presented. The modelling details and considerations can be found in (Radulović et al., 2014).

Funded by the European Union

Funded by the European Union. Views and opinions expressed are however those of the author(s) only and do not necessarily reflect those of the European Union or the European Atomic Energy Community ('EC-Euratom'). Neither the European Union nor the granting authority can be held responsible for them.

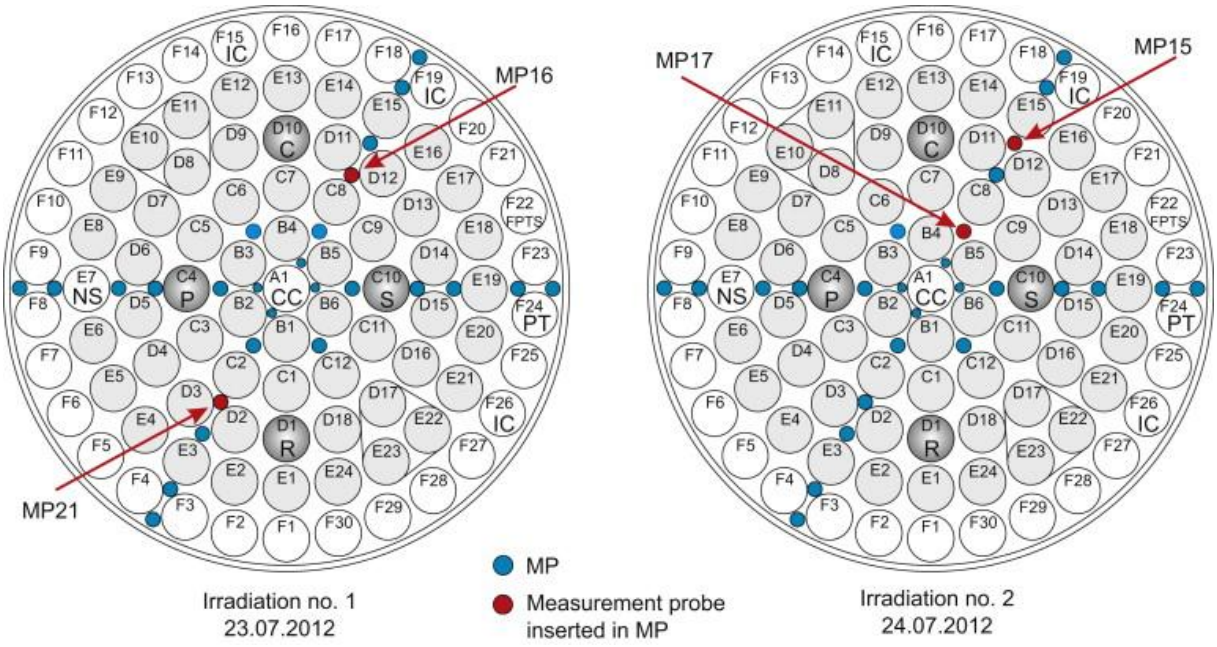

Figure 5-11: Measurement positions of the two probes during the two separate irradiations.

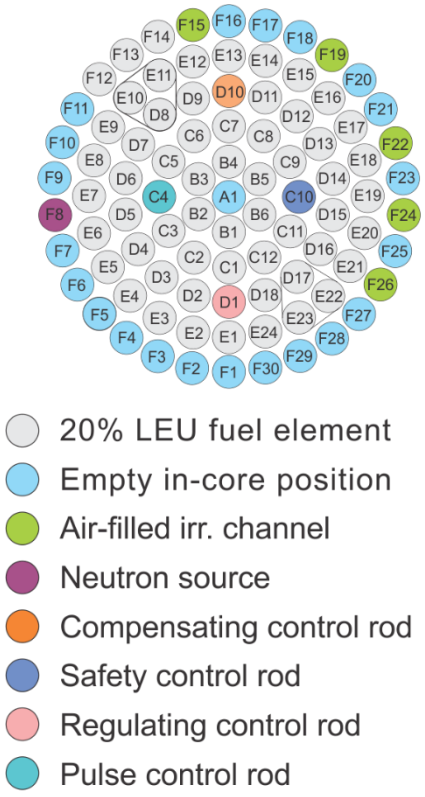

Figure 5-12: JSI TRIGA core configuration no. 190 and 192.

Funded by the European Union

Funded by the European Union. Views and opinions expressed are however those of the author(s) only and do not necessarily reflect those of the European Union or the European Atomic Energy Community ('EC-Euratom'). Neither the European Union nor the granting authority can be held responsible for them.

5.3.1.3. Results

This section present the absolute axial profiles of $^{197}Au(n,\gamma)^{198}Au$ reactions in different MP positions as measured and calculated using the JSI TRIGA MCNP model, the MCNP code and ENDF/B-VII.1 nuclear data libraries (Figure 5-13 to Figure 5-16). Results are available in csv format.

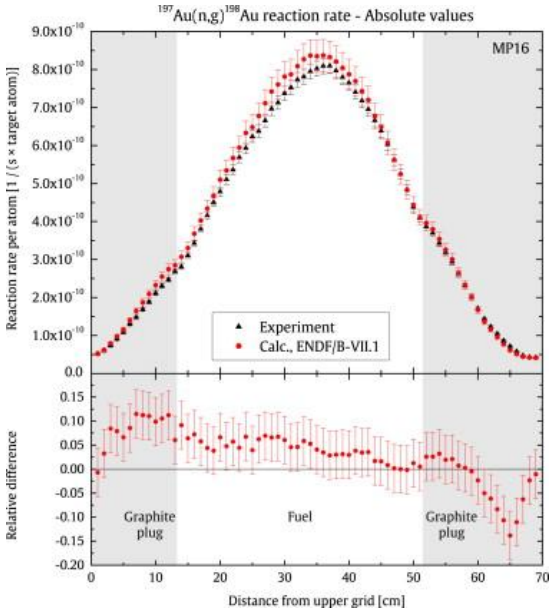

Figure 5-13: Axial profile of $^{197}Au(n.\gamma)^{198}Au$ reaction rates in MP16: measurements and simulations.

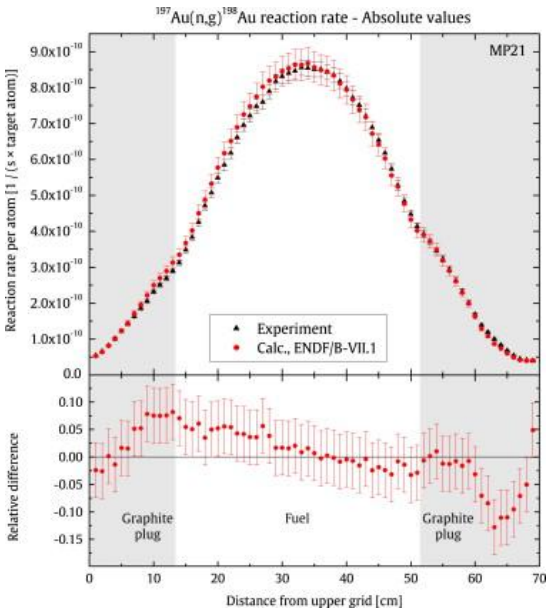

Figure 5-14: Axial profile of $^{197}Au(n.\gamma)^{198}Au$ reaction rates in MP21: measurements and simulations.

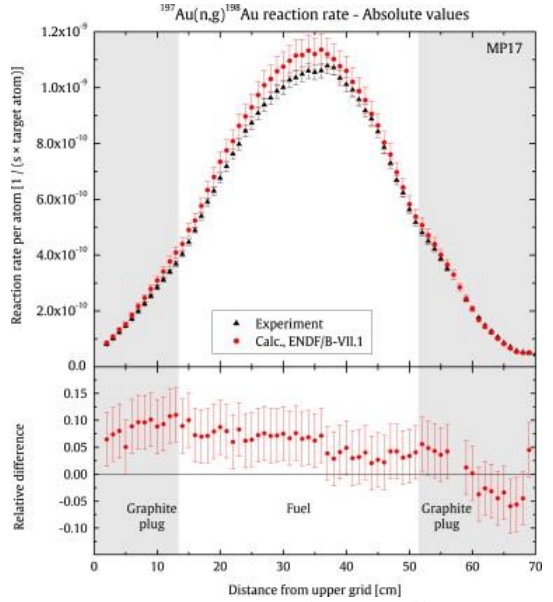

Figure 5-15: Axial profile of $^{197}Au(n.\gamma)^{198}Au$ reaction rates in MP17: measurements and simulations.

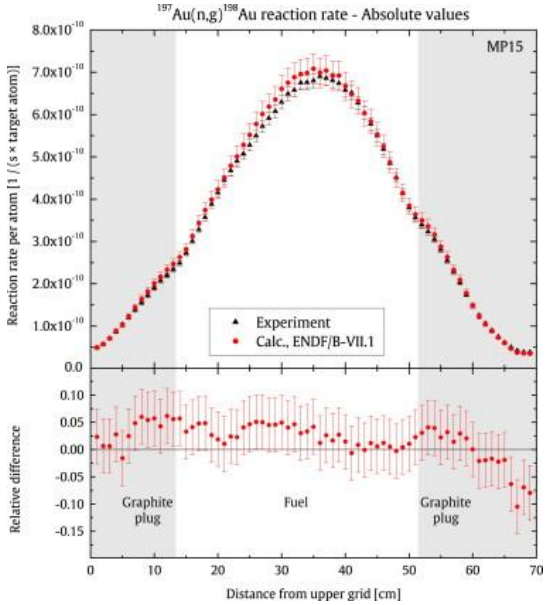

Figure 5-16:: Axial profile of $^{197}Au(n.\gamma)^{198}Au$ reaction rates in MP15: measurements and simulations.

The agreement between the calculated and the experimental absolute reaction rate values is within 5% for all cases. The calculated values are systematically greater than the experimental one, attributable to a relatively large uncertainty in the power calibration, directly affecting the calculations of the absolute values. The largest discrepancies are observed in the position MP17, which is closest to the core centre, next to the fuel elements with the largest burn-up. However, burn-up analysis was not performed in this scope, and the agreement is within the uncertainties.

Funded by the European Union

Funded by the European Union. Views and opinions expressed are however those of the author(s) only and do not necessarily reflect those of the European Union or the European Atomic Energy Community ('EC-Euratom'). Neither the European Union nor the granting authority can be held responsible for them.

5.3.1.4. Discussion

We present experimental $^{197}Au(n,\gamma)^{198}Au$ reaction rate profiles across four core locations. The comparison with the simulation results shows excellent agreement within 5% when scaled to the known reactor power, a highly favourable outcome given the inherent uncertainties in absolute power calibration.

5.3.2. Fission rate axial profile measurement

5.3.2.1. Introduction

A benchmark quality measurement of fission rate (see section 2.1) axial profiles has been measured with two absolutely calibrated fission chambers with fissile deposit of ^{235}U, being sensitive primarily to thermal neutrons, and ^{238}U for fast neutron measurements, developed, manufactured and calibrated by the Commissariat à l'Énergie Atomique et aux Énergies Alternatives (CEA). The measurements were reproduced with simulations using Monte Carlo particle transport code MCNP v 6.1 (Goorley et al., 2012) showing an agreement within their respective uncertainties. While the simulations results are also present, the modelling details and considerations are outside the scope of this report, and can be found in (Štancar et al., 2018). Only the modelling aspect for the assessment of uncertainties and biases is shown in this document.

5.3.2.2. Detector setup

Watertight, miniature fission chambers with different fissile materials were used for the measurements. The fission chambers have a diameter of 3mm, a connecting cable with mineral insulation. The structural components are made of stainless steel, and Al_2O_3 serving as an electrical insulator. The chamber is filled with a mixture of argon and nitrogen. The fission chamber has a concentric electrode design, where the fissile deposit is applied on the inner electrode. The material composition of the fissile deposit in the fission chamber is shown in Table 5-1.

Table 5-1: Isotopic composition of fissile deposit in the fission chambers.

Fission chamber	^{234}U [%at.]	^{235}U [%at.]	^{236}U [%at.]	^{238}U [%at.]	Total deposit mass [µg]
FC ^{235}U	0.063	98.490	0.038	1.409	8.86
FC ^{238}U	0.0003	0.0359	0	99.964	91.67

The chambers are designed to be operated in different regimes:

- Pulse mode, where pulses from individual events are separated, and can be counted effectively. Discrimination between gamma and neutron contributions is possible in this mode.
- Fluctuation or Campbell mode, where individual pulses are overlapping, and the signal is deduced from the variance of the signal.
- Current mode, where individual pulses sum up to make a constant flowing current signal.

In this particular experiment, reactor power was kept below 1 kW, corresponding to neutron flux levels of 10^{10} - 10^{11} $cm^{-2}s^{-1}$ to retain the readout capabilities in the pulse-mode regime, and to be sure that neutron and gamma contributions to the measurement signal can be separated.

Two different signal acquisition systems were used for this experiment: a spectroscopy amplifier i.e. Pulse-Height Analysis - PHA to analyse the detector's fission spectra, and a fast current amplifier for time-dependent count rate measurements (Multi-Channel Scaling mode- MCS), used for measurements of fission rates. PHA method was also used for the absolute calibration of the fission chambers performed in the zero-

Funded by the European Union

Funded by the European Union. Views and opinions expressed are however those of the author(s) only and do not necessarily reflect those of the European Union or the European Atomic Energy Community ('EC-Euratom'). Neither the European Union nor the granting authority can be held responsible for them.

power MINERVE reactor (Štancar et al., 2018). A schematic overview of the data acquisition system setup is shown in Figure 5-17.

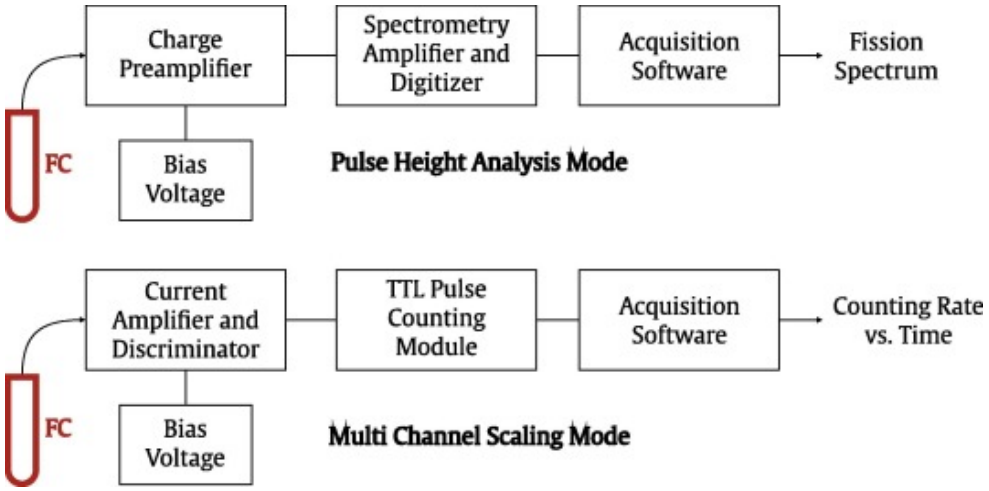

Figure 5-17: Schematic of the MCS and PHA acquisition system used for the analysis of fission chamber signals.

The fission chambers were inserted into the JSI TRIGA reactor core from the reactor platform. An aluminium guide-tube (Figure 5-18) was used for position holding inside the core's MP positions: MP14, MP15, MP16, MP17, MP20, MP21, MP23 and MP25. Cambers were moved within the aluminium guide-tube using the FC's stiff cables. The axial position was insured by a custom pneumatic grappler system with a microcontroller and a displacement sensor with the reference position being the end of the guide tube. The entire system was installed on a horizontal support beam installed on the reactor platform, extending over the reactor pool (Figure 5-19), along with the pneumatic control system (Figure 5-20). The accuracy of the system was within 0.1 mm and the repeatability of about 0.3 mm. The measurements were performed in increments of approximately 25 mm at heights corresponding to the fuel meat and a larger interval of approximately 50 mm near the fuel element edges.

Core configurations No. 190 and No. 192, which have the same loading pattern, were used for the reported measurements.

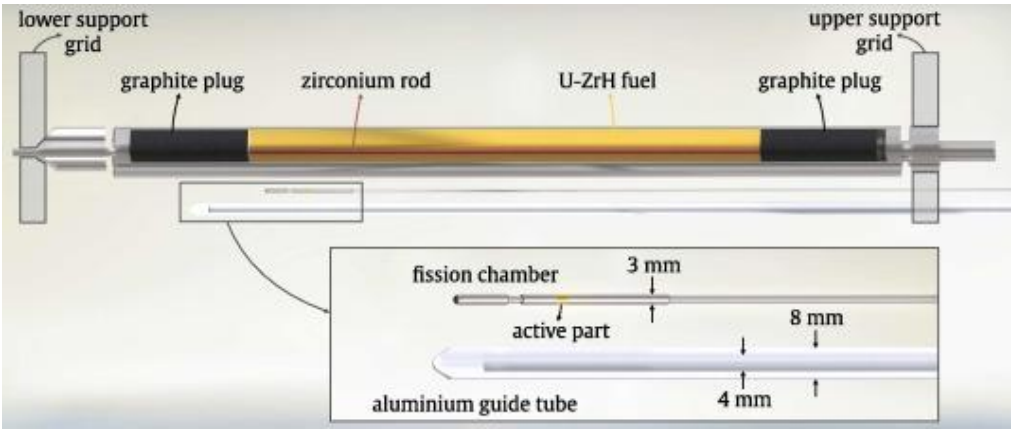

Figure 5-18: Cut view of the fuel element and the fission chamber. inserted inside an aluminium guide tube.

Funded by the European Union

Funded by the European Union. Views and opinions expressed are however those of the author(s) only and do not necessarily reflect those of the European Union or the European Atomic Energy Community ('EC-Euratom'). Neither the European Union nor the granting authority can be held responsible for them.

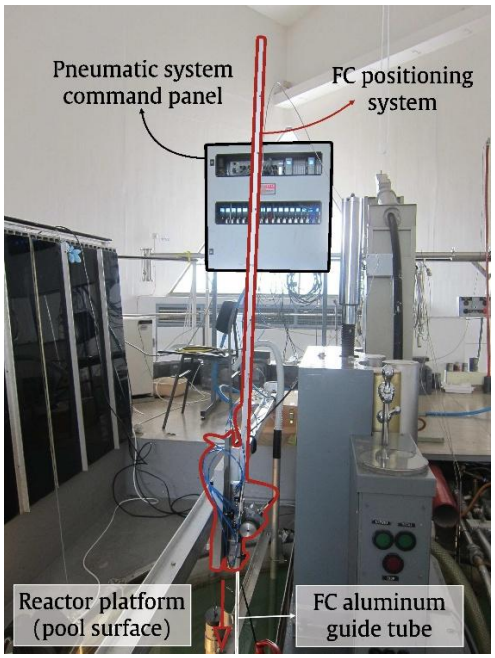

Figure 5-19: FC positioning system installed above the pool of the JSI TRIGA reactor. with denoted system control panel and the aluminium guide tube for FC in-core insertion.

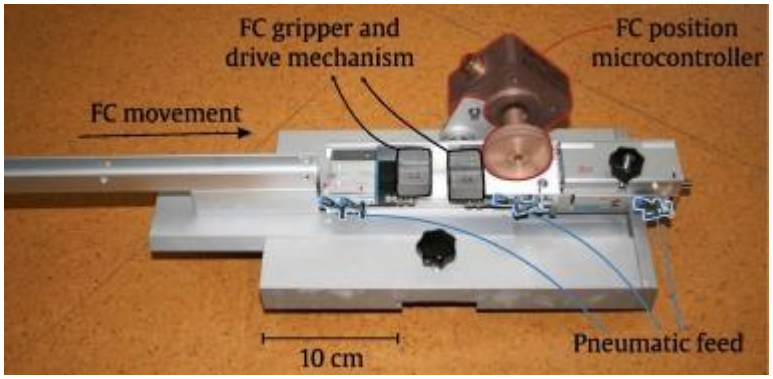

Figure 5-20: Close-up of the FC positioning system with position control microcontroller and pneumatic gripper and drive mechanism.

5.3.2.3. Uncertainty evaluation

The uncertainty qualification was performed computationally using the MCNP v6.1 code. starting with the identification of uncertainty sources and their implementation in the computational model. The effects were studied for individual fission chambers, as well as for individual measuring positions and the axial position of the FC with respect to the core. These are a consequence of an alteration in local physical conditions, such as neutron spectrum and core composition change, which have a strong dependence on the FC's position in the core. Two uncertainty metrics were employed: the maximum relative deviation from the nominal value L_{nat}. and a relative standard uncertainty across the axial profile L_{rs}, as shown in Equations (4 and (5.

$$L_{nat} = max_{i=1}^{N} \left| \frac{R_{i,var}}{R_{i,0}} - 1 \right| \quad (4)$$

$$L_{rs} = \sqrt{\frac{\sum_{i=1}^{N} \left(\frac{R_{i,var}}{R_{i,0}} - 1 \right)^2}{N}} \quad (5)$$

Funded by the European Union

Funded by the European Union. Views and opinions expressed are however those of the author(s) only and do not necessarily reflect those of the European Union or the European Atomic Energy Community ('EC-Euratom'). Neither the European Union nor the granting authority can be held responsible for them.

where $R_{i,0}$ is the reference reaction rate value at position i. and $R_{i,var}$ the perturbed value in position i.

It was discovered that the perturbation of the majority of parameters results in small fission rate changes. generally, below- or of the order of magnitude of the computational statistical uncertainty of ~0.3%. The absolute uncertainty of the uncertainty estimation is evaluated to be of the order of 0.5 %.

The axial positioning of the FC involves a total uncertainty of approximately ±3 mm, primarily due to manufacturing tolerances of the aluminium guide tubes. Since reaction rates vary with the axial position in the core, the displacement uncertainty directly impacts measurement accuracy. We utilize the reaction rate axial gradient to estimate the uncertainty. as shown by Equation (6).

$$\frac{1}{R_i}\left|\frac{dR_i}{dz_i}\right| = \frac{1}{R_i}\left|\frac{R_{i+1} - R_{i-1}}{z_{i+1} - z_{i-1}}\right| \quad (6)$$

Gradients at the core-mid height were 0.5%/mm, increasing to up to 2.5%/mm at the core edges as shown in Figure 5-21. Since differences in gradients at different MP positions are small, a conservative combined gradient estimate was performed across all used MP positions and across all axial positions. with values of 0.82%/mm for the FC ^{235}U and 0.86%/mm FC ^{238}U. Taking into account the position system accuracy to ~3 mm, leading to a conservative uncertainty estimate due to axial position uncertainty of 2.5% for FC ^{235}U and 2.6%/mm FC ^{238}U.

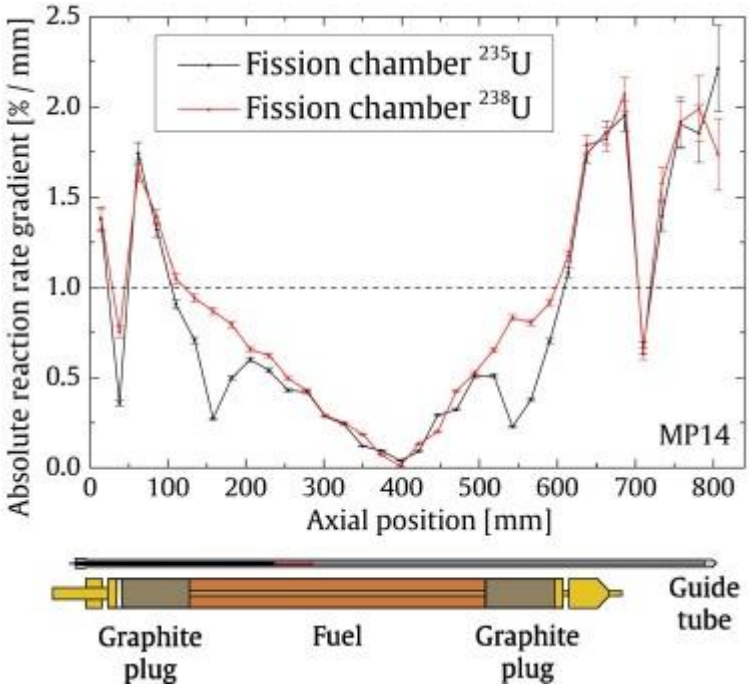

Figure 5-21: Fission reaction rate axial gradients in position MP14.

Since the inner diameter of the aluminium guide tube is 4 mm, and the outer diameter of the FCs is 3 mm, 0.5 mm of side movement is possible. To estimate this uncertainty contribution, the radial gradient throughout the TRIGA core was calculated for both FCs. Radial fission rate gradient profiles for both fission chambers at the reactor core mid-plane are shown in Figure 5-22.

Funded by the European Union

Funded by the European Union. Views and opinions expressed are however those of the author(s) only and do not necessarily reflect those of the European Union or the European Atomic Energy Community ('EC-Euratom'). Neither the European Union nor the granting authority can be held responsible for them.

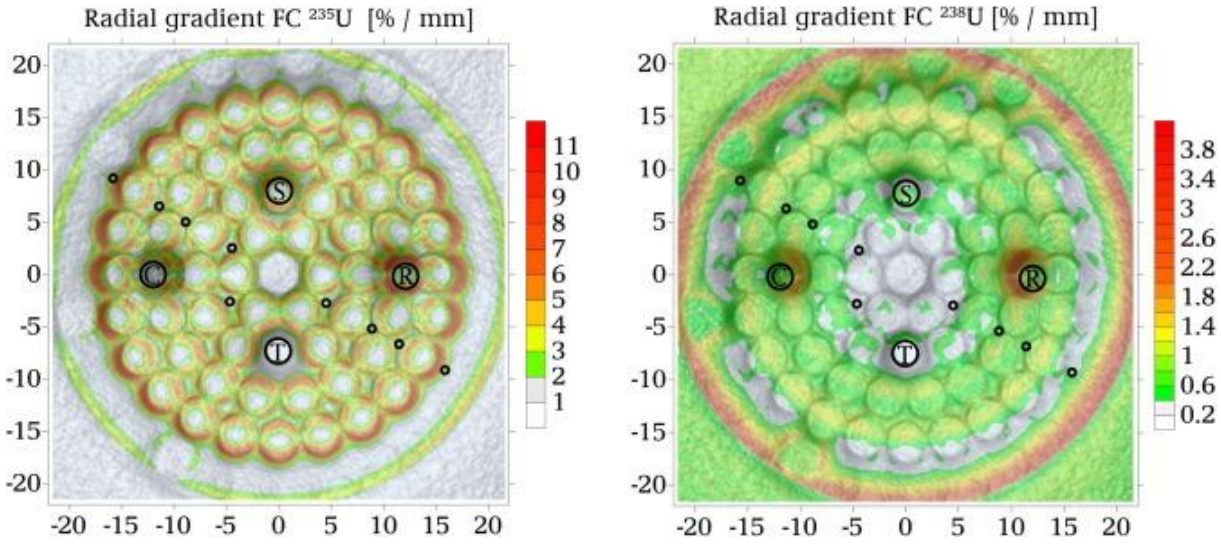

Figure 5-22: Radial fission reaction rate gradients for both fission chambers at the core mid-plane.

The calculations were performed on a rectangular mesh, superimposed over the entire reactor core with characteristic mesh voxel size of 1.5 cm. The radial gradient was calculated using the Equation (7).

$$\left|\frac{dR}{dr}\right|_{i,j} = \left(x_{i,j}^2 + y_{i,j}^2\right)^{-1/2} \left(x_i \left|\frac{R_{i+1,j} - R_{i-1,j}}{x_{i+1} - x_{i-1}}\right| + y_j \left|\frac{R_{i,j+1} - R_{i,j-1}}{y_{i+1} - y_{i-1}}\right|\right) \quad (7)$$

Where $R_{i,j}$ is the reaction rate value, $x_{i,j}$ is the x-axis component of the mesh, and the $y_{i,j}$ the -axis component of the mesh in the i,j position of the two-dimensional profile. The gradient fields differ strongly between FC ^{235}U and FC ^{238}U, particularly at the fuel element edges. where neutron spectrum changes rapidly in water. Due to small variations in the radial reaction rate gradients over the axial height, a value averaged over the entire height in each particular MP was considered, leading to calculated values of 1.59%/mm for FC ^{235}U and 0.36%/mm for the FC ^{238}U. Taking into account the upper uncertainty limit in the RC's radial position of 0.5 mm, this results in the uncertainty of 0.8% for FC ^{235}U and 0.2% for FC ^{238}U respectively.

Uncertainties in fission rates due to material composition and impurities have also been considered. The uncertainty in uranium mass of 072% for fuel elements and d1.27% for the fuel-followers in control rods were modelled by varying the fuel density, which resulted in a multiplication factor defect of $\Delta k = 22\ \mathrm{pcm} \pm 4\ \mathrm{pcm}$. leading to an average change in fission rates by approximately ±1.4%. We also evaluated the presence of ^{234}U (0.18 wt%) and ^{236}U (0.22 wt%) in the nuclear fuel against the impurity-free model. The standard uncertainty in the fission rate (Figure 5-23) distribution was evaluated at 1.4%. albeit the differences appear largely statistical in nature.

Hafnium impurities in zirconium were also evaluated, using the benchmark value of 50 ppm(John D. Bess et al., 2011), which resulted in a relative standard uncertainty in the fission rate distribution of approximately 1.3%. Effect of impurities in the axial graphite plugs of approximately 0.005 wt% were assessed to have a negligible both on the multiplication factor and the computed fission rate distribution.

The JSI TRIGA reactor power is managed using four control rods, with a position uncertainty of 3 steps out of a ~700 step range. During the experiment, Safety and Transient control rods are fully withdrawn, while the Regulating and Compensating(C) rods were partially inserted to maintain criticality. At these positions, their approximate reactivity worth gradients are between 5-6 pcm/step, leading to total uncertainty in k_{eff} of ±15-18 pcm. The effect of flux tilt (Kaiba et al., 2015) due to un-even withdrawal of the Regulating and Compensating control was also evaluated by varying their positions by ±5, ±10 and ±50 steps (Figure 5-24), and the difference then scaled down to 3-steps. In both cases, control rod position uncertainty and the flux redistribution evaluate to relative fission reaction rate uncertainties of roughly 0.3%.

Funded by the European Union

Funded by the European Union. Views and opinions expressed are however those of the author(s) only and do not necessarily reflect those of the European Union or the European Atomic Energy Community ('EC-Euratom'). Neither the European Union nor the granting authority can be held responsible for them.

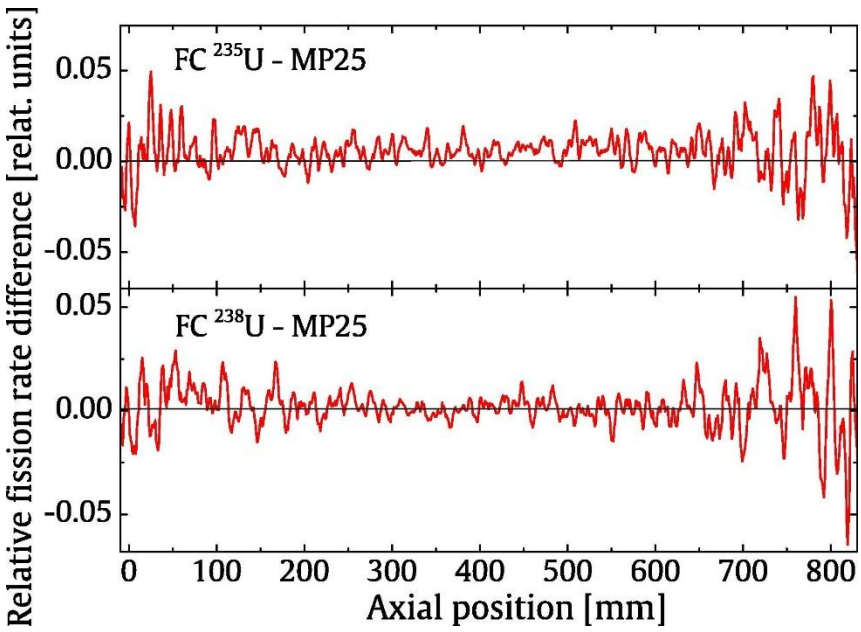

Figure 5-23: Relative difference in fission rate axial profile calculations between the reference model. and model with the additional of ^{234}U and ^{236}U impurities in MP25.

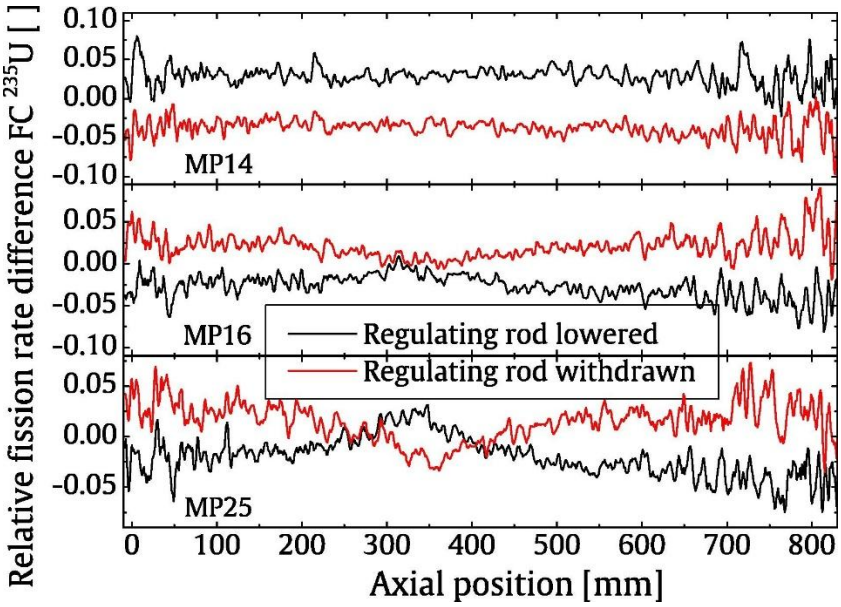

Figure 5-24: Axial distribution of the relative difference in fission rate with Regulating control rod position varied by 50 steps in different measurement positions MP.

Apart from the previously discussed contributions, we also studied the potential fuel element axial misalignment as bowing, as well as the effect of Xenon poisoning during the experimental campaign, which were both found to be negligible.

We combined the individual uncertainty sources for the experiment (Table 5-2), where individual contributions were treated as independent.

Funded by the European Union

Funded by the European Union. Views and opinions expressed are however those of the author(s) only and do not necessarily reflect those of the European Union or the European Atomic Energy Community ('EC-Euratom'). Neither the European Union nor the granting authority can be held responsible for them.

Table 5-2: Evaluation of the effects of experimental uncertainties of the fission rate axial profile measurements.

Uncertainty source	FC ^{235}U uncertainty [%]	FC ^{238}U uncertainty [%]
FC calibration	2.7	3.7
Fuel composition	1.4	1.4
^{234}U and ^{236}U impurities	1.4	1.4
Hf impurities	1.3	1.3
Graphite impurities	Negligible	Negligible
FC axial position	2.5	2.6
FC radial position	0.8	0.2
Fuel element axial position & bowing	Negligible	Negligible
Control rod position	0.3	0.3
Xenon poisoning	Negligible	Negligible
Combined	**4.5**	**5.1**

Funded by the European Union

Funded by the European Union. Views and opinions expressed are however those of the author(s) only and do not necessarily reflect those of the European Union or the European Atomic Energy Community ('EC-Euratom'). Neither the European Union nor the granting authority can be held responsible for them.

5.3.2.4. Results

Below is the comparison of both experimentally and computationally obtained reaction rate profiles, with the associated uncertainties for MP15 and MP20 with both FCs. Additional data are available on request.

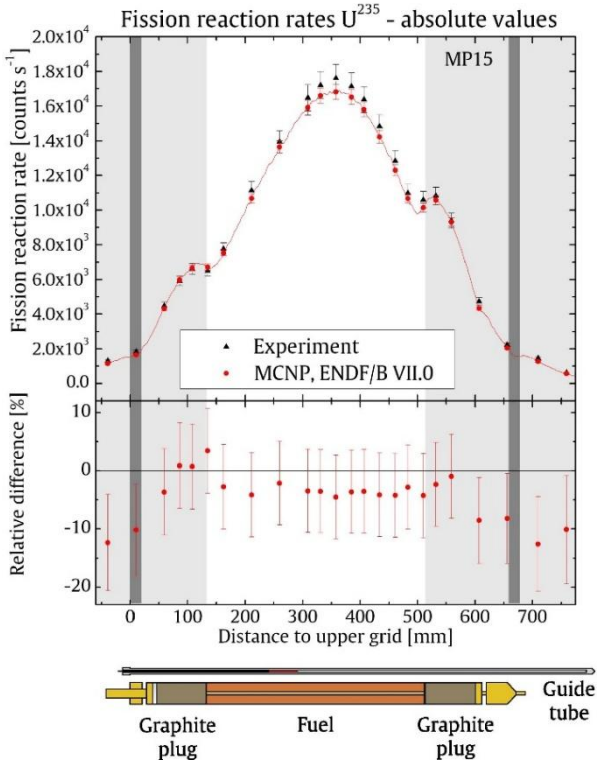

Figure 5-25: Axial fission rate profile measurements with FC ^{235}U in MP15.

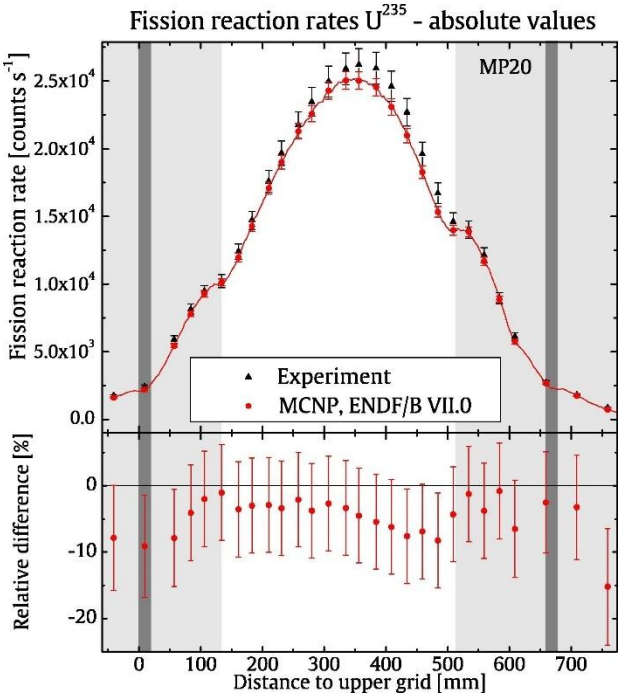

Figure 5-26: Axial fission rate profile measurements with FC ^{235}U in MP20.

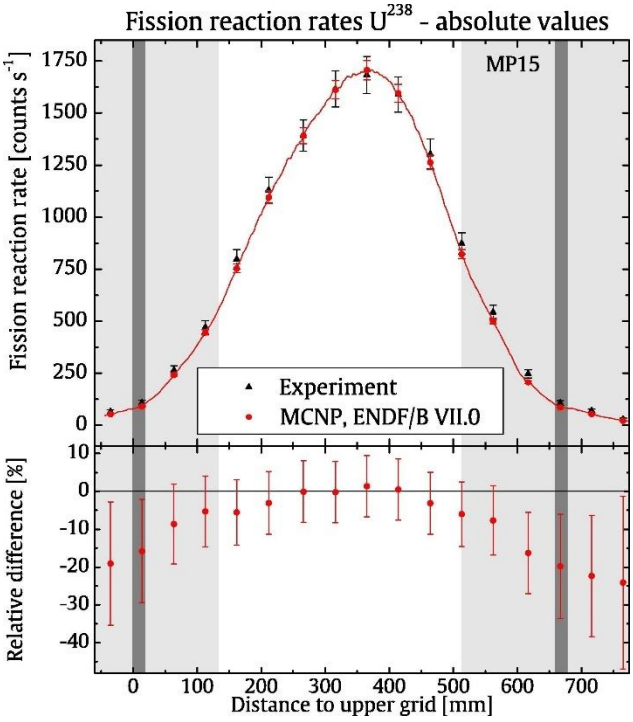

Figure 5-27: Axial fission rate profile measurements with FC ^{238}U in MP15.

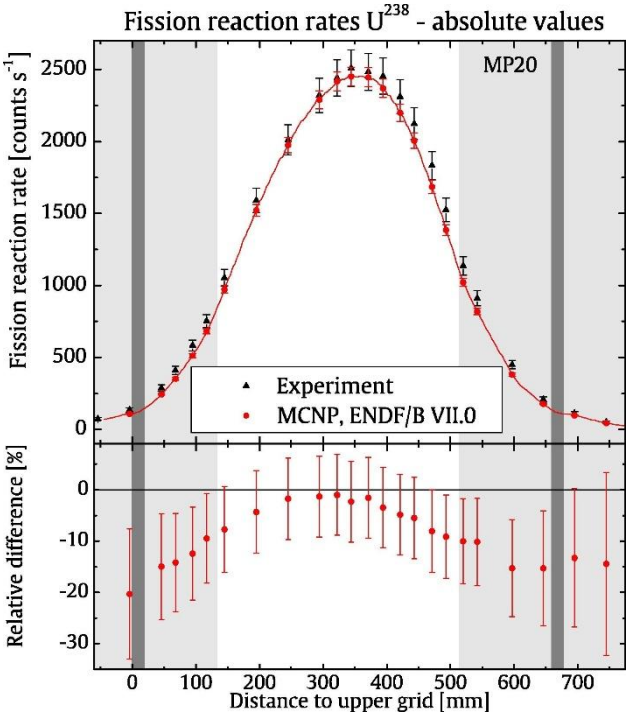

Figure 5-28: Axial fission rate profile measurements with FC ^{238}U in MP20.

Funded by the European Union

Funded by the European Union. Views and opinions expressed are however those of the author(s) only and do not necessarily reflect those of the European Union or the European Atomic Energy Community ('EC-Euratom'). Neither the European Union nor the granting authority can be held responsible for them.

5.3.2.5. Discussion

Absolute fission rate scans at nine radial positions were performed. The study determined a total experimental uncertainty of approximately 5%, primarily caused by fission chamber calibration and positioning errors. Water temperature measurements in the reactor pool.

Funded by the European Union

Funded by the European Union. Views and opinions expressed are however those of the author(s) only and do not necessarily reflect those of the European Union or the European Atomic Energy Community ('EC-Euratom'). Neither the European Union nor the granting authority can be held responsible for them.

5.3.3. Water temperature measurements

5.3.3.1. Introduction

Temperature measurements of the water have been performed at over 60 different positions of the JSI TRIGA Mark II reactor core during steady state operation and two transients for validation of thermal hydraulics computational model of the reactor tank. Measured data revealed the cooling dynamics inside the pool and allowed for the estimation of the bulk coolant velocity above the reactor core. The experiments were reproduced by CFD modelling based on the Unsteady RANS turbulence model. The results show that the simple geometry of the TRIGA reactor makes it a suitable candidate for a simple natural convection benchmark in cylindrical geometry. The results reported in this section summarize the work presented in (Henry et al., 2017).

5.3.3.2. Experimental setup

While the JSI TRIGA Mark II reactor has been characterized in great detail in terms of neutron and gamma field characteristics. few experiments related to the thermal hydraulics were performed. A set of experiments were performed to measure the temperature field of the coolant. Low power TRIGA reactors (<2 MW) generally rely on natural convection for cooling, additional cooling is installed to maintain the average water temperature below 40 °C, connected to a heat exchanger, as shown in Figure 5-29.

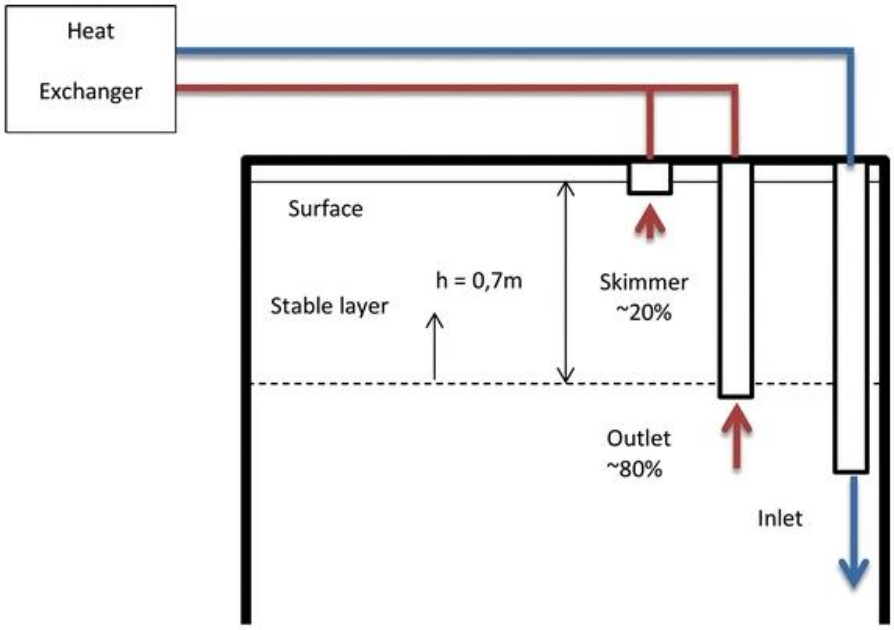

Figure 5-29: Schematic drawing of the JSI TRIGA MARK II cooling system.

The available space above the reactor core for accommodation of a large number of thermocouples is limited. due to existing infrastructure such as control-rods and irradiation channels. K-type thermocouples were selected due their performance and low neutron activation affinity, along with a National Instrument module (NI PXIe-4353) and a terminal block (TB-4353) with a powerful cold-junction compensation and declared accuracy of 0.36 °C, with an acquisition frequency of 1-2 Hz.

The size of the thermocouples was based on the required response time and the acquisition frequency. The junction was approximated as a sphere with diameter d. area S. volume V, mass m, specific heat capacity c_p. density ρ and temperature T, immersed in the fluid flow with a heat transfer coefficient h and temperature T_{ext}. as described by Equation (8).

Funded by the European Union

Funded by the European Union. Views and opinions expressed are however those of the author(s) only and do not necessarily reflect those of the European Union or the European Atomic Energy Community ('EC-Euratom'). Neither the European Union nor the granting authority can be held responsible for them.

$$S(T - T_{ext})h = mc_p \frac{dT}{dt} \quad (8)$$

The temporal response constant τ was calculated using Equation (9).

$$\tau = \frac{c_p \cdot \rho \cdot V}{h \cdot S} \quad (9)$$

By expressing the volume and the surface area in terms of the sensor diameter, we obtain the maximum diameter satisfying the requested τ using Equation (10).

$$d = \frac{6 \cdot h \cdot \tau}{c_p \cdot \rho} \quad (10)$$

This gave us a limiting diameter of 1.5 mm. Hence, thermocouple wires with diameter of 0.5 mm and PVC insulation were used for the experiment. To maintain the fast response and trustworthy temperature readings, the thermocouples were fused and left unsheathed.

A custom thermocouple supporting structure was made of aluminium due to its short decay half-life, to fit into the pool with all the obstacles, providing a rigid support and positional stability for 30 thermocouples into 10 evenly spaced (0.4 m) rows, each row comprising of 3 sensors, as shown in Figure 5-30. Two such structures with sensors were deployed, form maximum coverage over the pool. The bottom of the structures was equipped with an adjustable foot, which was placed against the reflector ring, keeping the structure at a fixed position. The lowest row of thermocouples was located 1.45 m above the top of the core. The installed supporting structure with installed thermocouples can be seen in Figure 5-31.

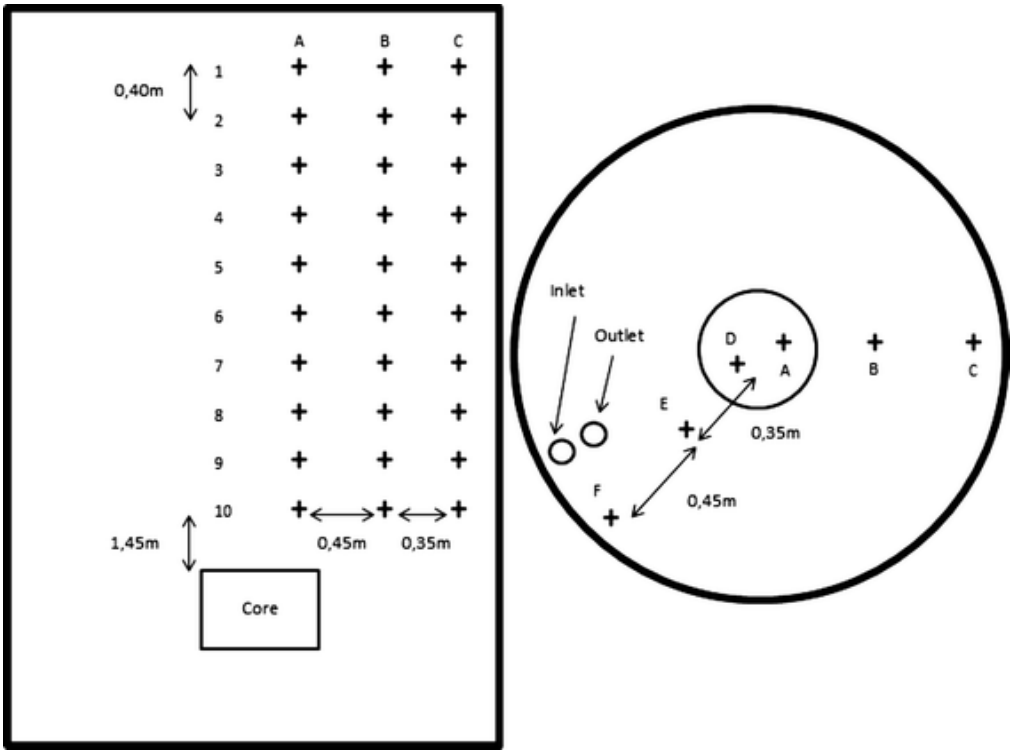

Figure 5-30: Schematic view of the thermocouple locations inside the reactor tank. with marked axial levels and different column letters.

Funded by the European Union

Funded by the European Union. Views and opinions expressed are however those of the author(s) only and do not necessarily reflect those of the European Union or the European Atomic Energy Community ('EC-Euratom'). Neither the European Union nor the granting authority can be held responsible for them.

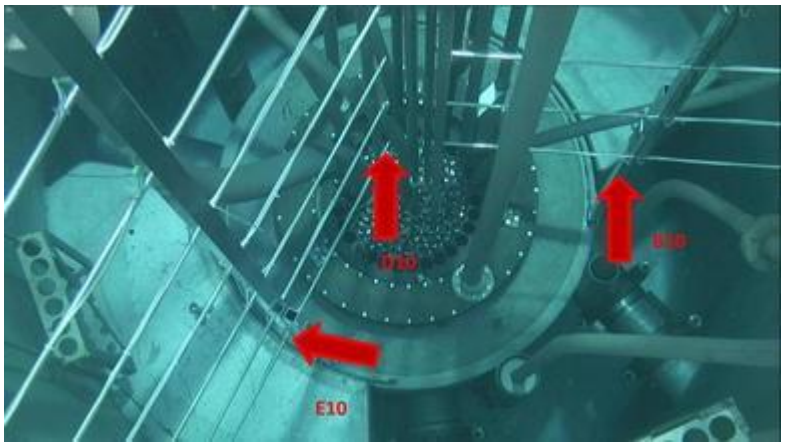

Figure 5-31: Top view of the two supporting structures with thermocouples inside the reactor pool.

A data acquisition application was developed in LabView for data acquisition and statistical analysis. PXI express chassis with an integrated controller was used with two PXIe-4353 modules and corresponding TB-4354 terminal blocks for cold-junction compensation. The hardware and the software were tested to ensure operation within published specifications, by placing detector assemblies inside the reactor pool after several days of last reactor operation in a constant temperature environment, where all of 60 thermocouples exhibited stability withing the 0.2 °C uncertainty band. In addition, spatial positioning as well as the temporal resolution contribute to the final uncertainty estimate, as reported in Table 5-3.

Table 5-3: Experimental uncertainty of the temperature. position and time measurements.

ΔT [°C]	Δx [cm]	Δy [cm]	Δz [cm]	Δt [s]
±0.36	±5	±5	±2	±1

Even though the described experimental facility was not meant to be used for the deduction of the velocity field using the cross-correlation method, a basic indication of the fluid bulk velocity withing the pool was obtained. following the Equation (11).

$$v_{conv,i} = \frac{z_{i+1} - z_i}{t_{i+1} - t_i}, \Delta v_{conv} = \sqrt{\left(\frac{\Delta z}{t_{i+1} - t_i}\right)^2 + \left(\frac{(z_{i+1} - z_i)\Delta t}{(t_{i+1} - t_i)^2}\right)^2} \quad (11)$$

Where i represents the axial layer index.

The core loading no. 218, as schematically shown in Figure 5-32 was used for the experimental campaign.

Modelling of the experiment was also performed using the ANSYS® CFX code, and a detailed model of the JSI TRIGA reactor. The simulation results are also presented, however modelling considerations are beyond the scope of this report, and can be found in (Henry et al., 2017).

Funded by the European Union

Funded by the European Union. Views and opinions expressed are however those of the author(s) only and do not necessarily reflect those of the European Union or the European Atomic Energy Community ('EC-Euratom'). Neither the European Union nor the granting authority can be held responsible for them.

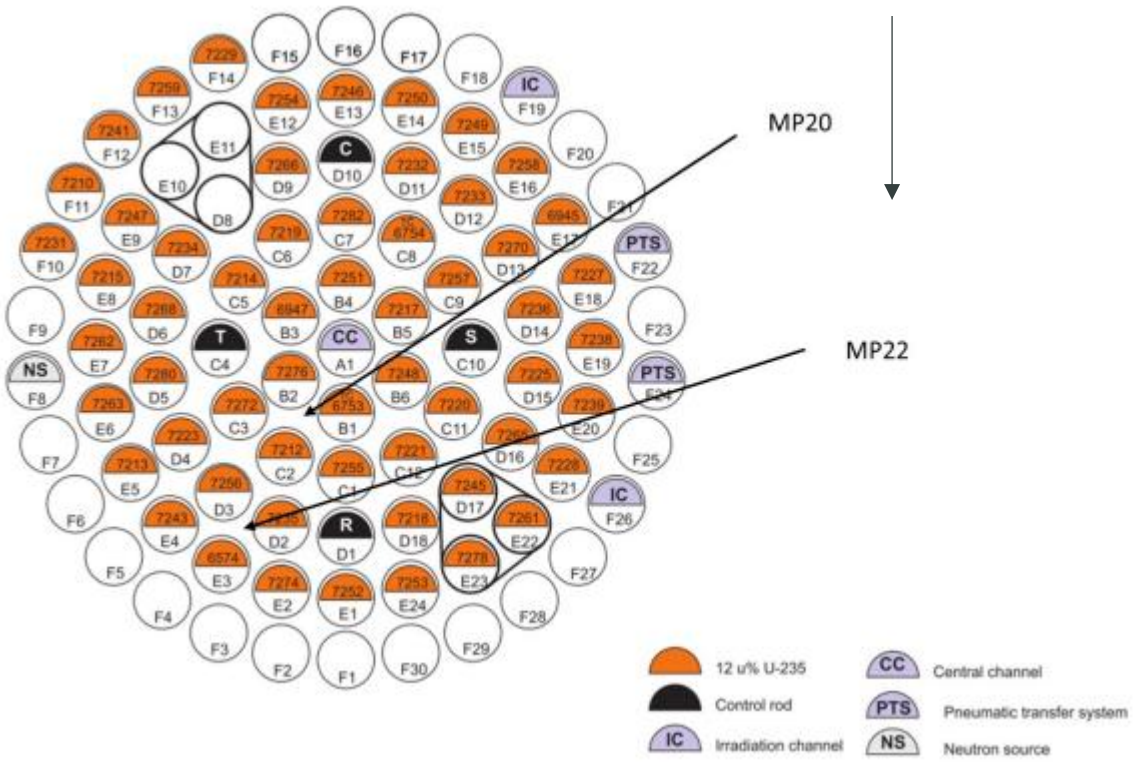

Figure 5-32: Core loading pattern no. 218 used in the experiments. with the arrow denoting north direction.

5.3.3.3. Results

Experimental and computational results of three different operational scenarios are presented here:

- Steady state operation with external cooling
- Steady state operation without external cooling

Steady state operation with cooling

The reactor was operated at a constant power level of 240 kW and the produced heat was removed via the external cooling system. Mixed convection drives the coolant flow through the core. Average recorded temperature evolutions in the pool during 600 s were compared with the converged steady-state temperature profile. Low temperature differences are observed across the pool, making this mode less attractive for measurements and simulations. Results of measurements and simulations are reported in Table 5-4. While steady state operation is interesting from a steady-state perspective, it provides little value in terms of thermal-hydraulic benchmarking.

Table 5-4: Mean coolant temperature at various positions in the pool. during steady-state operation.

	Measured [°C]	Computed [°C]
Maximum	28.3	28.4
Average	27.5	27.2
Minimum	26.8	25.8

Funded by the European Union

Funded by the European Union. Views and opinions expressed are however those of the author(s) only and do not necessarily reflect those of the European Union or the European Atomic Energy Community ('EC-Euratom'). Neither the European Union nor the granting authority can be held responsible for them.

Steady state operation without cooling

In this case, the external cooling was turned off, and the reactor was turned on to full power (250 kW) for the duration of 70 min, representing a pure natural convection case. Ryleigh number was calculated using Equation (12) with a value of around 10^{13}.

$$Ra = \frac{g\beta}{\upsilon\alpha\lambda} q'' L_c^4 \tag{12}$$

where g is the gravitational acceleration. β is the volumetric thermal expansion coefficient. υ the kinematic viscosity, α the thermal diffusivity, λ the thermal conductivity and q'' the heat flux. The characteristic length L_c value of 0.5 m was used.

The experiment was performed, starting with a reactor coolant slightly above 18 °C. Temperatures in the core were recorded during the entire period of the pool heating, which allowed for the interpretation. Figure 5-33 shows the course of measured and calculated coolant temperatures at various positions in the core. It was observed that temperature distributions along columns B and E as well as C and F have very similar profiles.

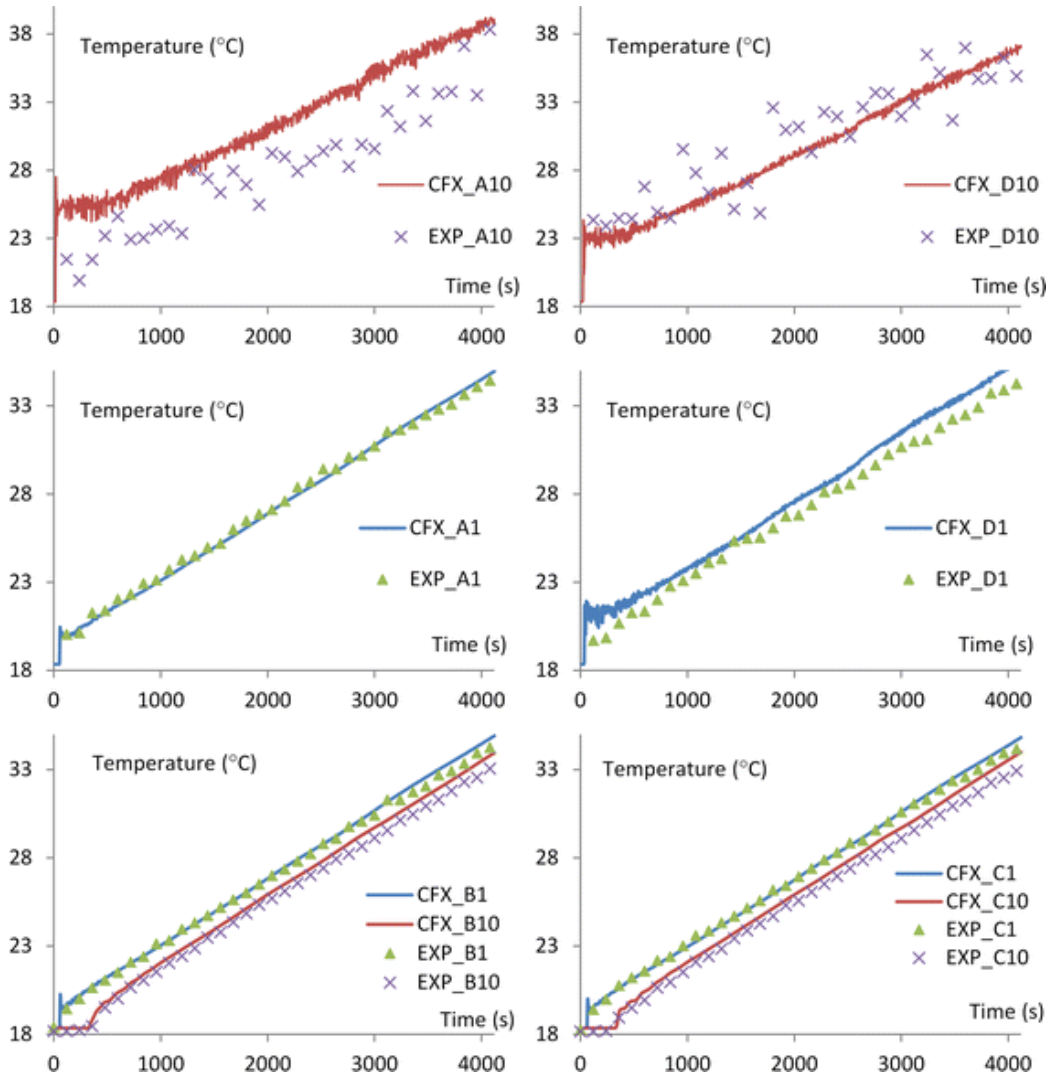

Figure 5-33: Temporal temperature evaluation at specific thermocouple points during full power operations: (EXP) - experiments. (CFX) computational fluid analysis.

Funded by the European Union

Funded by the European Union. Views and opinions expressed are however those of the author(s) only and do not necessarily reflect those of the European Union or the European Atomic Energy Community ('EC-Euratom'). Neither the European Union nor the granting authority can be held responsible for them.

The thermal-hydraulic behaviour of the reactor pool undergoes a distinct transformation during the start-up phase, transitioning from initial heating to a stable natural convection regime within approximately 500 s (Figure 5-34). The heat release from the core triggers an initial upward motion of water, creating a narrow, highly turbulent column of heated fluid directly above the active core. This region is characterized by chaotic behaviour and intense mixing as hot water rising from the fuel meets colder pool water. Significant temperature fluctuations – up to 30 °C – are observed and are further exacerbated by the presence of non-fuelled components, like the transient control rod, creating sharp temperature gradients and localized flow disturbances.

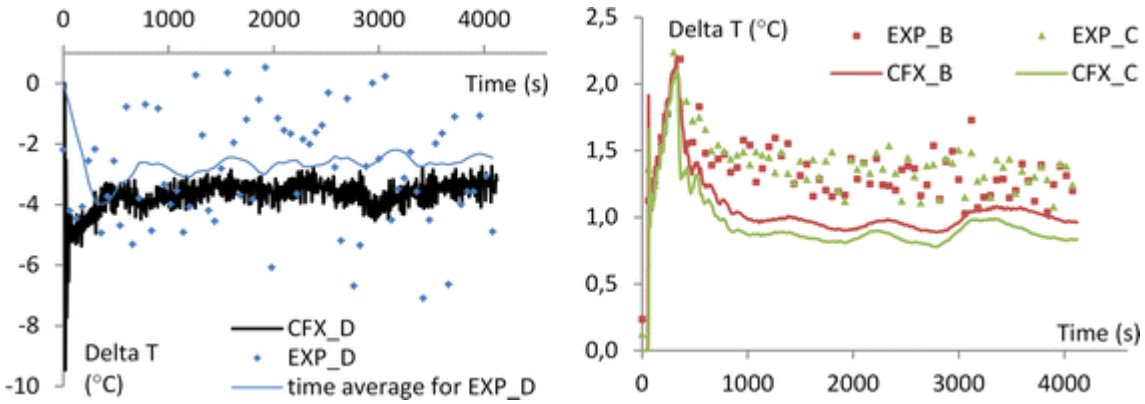

Figure 5-34: Temperature difference between top (position 10) and bottom (position 1) for three thermocouple columns.

After the initial transient, the flow patterns stabilize into a steady state natural circulation and the pool enters a phase where the mean temperature rises linearly. Interestingly, once the steady state is established, the relative temperature differences between various points in the pool remain unchanged. This suggest that a reduced number of thermocouples (1-2) can be used for the assessment of the average pool temperature.

The initial plume of hot water allowed for the assessment of the vertical fluid velocity, as outlined in Table 5-5. The power ramp-up was modelled as a Heaviside function, while in reality it takes roughly 20 s for the reactor power to transition from 20 % to full power, which was considered as the uncertainty estimate of simulations.

The spatial distribution of heat is highly non-uniform; while the central column above the core experiences the highest temperatures and most rapid fluctuations. the water near the pool walls and the bottom annulus remains significantly cooler and more stable. In the centre, a secondary flow is induced that pulls coolant from the sides toward the centreline, reinforcing the stable rising plume. Ultimately, the study demonstrates that while the initial minutes of reactor operation are marked by complex, high-amplitude thermal oscillations, the system quickly settles into a predictable, linear heating trend governed by a well-defined buoyancy-driven flow.

Table 5-5: Position and temporal delay of measured and calculated temperature perturbation due to the initial hot water plume and estimations of vertical velocity v_{conv}.

Thermocouple	Detection time [s] - experimental	Detection time [s] - calculated	v_{conv} – exp. [cm/s]	v_{conv} – calc. [cm/s]
A1	57	54	7.1	9.0
A10	6	14		
B1	63	58	-1.1	-1.3

Funded by the European Union

Funded by the European Union. Views and opinions expressed are however those of the author(s) only and do not necessarily reflect those of the European Union or the European Atomic Energy Community ('EC-Euratom'). Neither the European Union nor the granting authority can be held responsible for them.

B10	377	344		
C1	65	62	-1.2	-1.2
C10	359	352		
D1	55	54	7.5	9.0
D10	7	14		
E1	73	56	-1.2	-1.1
E10	379	370		
F1	59	64	-1.1	-1.2
F10	399	374		

5.3.3.4. Discussion

The water temperature measurement in the pool of the JSI TRIGA reactor are performed at 60 different locations using K-type thermocouples Steady-state operation offered limited thermal-hydraulic insight due to low temperature gradients. The study's most significant findings emerged during the transient analysis, specifically regarding the development of natural convection.

A key observation was the 500-second transition period required for the natural convection profile to fully develop. During this phase, time-lag measurements of temperature perturbations allowed for the estimation of propagation velocities, a process the simulation reproduced with high precision. Once this steady velocity field was established. the pool entered a quasi-linear heating phase. The flow was characterized by a narrow, highly turbulent plume directly above the core where the majority of mixing occurred, contrasted by the relatively stable and linear temperature rise in the rest of the pool.

Funded by the European Union

Funded by the European Union. Views and opinions expressed are however those of the author(s) only and do not necessarily reflect those of the European Union or the European Atomic Energy Community ('EC-Euratom'). Neither the European Union nor the granting authority can be held responsible for them.

5.3.4. In-core temperature measurements

5.3.4.1. Introduction

An experimental campaign focused on the coolant temperatures in the core of the JSI TRIGA reactor has been performed in order to have experimental data for validation of multi-physics coupling of neutronics and thermal-hydraulics phenomena. A specialized support structure was developed to house the thermocouples in a vertical arrangement, prioritizing three factors: shielding of the sensors from direct contact with the hot fuel element surface, ensuring good thermal contact of thermocouple tips with the coolant, and utilizing materials that minimize neutron activation. This section summarizes previously published work by (Henry & Matkovič, 2016) and (Henry, 2017).

5.3.4.2. Experimental setup

To perform axial coolant temperature profile measurements within the reactor core, a custom support structure was designed and built in-house to accommodate 10 thermocouples in a vertical column within the Measuring Position (MP) of the reactor core (Figure 5-6), keeping the tips of thermocouples exposed and in contact with the coolant, while shielding the temperature sensors from the hot fuel surface. The outer diameter of the assembly is 8mm, so that it first into all major MP positions. The exposed thermocouples are aligned in one direction and exposed to the coolant, as shown in Figure 5-35. Their distanced from the top plane of the bottom grid and naming convention is shown in Figure 5-36. Same core configuration (no. 218) as in the experiment described in Section 0 was used, as well as the same data acquisition system along with the same acquisition frequency and thermocouple types. Uncertainty estimates are based on the positional uncertainty within the larger diameter MP and the data acquisition system, and are reported in Table 5-6.

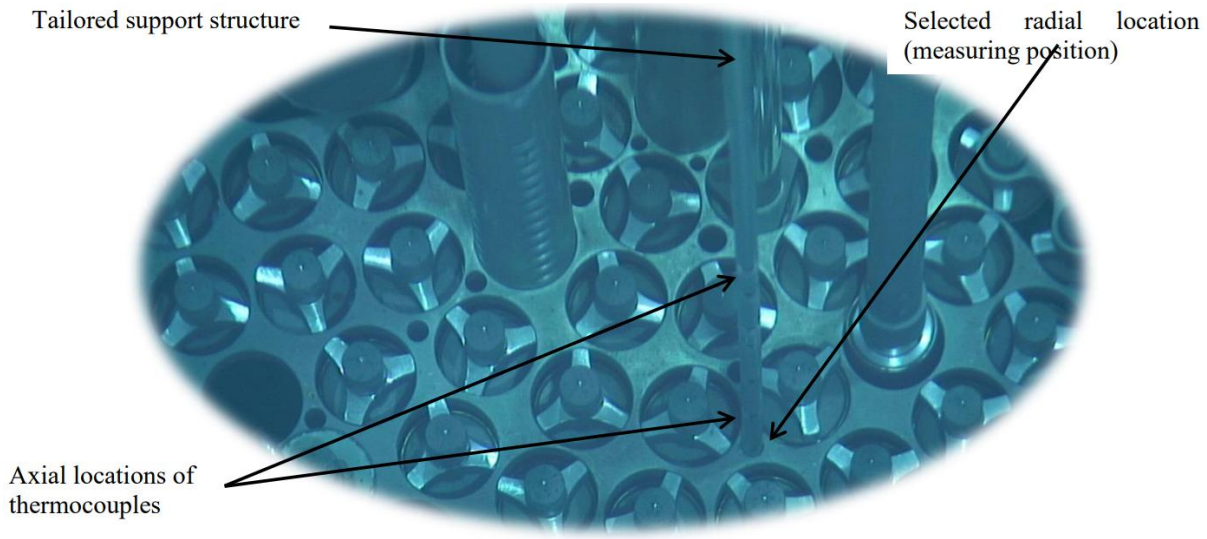

Figure 5-35: The insertion of the probe equipped with the thermocouples into the MP position of the reactor core.

Table 5-6: Reported experimental uncertainties for in-core temperature measurements.

ΔT [°C]	Δx [cm]	Δy [cm]	Δz [cm]	Δt [s]
±0.36	±0.4	±0.4	±0.2	±1

Funded by the European Union

Funded by the European Union. Views and opinions expressed are however those of the author(s) only and do not necessarily reflect those of the European Union or the European Atomic Energy Community ('EC-Euratom'). Neither the European Union nor the granting authority can be held responsible for them.

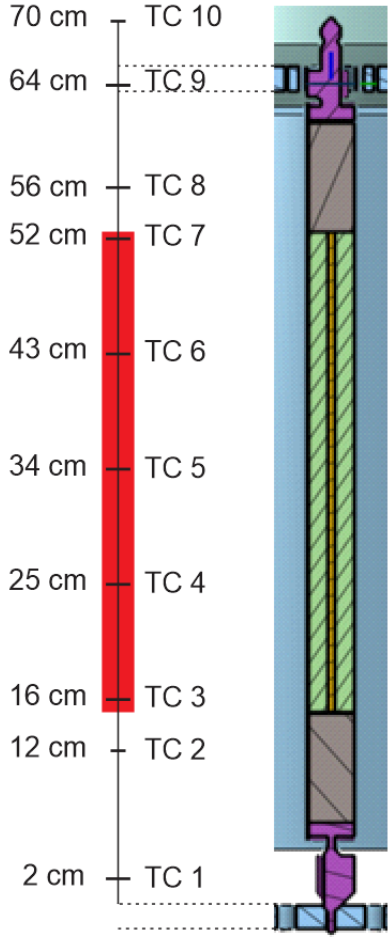

Figure 5-36: Thermocouple distances from the top plane of the bottom grid. and. their naming convention. and location with respect to the fuel element. Red area denotes the fuel meat height

Measurements were performed in multiple MP positions. Since the holes for the thermocouples are located only on one side of the guide-tube. the experiment was repeated with different orientations of the thermocouple assembly. Temperature measurements were performed during steady state operation i.e. full power (250 kW) with external cooling on. to keep the reactor coolant temperature at 27 °C on average. Each experiment lasted for roughly 5 min per experiment and the results are averaged out, since numerous temperature oscillations are observed, with error bars representing temperature variation during the experiment. Modelling of the experiments was performed using the ANSYS CFX code, with the present results. However, modelling considerations are not discussed in this report, and the reader is directed to (Henry, 2017; Henry & Matkovič, 2016).

5.3.4.3. Results

In this section we present the temperature measurements at different MP locations: 5, 14, 16 and 21, and different orientations, during full power, steady state operation and the corresponding CFD computational results. Results in Figure 5-37 to Figure 5-40 are given in terms of temperature differences with respect to the lower thermocouple-TC1.

Funded by the European Union

Funded by the European Union. Views and opinions expressed are however those of the author(s) only and do not necessarily reflect those of the European Union or the European Atomic Energy Community ('EC-Euratom'). Neither the European Union nor the granting authority can be held responsible for them.

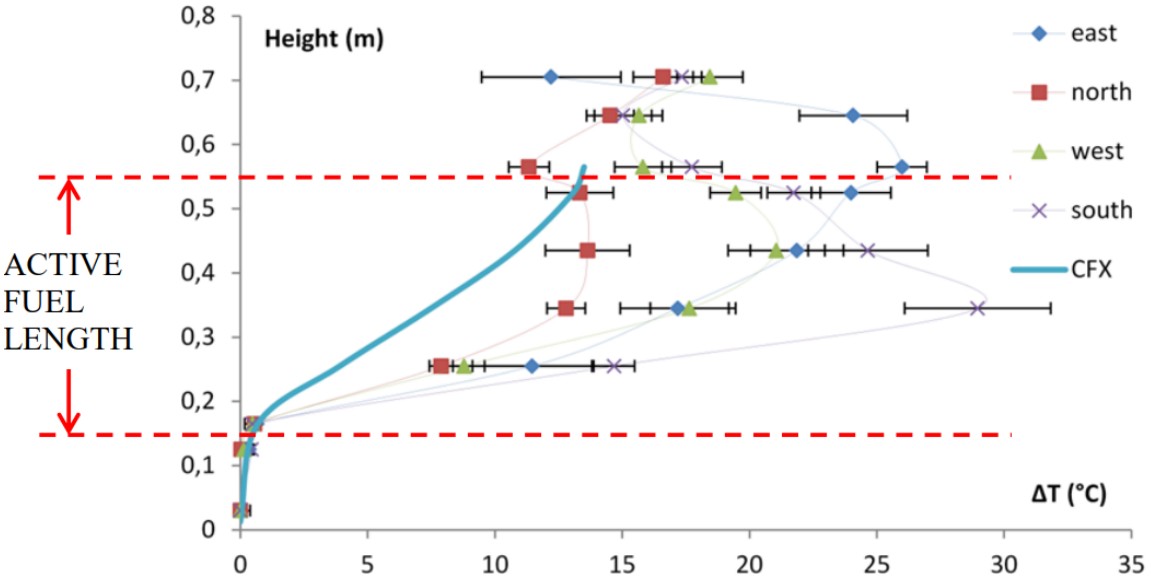

Figure 5-37: Simulated and measured temperature differences (with different thermocouple holder orientations) with respect to TC1 at full reactor power in MP5 position.

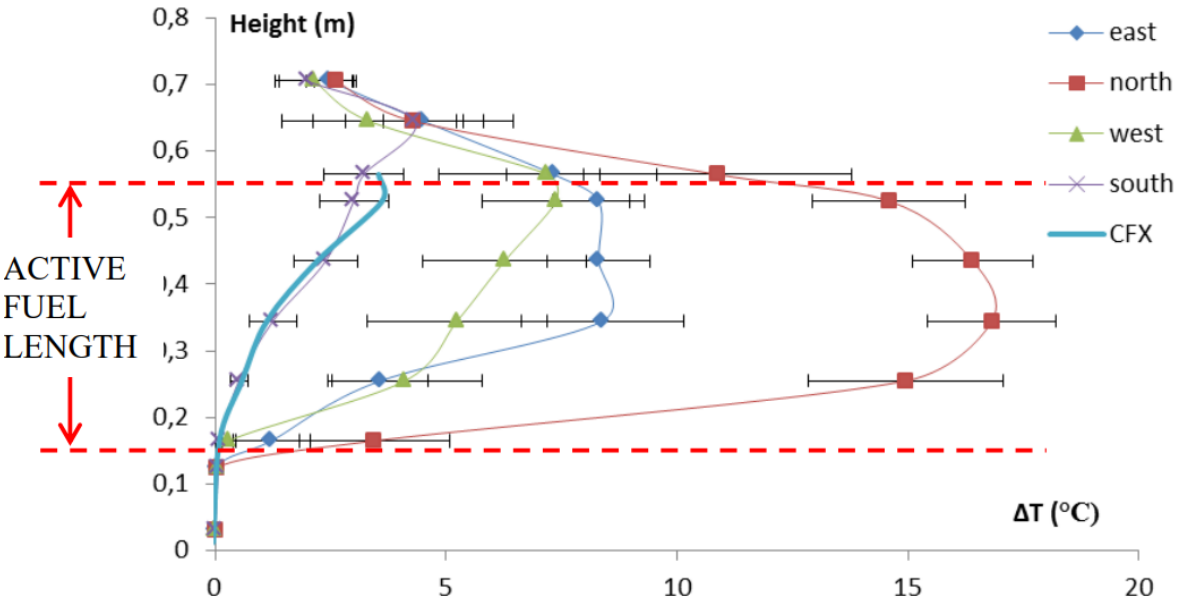

Figure 5-38: Simulated and measured temperature differences (with different thermocouple holder orientations) with respect to TC1 at full reactor power in MP14 position.

Funded by the European Union

Funded by the European Union. Views and opinions expressed are however those of the author(s) only and do not necessarily reflect those of the European Union or the European Atomic Energy Community ('EC-Euratom'). Neither the European Union nor the granting authority can be held responsible for them.

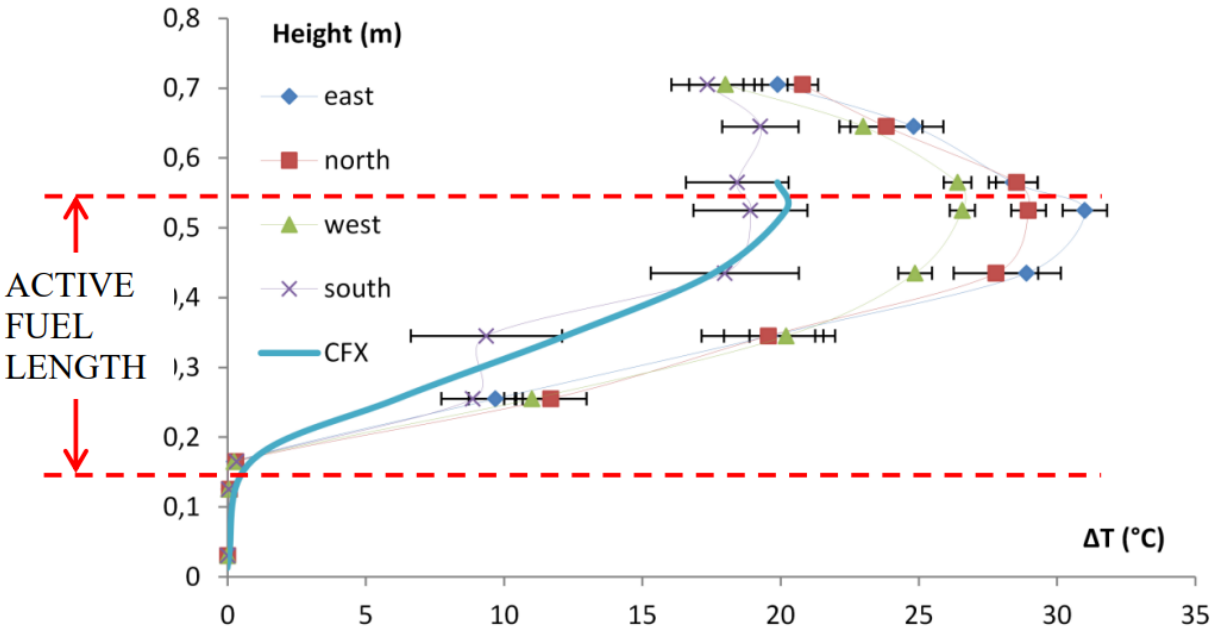

Figure 5-39: Simulated and measured temperature differences (with different thermocouple holder orientations) with respect to TC1 at full reactor power in position MP16.

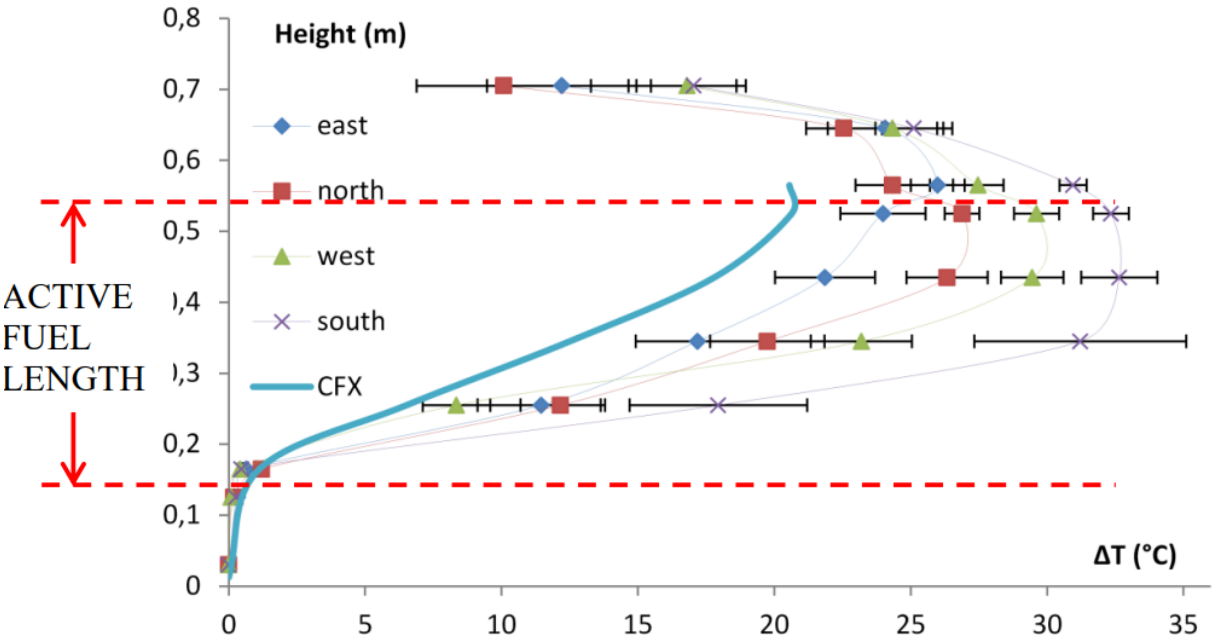

Figure 5-40: Simulated and measured temperature differences (with different thermocouple holder orientations) with respect to TC1 at full reactor power in position MP21.

Generally, the calculations slightly underestimate the measured temperatures and a detailed sensitivity analysis should be performed to determine which assumptions of the modelling require improvements.

Measurements within the reactor core reveal that mixing is most intense along the active fuel length, with temperature profiles varying significantly based on a sensor's proximity to specific heat sources. Higher temperature gradients were observed near the hotter fuel elements of the C-ring compared to the D-ring or the reflector, while the presence of non-heated components like the transient rod introduced chaotic flow

Funded by the European Union

Funded by the European Union. Views and opinions expressed are however those of the author(s) only and do not necessarily reflect those of the European Union or the European Atomic Energy Community ('EC-Euratom'). Neither the European Union nor the granting authority can be held responsible for them.

through strong thermal heterogeneities. By applying an energy balance to these vertical temperature profiles, the initial estimate of the coolant flow velocity within the core appears to be between 10 and 20 cms^{-1}.

5.3.4.4. Discussion

To investigate internal reactor dynamics, an experimental campaign paired with a CFD modelling was performed to map coolant temperature profiles within the core. While preliminary simulations were promising, experimental data revealed significant mixing between fuel rods, evidenced by drastically different temperature profiles recorded when simply rotating the measuring device at a single location. Consequently, the study highlights the need for further research to accurately assess this localized coolant mixing and recommends a sensitivity analysis regarding core inlet velocity to refine the current bulk velocity estimations.

5.3.5. Pulse experiments Benchmark Database

5.3.5.1. Scope

The JSI TRIGA Pulse Database (Švajger, 2023) represents an exhaustive, 26-year empirical archive of transient nuclear operations. Initiated following the reactor's 1991 reconstruction, the database systematically catalogues 289 distinct pulse experiments. The dataset transitions from highly controlled initial tests using a compact, fresh, and homogeneous core, to complex transient events performed across a wide spectrum of core configurations, isotopic variations, and accumulated fuel burnups. By explicitly recording the physical conditions and raw signal outputs of every single pulse, the database provides an unparalleled empirical foundation for evaluating high-energy transient reactor states without relying on theoretical interpolation. The details are described in (Švajger et al., 2024).

5.3.5.2. Pulse experiments and core geometry

The database meticulously logs the exact hardware and geometric parameters of the reactor at the time of each transient event. While the JSI TRIGA reactor maintains a nominal steady-state power of 250 kW, it also allows for a pulse operation, reaching peak powers of up to 1 GW for millisecond durations.

The exact spatial arrangement of standard fuel elements, which are composed of 12 wt% of 20% enriched uranium uniformly mixed with zirconium-hydride and instrumented fuel elements is mapped for every pulse. This precise geometric logging is critical, as the total physical fuel mass acts as the primary thermal sink during a pulse, directly dictating the empirical power peak and thermal diffusion rates.

5.3.5.3. Mechanics of pulse operation and control rod data

Every pulse recorded in the database is initiated by a strictly physical mechanism: the rapid pneumatic ejection of a dedicated fourth control rod, known as the “Transient” or “Pulse” control rod (Figure 5-7).

The fuel-followed transient control rod is ejected at high speed, extracting a total of 15 inches from the core—a distance that directly corresponds to the entire active length of the reactor core. The instantaneous removal of this neutron absorber plunges the core into a prompt-super-critical state.

Because the exact amount of inserted reactivity fundamentally defines the pulse, the database contains rigorous pre-pulse calibration curves. Over the 26-year period, two empirical methods were utilized to measure the reactivity "worth" of the control rods:

- Rod-Exchange Method: Utilized for the first 14 foundational pulses, mapping rod worth relative to physically swapped calibrated rods.
- Digital Rod-Insertion Method: Adopted for all subsequent pulses, leveraging a digital reactivity meter (DMR) to dynamically record real-time reactivity changes as the drive mechanism inserts the rod into a critical core.

Funded by the European Union

Funded by the European Union. Views and opinions expressed are however those of the author(s) only and do not necessarily reflect those of the European Union or the European Atomic Energy Community ('EC-Euratom'). Neither the European Union nor the granting authority can be held responsible for them.

The database logs the initial pre-pulse position of all control rods alongside these calibration curves, allowing researchers to trace the exact physical insertion parameters that triggered each specific 1 GW power spike.

5.3.5.4. Pulse dynamics measurements database

The core of the database consists of the raw energy, power, and temporal measurements extracted directly from the pulse detector channels. Due to the homogeneous U-ZrHx fuel mixture, the reactor possesses a strong prompt negative temperature reactivity coefficient. This physical property ensures that as the fuel matrix instantaneously heats up, the nuclear chain reaction is naturally choked off, forcing the pulse to safely terminate within milliseconds.

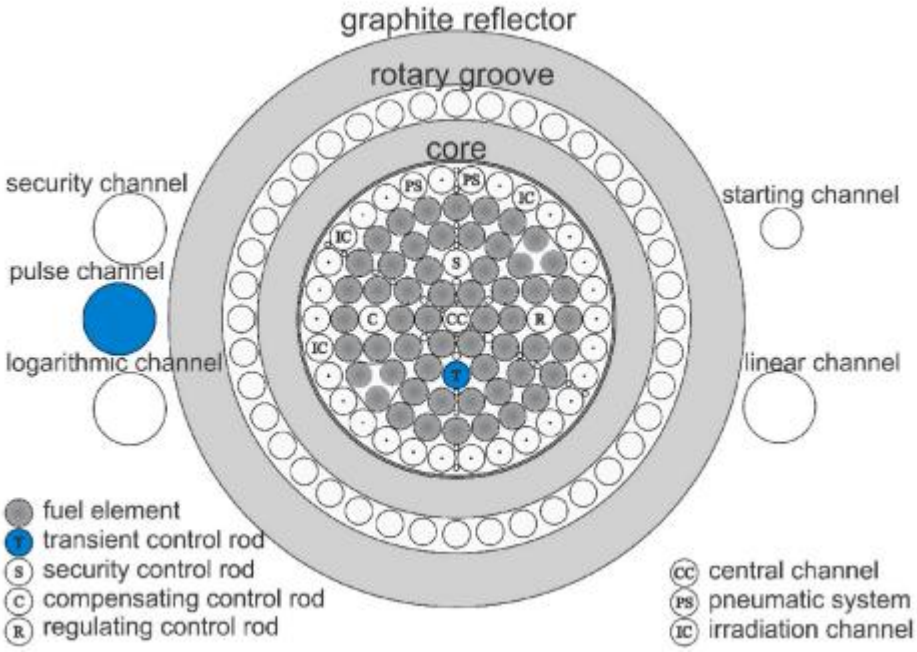

The primary energetic data points archived for all 289 pulses include:

- Prompt Reactivity Insertions: The physical trigger values, ranging empirically from 0.50 $(low transients) up to over 2.00$ (maximum transients).
- Peak Power Output: The absolute highest recorded power burst. Depending on the reactivity inserted and the physical core configuration (46 vs. 56 elements), empirical peak powers span from roughly 60 MW up to ~829 MW, with modern testing pushing the upper limits toward 1 GW.
- Total Energy Released: Calculated via the strict numerical integration of the raw power signal curves. Despite the massive megawatt/gigawatt power spikes, the total physical energy deposited in the core remains relatively low, typically constrained to a few megajoules (ranging from ~2.1 MWs up to ~11.2 MWs per pulse) due to the ultra-short duration of the event.
- Full Width at Half Maximum (FWHM): The empirical duration of the power spike. The hardware limits the fastest, highest-power pulses to an FWHM of approximately 12.8 milliseconds, while slower, low-power pulses stretch to roughly 57.9 milliseconds.

5.3.5.5. Thermodynamic and core state variables

To map the extreme thermal forces generated by the megajoule energy deposits, the database archives high-resolution temperature telemetry.

- Instrumented Fuel Elements: Internal fuel temperatures are captured via two specialized fuel elements equipped with internal thermocouples. The database logs the specific placement of these sensors (e.g., permanently fixed in the inner B ring, or rotated between the A, C, and D rings).

Funded by the European Union

Funded by the European Union. Views and opinions expressed are however those of the author(s) only and do not necessarily reflect those of the European Union or the European Atomic Energy Community ('EC-Euratom'). Neither the European Union nor the granting authority can be held responsible for them.

- Heat Conduction Constraints: A crucial empirical factor noted in the dataset is the physical heat conduction delay. Because there is a measurable temporal gap between the thermal generation in the uranium-zirconium fuel and its conduction to the thermocouple sensor, the measured maximum temperatures mathematically lag behind the actual peak temperatures at the centre of the fuel element. The database provides the raw, unadjusted temperature signals, explicitly forcing researchers to account for this physical conduction barrier. Furthermore, the ambient bulk water temperature inside the reactor tank is logged continuously to contextualize the core's boundary conditions.

5.3.5.6. Fuel Burnup and Environmental Reactivity Influences

A pulse cannot be treated in isolation; its energetics are intimately tied to the reactor's long-term operational history. Between pulse events, the JSI TRIGA Mark II operates in standard steady-state mode, which systematically alters the core's physical and chemical makeup.

- Isotopic Depletion: The database exhaustively tracks the cumulative burnup of each of the 91 fuel pins. It documents the shifting isotopic composition of the uranium fuel over decades of steady-state use. This is corroborated by multi-zone depletion measurements tracking precise isotopic shifts.
- Xenon Poisoning Dynamics: The database also tracks the empirical accumulation of Xenon—a powerful neutron poison. In early experiments, pulses were initiated from a sub-critical state, and the physical presence of Xenon directly suppressed pulse reactivity. In later operations initiated from a critical state, Xenon forced operators to manually reposition standard control rods prior to the pulse. This physical repositioning altered the core's neutron flux distribution, tangibly changing the transient rod's total reactivity worth. All of these pre-pulse configurations are logged to explain minor statistical variances between pulses of identical intended reactivity.

The fidelity of the TRIGA Pulse Database relies on a robust and highly responsive physical instrumentation array capable of capturing data during gigawatt-scale, millisecond-duration transients. An example of data for pulse No. 760 is showcased in Figure 5-41.

5.3.5.7. Hardware Infrastructure:

During a pulse, flux and power signals are captured by a dedicated pulse detector channel utilizing an uncompensated ion chamber. To ensure no transient data is lost, this hardware feeds directly into a digital processing computer that logs the entire event at a rapid sampling rate of 20 kHz.

Every individual entry in the database is essentially a "snapshot" of the reactor's absolute physical state. By accessing the database, researchers retrieve:

- The raw 20 kHz digital power and temperature waveform signals.
- The exact dimensional and geometric layout of the core.
- The specific calibration curves and physical displacement (in inches) of the transient and regulating control rods.
- The empirical megawatt peak, the megajoule energy integral, and the precise FWHM duration.
- The depleted isotopic state and Xenon concentration of the surrounding fuel matrix at the millisecond the pulse was fired.

Through this rigorous empirical approach, the JSI TRIGA database effectively removes the reliance on theoretical pulse modelling, providing the international nuclear community with an unparalleled physical dataset of extreme transient reactor states. Additional improvements in reactor power measurements have recently been made by using a Cherenkov light detection system, which is described by (Peric et al., 2026).

Funded by the European Union

Funded by the European Union. Views and opinions expressed are however those of the author(s) only and do not necessarily reflect those of the European Union or the European Atomic Energy Community ('EC-Euratom'). Neither the European Union nor the granting authority can be held responsible for them.

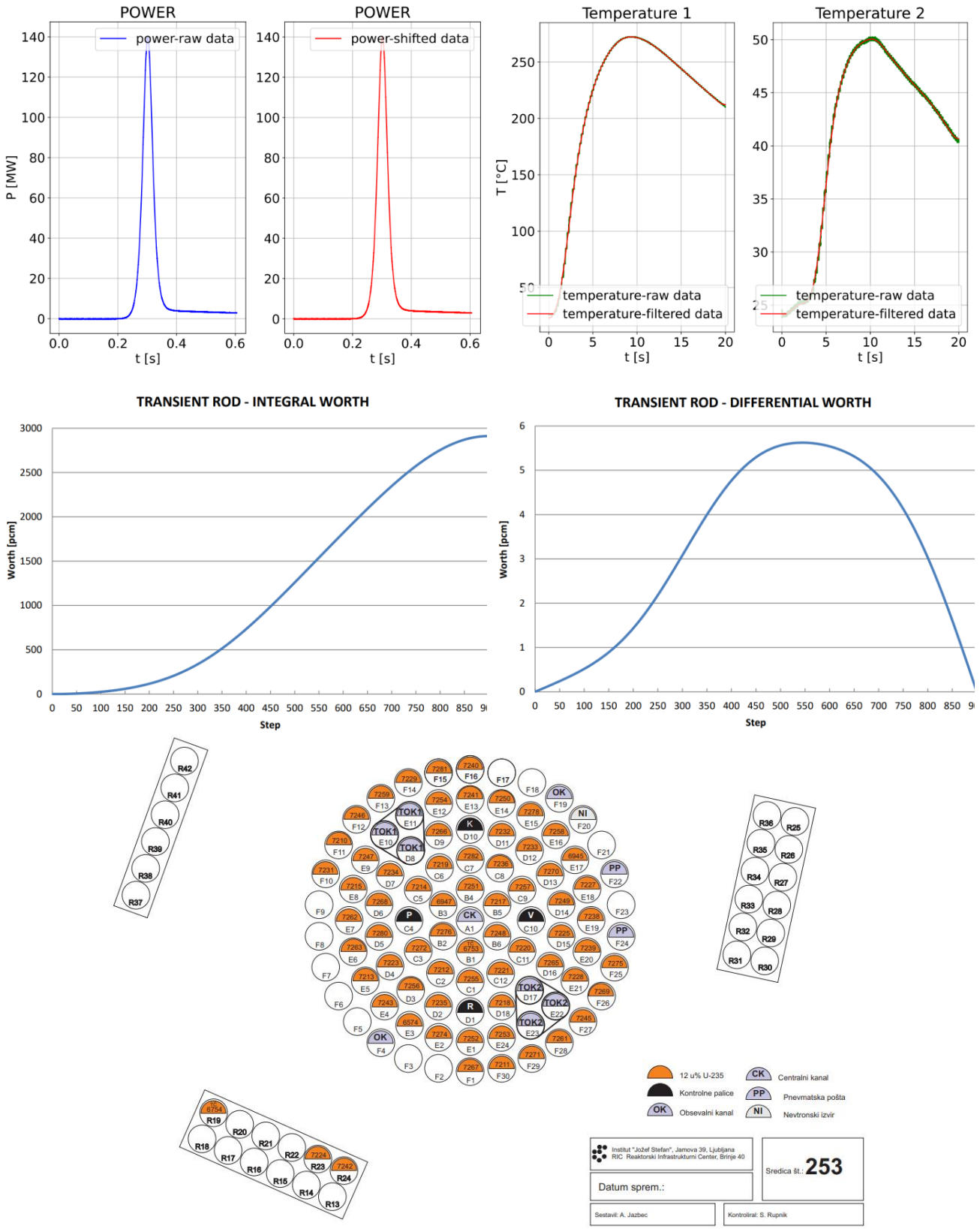

Figure 5-41: Example of Power and fuel temperature evolution during reactor pulse (top), reactivity worth of the Transient control rod (middle) and reactor core loading pattern used in the experiment (bottom).

Funded by the European Union

Funded by the European Union. Views and opinions expressed are however those of the author(s) only and do not necessarily reflect those of the European Union or the European Atomic Energy Community ('EC-Euratom'). Neither the European Union nor the granting authority can be held responsible for them.

6. Conclusions and future applications

The comprehensive experimental campaigns detailed in this deliverable represent a significant contribution to the Multiphysics characterization of nuclear research reactors. By rigorously applying established methodologies—such as Neutron Activation Analysis (NAA), inverse kinetics for reactivity determination, and high-frequency digital signal acquisition for transient events—this document successfully bridges the gap between raw physical measurements and advanced computational modelling. The compiled datasets provide the high-fidelity, benchmark-quality empirical data required to validate modern multi-physics coupling, Monte Carlo neutron transport codes, and computational fluid dynamics (CFD) models.

6.1. Facility-specific Achievements and Experimental Milestones

The scope of this deliverable highlights critical baseline updates and advanced diagnostic achievements across three distinct European facilities:

6.1.1. BME Training Reactor:

The campaigns at the BME Training Reactor fundamentally updated the facility's operational baselines. Most notably, the new activation- and calorimetry-based power calibration established a measured-to-nominal power ratio of 1.44±0.03, ensuring that future computational models are anchored to accurate thermal outputs. The precise quantification of integral and differential control rod worth, alongside detailed assembly reactivity measurements, provides a complete neutronic profile of the core.

The extensive thermal-hydraulic mapping during 17 distinct operational transients revealed clear axial thermal stratification and recirculation time delays, generating an ideal empirical dataset for validating coupled TRACE/PARCS multi-physics simulations.

6.1.2. Budapest Research Reactor (BRR)

The experimental campaign at BRR successfully mapped continuous axial flux profiles across the full 60 cm length of fuel elements within fast-flux irradiation channels. By utilizing carefully calibrated high-purity iron and aluminium-gold activation wires, the measurements provided a high-resolution snapshot of daughter creation rates. Furthermore, the meticulous accounting for detector geometric anomalies (such as Pb slit imperfections) using MCNP efficiency integrations establishes a rigorous framework for absolute flux validation in high-power research environments.

6.1.3. JSI TIGA reactor

The JSI TRIGA campaigns provided exhaustive data across both steady-state and extreme transient domains. Absolute axial fission rate measurements using miniature ^{235}U and ^{238}U fission chambers and neutron dosimetry foils. Furthermore, the pool-wide temperature mappings successfully tracked the core's transition from chaotic, localized turbulent heating to a stable natural convection regime.

The crowning experimental achievement remains the JSI TRIGA Pulse Database. By systematically archiving 26 years of prompt-super-critical events (including gigawatt-scale power peaks, exact control rod calibrations, and evolving core geometries for 289 individual pulses) this dataset removes the reliance on theoretical interpolation for transient states.

6.2. Implications for Computational Benchmarking

The value of these experimental datasets lies in their immediate application. As the nuclear engineering community pushes toward high-fidelity simulation frameworks, the demand for pristine, well-documented physical data is critical. The empirical profiles established in this deliverable provide method and code

Funded by the European Union

Funded by the European Union. Views and opinions expressed are however those of the author(s) only and do not necessarily reflect those of the European Union or the European Atomic Energy Community ('EC-Euratom'). Neither the European Union nor the granting authority can be held responsible for them.

developers with the exact boundary conditions and target metrics required to prove computational safety and accuracy.

6.3. Future outlooks and planned developments

Looking ahead, the scope of this project will continue to expand to capture even more granular reactor dynamics. New experimental developments are planned further down the project timeline, focusing on the deployment of novel, high-fidelity, non-contact measurement techniques.

By transitioning to advanced, non-intrusive diagnostic tools, future campaigns aim to eliminate physical probe effects (such as localized flow obstructions or minor flux perturbations) and capture unprecedented spatial and temporal resolution, continuing to push the boundaries of multi-physics reactor benchmarking.

Bibliography

Anderson, H. L., Fermi, E., Wattenberg, A., Weil, G. L., & Zinn, W. H. (1947). Method for Measuring Neutron-Absorption Cross Sections by the Effect on the Reactivity of a Chain-Reacting Pile. *Physical Review*, *72*(1), 16–23. https://doi.org/10.1103/PhysRev.72.16

ANSYS. (2011). *User's guide, ANSYS 14.0 Documentation*.

Fazekas, B., Molnár, G., Belgya, T., Dabolczi, L., & Simonits, A. (1997). Introducing HYPERMET-PC for automatic analysis of complex gamma-ray spectra. *Journal of Radioanalytical and Nuclear Chemistry*, *215*(2), 271–277. https://doi.org/10.1007/BF02034477

Goorley, T., James, M., Booth, T., Brown, F., Bull, J., Cox, L. J., Durkee, J., Elson, J., Fensin, M., Forster, R. A., Hendricks, J., Hughes, H. G., Johns, R., Kiedrowski, B., Martz, R., Mashnik, S., McKinney, G., Pelowitz, D., Prael, R., … Zukaitis, T. (2012). Initial MCNP6 Release Overview. *Nuclear Technology*, *180*(3), 298–315. https://doi.org/10.13182/NT11-135

Henry, R. (2017). *Neutronic and thermal-hydraulics coupling for simulations of the TRIGA Mark II reactor* [Ph. D. Thesis]. University of Ljubljana, Slovenia.

Henry, R., & Matkovič, M. (2016). Coolant Temperature Measurements in the Core of TRIGA Research Reactor. *Proceedings of the 25th Internaitonal Conference Nuclear Energy for New Europe - NENE 2016*.

Henry, R., Tiselj, I., & Matkovič, M. (2017). Natural and mixed convection in the cylindrical pool of TRIGA reactor. *Heat and Mass Transfer*, *53*(2), 537–551. https://doi.org/10.1007/s00231-016-1833-2

John D. Bess, Thomas L. Maddock, Margaret A. Marshall, & Leland M. Montierth. (2011). *Fresh-Core Reload of the Neutron Radiography (NRAD) Reactor with Uranium(20)-Erbium-Zirconium-Hydride Fuel*. https://doi.org/10.2172/1004283

Jones, M., & Elliot, A. (1974). *A simplified method of power calibration*.

Kaiba, T., Žerovnik, G., Jazbec, A., Štancar, Ž., Barbot, L., Fourmentel, D., & Snoj, L. (2015). Validation of neutron flux redistribution factors in JSI TRIGA reactor due to control rod movements. *Applied Radiation and Isotopes*, *104*, 34–42. https://doi.org/10.1016/j.apradiso.2015.06.026

Funded by the European Union

Funded by the European Union. Views and opinions expressed are however those of the author(s) only and do not necessarily reflect those of the European Union or the European Atomic Energy Community ('EC-Euratom'). Neither the European Union nor the granting authority can be held responsible for them.

Keresztúri, A., Hegyi, Gy., Marázcy, Cs., Panka, I., Telbisz, M., Trosztel, I., & Hegedüs, Cs. (2003). Development and validation of the three-dimensional dynamic code—KIKO3D. *Annals of Nuclear Energy*, *30*(1), 93–120. https://doi.org/10.1016/S0306-4549(02)00043-9

Klujber, G., & Horváth, A. (2021). *Benchmark description of the BME Training Reactor, version 3.2*.

Kovács, M. (2011). *Mechanical design of BME TR spent fuel transportation* [Master Thesis]. Budapest University of Technology and Economics.

Leppänen, J., Valtavirta, V., Rintala, A., & Tuominen, R. (2025). Status of Serpent Monte Carlo code in 2024. *EPJ Nuclear Sciences & Technologies*, *11*, 3. https://doi.org/10.1051/epjn/2024031

Peric, J., Snoj, L., & Radulović, V. (2026). Cherenkov reactor power meter: Development of an innovative and cost-effective technique for reactor power monitoring. *Nuclear Engineering and Technology*, *58*(3), 104042. https://doi.org/10.1016/j.net.2025.104042

Por, G., Berta, M., & Csuvar, M. (2003). Measurement of the coolant flow rate using correlation of temperature fluctuations. *Progress in Nuclear Energy*, *43*(1–4), 281–288. https://doi.org/10.1016/S0149-1970(03)00038-6

Radulović, V., Štancar, Ž., Snoj, L., & Trkov, A. (2014). Validation of absolute axial neutron flux distribution calculations with MCNP with 197Au(n,γ)198Au reaction rate distribution measurements at the JSI TRIGA Mark II reactor. *Applied Radiation and Isotopes*, *84*, 57–65. https://doi.org/10.1016/j.apradiso.2013.11.027

Radulović, V., Thiollay, N., Carcreff, H., Pungerčič, A., Ambrožič, K., Destouches, C., & Trkov, A. (2024). Epithermal neutron activation dosimetry–(n, γ) reactions under boron-based filters. *Scientific Reports*, *14*(1), 28604. https://doi.org/10.1038/s41598-024-78034-w

Rising, M. E., Armstrong, J. C., Bolding, S. R., Bull, J. S., Clark, A. R., Frederick, C. S., Giron, J. F., Grieve, A. S., Haeck, W., Jones, F. B., Josey, C. J., Kulesza, J. A., Lively, M. A., Swaminarayan, S., Sweezy, J. E., Weaver, C. A., & Zukaitis, A. J. (2025). *MCNP® Code Version 6.3.1 Release Notes*.

Štancar, Ž., Barbot, L., Destouches, C., Fourmentel, D., Villard, J.-F., & Snoj, L. (2018). Computational validation of the fission rate distribution experimental benchmark at the JSI TRIGA Mark II research reactor using the Monte Carlo method. *Annals of Nuclear Energy*, *112*, 94–108. https://doi.org/10.1016/j.anucene.2017.09.039

Štancar, Ž., & Snoj, L. (2017). An improved thermal power calibration method at the TRIGA Mark II research reactor. *Nuclear Engineering and Design*, *325*, 78–89. https://doi.org/10.1016/j.nucengdes.2017.10.007

Švajger, I. (2023). *JSI TRIGA Pulse Database*. Https://Trigapulse.Ijs.Si.

Švajger, I., Čalič, D., Pungerčič, A., Trkov, A., & Snoj, L. (2024). Evaluation of reactor pulse experiments. *Nuclear Engineering and Technology*, *56*(4), 1165–1203. https://doi.org/10.1016/j.net.2023.11.021

Trkov, A., Žerovnik, G., Snoj, L., & Ravnik, M. (2009). On the self-shielding factors in neutron activation analysis. *Nuclear Instruments and Methods in Physics Research Section A: Accelerators, Spectrometers, Detectors and Associated Equipment*, *610*(2), 553–565. https://doi.org/10.1016/j.nima.2009.08.079

Ványi, A. S. (2023). *Experimental and numerical multi-physics analysis for the BME Training Reactor* [Ph. D. Thesis]. Budapest University of Technology and Economics.

Ványi, A. Sz., Babcsány, B., Böröczki, Z. I., Horváth, A., Hursin, M., Szieberth, M., & Czifrus, Sz. (2021). Steady-state neutronic measurements and comprehensive numerical analysis for the BME training reactor. *Annals of Nuclear Energy*, *155*, 108144. https://doi.org/10.1016/j.anucene.2021.108144

Funded by the European Union

Funded by the European Union. Views and opinions expressed are however those of the author(s) only and do not necessarily reflect those of the European Union or the European Atomic Energy Community ('EC-Euratom'). Neither the European Union nor the granting authority can be held responsible for them.

Ványi, A. Sz., Hursin, M., Aszódi, A., Adorján, L., Biró, B., Magyar, B., Mészáros, P., Bozsó, T., & Czifrus, Sz. (2023). Thermal-hydraulic measurements and TRACE system code analysis performed on the natural circulation cooled BME Training Reactor. *Annals of Nuclear Energy*, *189*, 109839. https://doi.org/10.1016/j.anucene.2023.109839

Ványi, A. Sz., Hursin, M., & Czifrus, Sz. (2023). Analysis of transient measurements with thermal feedback and coupled TRACE/PARCS calculations performed on the BME Training Reactor. *Annals of Nuclear Energy*, *194*, 110072. https://doi.org/10.1016/j.anucene.2023.110072

Funded by the European Union

Funded by the European Union. Views and opinions expressed are however those of the author(s) only and do not necessarily reflect those of the European Union or the European Atomic Energy Community ('EC-Euratom'). Neither the European Union nor the granting authority can be held responsible for them.